ABSTRACT

Title of Dissertation:	PROGRAMMING BACTERIAL CONSORTIA FOR AUTONOMOUS REGULATION AND COORDINATED ACTIVITY
	Kristina Therese Stephens, Doctor of Philosophy, 2020
Dissertation directed by:	Professor William E. Bentley, Fischell Department of Bioengineering

The potential of genetically engineered microbes seems nearly infinite with applications ranging from human health to bioprocessing. However, metabolic burden and unbalanced use of cell resources are frequent challenges when engineering cells to carry out synthetic functions. To work around this challenge, engineers are attempting to use co-cultures or synthetic consortia wherein labor is divided amongst subpopulations that work together. This emerging strategy requires new tools to regulate the composition of subpopulations and to enable robust coordination between subpopulations. Here, we investigated and rewired a native cell-cell communication process, quorum sensing, in order to develop tools to regulate co-cultures. We developed modules for signal regulated cell growth rate and cell-cell communication in bacteria, and we used these modules to construct co-cultures with autonomous composition control. Specifically, we developed a “controller” strain for signal

modulated cell growth rate by using quorum sensing signals to regulate levels of HPr, a protein involved in sugar transport. We developed a second “translator” strain that detects the universal quorum sensing signal AI-2 and translates it into a species-specific AI-1 signal. The composition of the resulting co-culture adjusts autonomously in response to AI-2. Importantly, we developed a simple mathematical model based on individual monocultures that predicts behavior of the co-culture. Then, we used our model to explore *in silico* alternate construct designs operating in varied environments. To complement the co-culture model, which explores behavior due to interactions between strains but does not encompass information about the genetic circuits underlying the quorum sensing process, we then developed a gene circuit model of a dual-input synthetic AI-2 quorum sensing system. Finally, we demonstrate that the strategies developed in our co-culture platform can be used to engineer co-cultures where the culture composition is controlled electrically. We also show that these strategies can be used to change the culture composition of a synthetic co-culture where each population is working together to produce pyocyanin, thereby changing the rate of pyocyanin production in the co-culture. The techniques developed here may enable further use of co-cultures or synthetic consortia by synthetic biologists and metabolic engineers for varied applications.

PROGRAMMING BACTERIAL CONSORTIA FOR AUTONOMOUS REGULATION AND COORDINATED ACTIVTY

by

Kristina Therese Stephens

Dissertation submitted to the Faculty of the Graduate School of the
University of Maryland, College Park, in partial fulfillment
of the requirements for the degree of
Doctor of Philosophy
2020

Advisory Committee:
Professor William E. Bentley, Chair
Professor Gregory F. Payne
Professor Rohan Fernandes
Professor Amy J. Karlsson
Professor Helim Aranda-Espinoza
Professor Nam Sun Wang, Dean's Representative

Dedication

To my parents, Jamie Stephens and Katie Martin-Stephens, who have always been my biggest supporters.

Acknowledgements

Many people have helped me throughout my dissertation research. I would first like to thank Professor Bentley for his encouragement and wise insight, and especially for providing me an environment where I could explore my interests with freedom to grow. I would also like to thank my fellow lab members for their advice and help, encouragement, lively scientific discussions, and camaraderie. A special thanks to Chen-Yu for patiently teaching me as a new graduate student, and Pricila, who involved me in a project early on, out of which much of my dissertation research grew. Finally, I would also like to acknowledge my friends and family for their constant support.

Table of Contents

List of Tables

List of Figures

List of Abbreviations

AHL: acyl-homoserine lactone
AI: autoinducer
cAMP: cyclic AMP (adenosine monophosphate)
CCR: carbon catabolite repression
CM: conditioned media
CRP: cAMP receptor protein
DPD: dihydroxy-pentane-dione
GI: gastrointestinal
IPTG: isopropyl β-D-1-thiogalactopyranoside
PCA: phenazine-1-carboxylic acid
PEP: phosphoenolpyruvate
PTS: phosphotransferase system
PYO: pyocyanin
QS: quorum sensing

Chapter 1: Introduction

1.1 Motivation

Metabolic engineering and synthetic biology have high potential to positively impact human health and the environment. These fields have led to the design of "smart" microbes that are able to survey their environment and initiate a response[1] and to microbes that are able to manufacture biomolecular products that either cannot be produced chemically or are environmentally unfriendly to manufacture[2]. However, metabolic burden and unbalanced use of cell resources are frequent challenges when engineering cells to carry out synthetic functions. To work around this challenge, engineers are attempting to use co-cultures or synthetic consortia wherein labor is divided amongst subpopulations that work together[3]. This emerging strategy requires new tools to regulate the composition of subpopulations and to enable robust coordination between subpopulations. Quorum sensing (QS), a native process for cell-cell communication[4], can be coopted to facilitate coordination between populations within a consortia. In this work, we investigate native cell-cell signaling processes and strategies for regulating bacterial co-cultures or synthetic consortia.

1.2 Dissertation Overview

The goal of this work was to engineer strategies for manipulation of individual strains within bacterial co-cultures or small consortia using cell-cell communication.

Chapter 2 provides a background on quorum sensing and on how engineers can use QS processes to manipulate both natural and synthetic microbial communities.

Chapters 3 and 4 focus on fundamental investigations into AI-2 QS and on methods for manipulating cell response to the AI-2 QS signal. Chapter 3 focuses on the effect of the phosphotransferase system (PTS) protein HPr on *E. coli* cell response to AI-2 and on AI-2 uptake. In Chapter 4, we show that a suite of AI-2 reporter cells with a range of behavior is created by overexpressing or deleting genes in the AI-2 QS pathway.

In Chapter 5, we present development of a synthetic co-culture that detects AI-2 in the environment and changes its culture composition accordingly. We constructed an AI-2 sensing strain that functions in media containing glucose (building off discoveries made in Chapter 3). We also developed QS signal-regulated cell growth rate. We developed a simple mathematical model based off of the monoculture experiments, and used the model to predict the co-culture behavior for a range of initial AI-2 concentrations and cell densities.

Chapter 6 presents design of a dual-input AI-2 QS circuit and a mathematical model that describes cell response to AI-2 using the synthetic QS circuit. Importantly, this new synthetic circuit incorporated inducible expression of LsrR, which lowered background expression from the *lsr* promoter. The model, which described both the synthetic circuit components as well as the relevant host components, predicts expression in systems containing the synthetic circuit for a range of inputs.

In Chapters 7 and 8, we apply the strategy for regulating cell growth rate developed in Chapter 5 to new synthetic systems. Chapter 7 describes a system for electronic control of bacterial cell growth rate, enabling electronic control of co-culture composition. Chapter 8 describes the application of the growth control module towards a co-culture system that is cooperatively producing the molecule pyocyanin. By modulating cell growth rate, we are able to modulate pyocyanin synthesis.

Chapter 2: Synthetic biology for manipulating quorum sensing in microbial consortia

This chapter is reproduced from the recently accepted review article: Stephens, K., Bentley, W.E. "Synthetic biology for manipulating quorum sensing in microbial consortia." *Trends in Microbiology.*

2.1 Synergy between quorum sensing research and synthetic biology

Although bacteria are unicellular organisms, it is now well understood that they are social and display population based behavior. Cell-cell communication can occur through quorum sensing (QS). In this process, bacteria secrete signaling molecules called autoinducers that accumulate in the extracellular milieu as the local cell density increases. Once a threshold autoinducer level is reached, the autoinducers alter gene expression within the cells collectively across the population. Early investigations of QS primarily consisted of growing a single strain in standard (well-mixed) laboratory conditions[5, 6]. Many recent studies, however, focus on the impact of QS between species and within consortia. The rapid expansion of microbiome research is likely to further reveal the impact of QS in natural environments.

Research on QS, in addition to revealing important fundamental science, was also instrumental in the early years of synthetic biology[7]. Synthetic biologists seek to design biological systems with programmable or predictable behavior. A hallmark of the field is the incorporation of engineering design principles. Many early studies in synthetic biology made use of QS circuits for programming cell behavior[8, 9], and QS

processes have continued to be a staple for synthetic biologists when creating synthetic circuits. This interest in QS by synthetic biologists lead to many QS processes and the parts (i.e. promoters, genes, and proteins) that make up those processes being well characterized with a focus on understanding ways to precisely and predictably manipulate responses to QS molecules. That is, QS and synthetic biology research have been highly complementary, with QS research expanding the synthetic biology toolkit and synthetic biology providing new tools for investigating QS. In recent years, both of these fields have been shifting focus away from research using single strains towards consortia and microbiome research.

In this review we discuss ways in which synthetic biology can be used to manipulate QS processes in microbial consortia. We first cover ways in which synthetic biology tools have been used to manipulate signal transduction and cell response to autoinducers. Then, we discuss how synthetic biology can be used to manipulate and interrogate QS processes in microbiomes and to create synthetic consortia.

2.2 Synthetic biology provides tools to manipulate quorum sensing signal transduction and quorum sensing-mediated cell phenotype

Several types of QS systems have been discovered. Here, we cover the AI-1 or acyl-homoserine lactone (AHL) and AI-2 QS systems. We give brief backgrounds on the genetic and molecular pathways that make up each QS process and then focus on examples of how these processes have been manipulated in order to engineer cellular responses.

AHL

The AHL systems are perhaps the most well-known QS systems. The process was originally discovered in the marine bacterium *Vibrio fischeri* and found to control luminescence production[10]. In *V. fischeri*, LuxI synthesizes the AHL molecule, which is able to freely diffuse across the cell membrane (**Figure 2.1**). AHL level increases as cell density increases, and once a threshold of AHL is reached, the AHL molecule binds LuxR and the bound complex activates the bidirectional *lux* promoter. Promoter activity results in transcription of the luciferase genes *luxCDABE* and additional transcription of *luxI* and *luxR*. This positive feedback loop is a hallmark of many QS systems. Several homologous AHL systems have been discovered in other organisms, including *Pseudomonas aeruginosa* and *Vibrio harveyi*[4]. Each organism produces a different AHL molecule, usually differing in the length of the fatty acid chain. Generally, organisms only recognize the AHL molecule that they produce, and so each AHL system is considered species-specific. In addition, several species use multiple QS signals and bacteria can use these to integrate multiple pieces of information, which is likely important in consortia or different niches (see reviews[5, 11]).

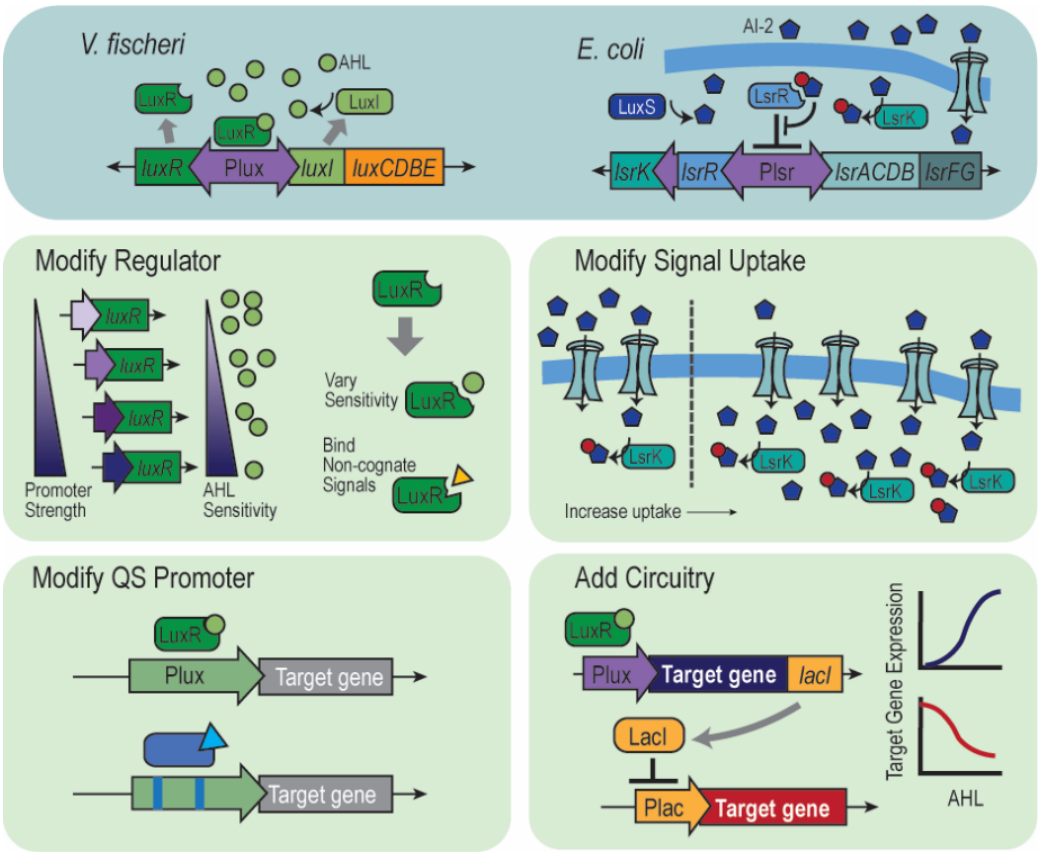

Figure 2.1. Synthetic biology allows manipulation of cell response to quorum sensing signals.

The native AHL and AI-2 QS pathways are shown in *V. fischeri* and *E. coli*, respectively (top panel). Several strategies for manipulating cell response are illustrated (bottom panels). The regulator (LuxR) can be manipulated to control sensitivity to AHL signals, either by regulating transcription to control the number of copies of LuxR or by modifying the AHL binding site. Signal uptake can be altered by, for instance, increasing the number of copies of proteins involved in AI-2 transport and processing. The QS promoter can be mutated to alter response to the relevant autoinducer. Additional circuitry can be incorporated into the cell response to create varied or programmed responses to the autoinducer.

Synthetic biologists frequently use the AHL QS systems. These systems require relatively few components, namely LuxR (or the homologous regulator), the AHL synthase, and the relevant promoter. AHL molecules cross the cell membrane without requiring specific transporters. These qualities allow the different components to be easily assembled in a range of hosts. The iGEM (International Genetically Engineered Machines) organization maintains a library of genetic "BioBricks" that can be used to build synthetic circuits, and the components comprising the AHL systems are amongst the most commonly used parts in the database (http://parts.igem.org/Frequently_Used_Parts).

Many efforts have been made to characterize responses to AHL and to engineer cells that respond to specific concentrations of AHL. This is frequently done by manipulating the regulator protein LuxR. For instance, Wang et al. expressed LuxR under a series of constitutive promoters with varying activity[12]. The varied expression levels resulted in populations that detected different ranges of AHL, with high constitutive expression of LuxR resulting in cells with the most sensitivity to AHL. Alternately, directed evolution of the regulator can change the sensitivity to its cognate AHL[13] or increase its sensitivity to non-cognate AHL molecules[14]. Shong et al. mutated an AHL responsive promoter by adding an additional binding site for the regulator in different locations[13]. This resulted in varied promoter activities, and in one case, reversed the effect of adding the AHL molecule. A mathematical approach can be used to rationally engineer QS cell response. For instance, Zeng et al. developed an approach that combines network enumeration with parameter

optimization, incorporating known information on biological parts to design an ultrasensitive QS switch[15].

The AHL systems are frequently used by synthetic biologists to engineer cells where the phenotype is dependent on cell density. For instance, You et al. engineered AHL producing cells where AHL activated a toxin within the cell, resulting in programmable stationary phase cell density[8]. Liu et al. linked chemotaxis with cell density for patterned behavior[16], and Swofford et al. engineered *Salmonella* that turn on gene expression in tumors where they accumulate at higher density than in other organs[17]. QS has also been used by metabolic engineers to autonomously redirect cell metabolism at a certain cell density[18, 19]. Gupta et al. engineered cells that produced the AHL signal at different rates, with higher rates of AHL production causing the metabolic switch to occur at lower cell densities[19]. They then selected the strain with the highest titers for the desired product. Additional genetic circuitry is also frequently added to develop more complex phenotypes[20-22]. Basu et al. engineered a system where the cells fluorescence only at medium concentrations of AHL and not low or high concentrations[9]. Danino et al used QS to synchronize a genetic clock amongst the cells in a culture[23]. Andrews et al. engineered a system for sequential or check-point controlled activation of target genes, using AHL QS components along with other small molecule induction systems[24].

AI-2

Unlike the AHL quorum sensing systems, the AI-2 QS system is used by multiple species. LuxS synthesizes AI-2 as a byproduct of the activated methyl cycle.

In *E. coli* (**Figure 2.1**), AI-2 is imported into the cell by the transporter LsrACDB [25]. It is then phosphorylated by the LsrK kinase. Phosphorylated AI-2 binds the repressor, LsrR, and relieves repression of the bidirectional *lsr* (LuxS regulated) promoter. This causes transcription of the *lsr* operon and overexpression of LsrACDB, LsrK, LsrR, and LsrFG, leading to rapid uptake of AI-2 and depletion of AI-2 from the extracellular media. LsrFG eventually metabolize the AI-2.

Due to the relatively complex signal transduction process and the fact that AI-2 does not diffuse across cell membranes [26], several more components are required for reconstructing the AI-2 system compared to the AHL systems. However, the additional complexity allows for multiple control points to regulate cell response. Overexpressing or deleting specific genes in the cascade can result in interesting dynamics. For instance, in a clonal population of *E. coli*, only a subset of the culture responds to AI-2. Deleting *lsrFG* from the genome, however, causes cells to be more sensitive to AI-2, and also changes the fraction of the population that responds to AI-2[27]. It was also found that overexpression of LsrACDB or LsrK leads to rapid uptake of AI-2 from the extracellular environment and decreased variability in cell response across the population[28]. Combining these two strategies lead to a suite of cells with varied responses to AI-2[29].

The AI-2 receptor may also be an avenue for manipulating cell responses to AI-2. AI-2 is derived from 4,5-dihydroxy-2,3-pentanedione (DPD), and can spontaneously cycle among a collection of molecules all known as AI-2. In *Vibrio* species, LuxP is responsible for initiating cell responses to AI-2 via a phosphorylation cascade while in *E. coli* and *Salmonella*, LrsB binds AI-2 and initiates transport via

an ABC-like transporter. These two receptors, importantly, bind different forms of AI-2. Recently, it was found that *Clostridium saccharobutylicum* has an LsrB-like receptor in which the binding site for AI-2 contains amino acid variations from what was previously determined to be critical for AI-2 binding, which may lead to discovery of additional species with ability to bind AI-2[30]. This same study revealed that *C. saccharobutylicum* begin to uptake AI-2 at a lower AI-2 threshold than *E. coli*. This difference in AI-2 uptake, along with the ability of different organisms to respond to different forms of AI-2 is interesting when considering these species may exist together in medically important niches. It may also provide avenues for synthetic biologists to manipulate the AI-2 signal in a given environment in ways that affect certain species more than others[31].

The *lsr* promoter in *E. coli* is also sensitive to carbon catabolite repression and is not active when glucose is present in the media[32]. It's been understood for many years that the promoter contains cyclic AMP (cAMP)-cAMP receptor protein (CRP) binding sites. However, it was also more recently shown that a cytosolic phosphotransferase system (PTS) protein involved in sugar transport, HPr, can post translationally regulate AI-2 quorum sensing[33]. HPr can bind LsrK and lower LsrK activity. The phosphorylation state of HPr, which is indicative of glucose transport, determines how effectively HPr binds LsrK. Others have similarly demonstrated a strong link between metabolism and AI-2 QS[34]. These results present challenges when engineering cells using the AI-2 system. That is, the cells may behave drastically differently depending on whether the media contains glucose. Zargar et al. showed that by decoupling expression of the AI-2 uptake and processing genes from

the *lsr* promoter, cells could be engineered to uptake AI-2 even in media containing glucose[35]. HPr mutants are also able to uptake AI-2 in the presence of glucose[33], as are catabolite repression insensitive strains[34].

Another challenge of using the *lsr* system is that the promoter is relatively weak. This has been overcome by coupling the *lsr* promoter with the strong T7 expression system[36]. T7 RNA polymerase is placed under the *lsr* promoter and activates expression of the gene of interest under the T7 promoter. Alternately, directed evolution of the promoter showed that mutations in the region thought to be regulated by cAMP lead to higher promoter activity[37].

The above works illustrate how synthetic biology techniques can be used to understand the function and relative importance of specific components of the AI-2 QS pathway, and to manipulate AI-2 levels or cell response to AI-2. Several mathematical models have also been developed from these results to predict and understand AI-2 QS[38-41].

2.3 Manipulating quorum sensing in microbiomes using synthetic biology

It is likely that QS plays an important role in niches where microbial communities exist, such as the gastrointestinal (GI) tract or plant microbiome. While experiments with single strains in shake flasks have been useful in identifying the molecular pathways that make up QS processes, it is likely that QS processes play as yet undiscovered roles in these complex niches. Synthetic biology may provide tools for understanding both the role of QS in microbiomes and for manipulating QS processes for positive health outcomes (**Figure 2.2**). Here we discuss recent studies

indicating the importance of QS in natural consortia and preliminary studies that use synthetic biology to manipulate QS processes in these environments.

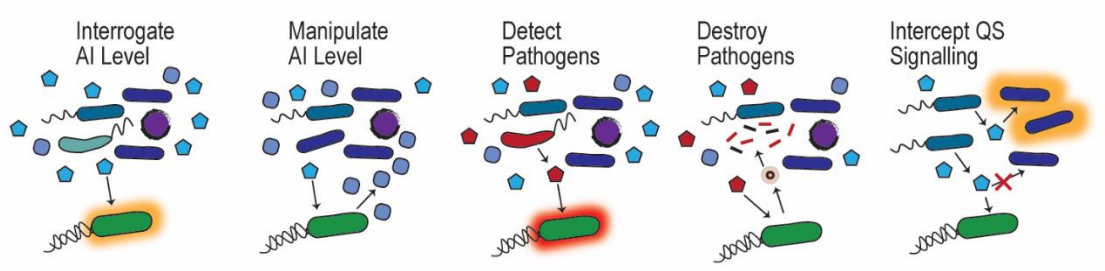

Figure 2.2. Synthetic biology for manipulating quorum sensing in microbiomes. Cells can be engineered to operate in native environments as diagnostic or therapeutic vehicles. As depicted, these strains can be designed to read varied autoinducer (AI) levels and respond with a measurable output (such as fluorescence). They can manipulate autoinducer levels by uptaking or secreting specific signals. Engineered cells can detect autoinducers from pathogens and respond by releasing molecules to destroy the pathogen. They can also intercept cell-cell communication that may be occurring between different strains by uptaking the relevant signal.

GI Tract

The microbiome of the GI tract is an exciting area of research due to its importance for human health. The human GI microbiome is important for nutrient and drug adsorption and digestion[42, 43], is the site of many pathogenic diseases, and has even been shown to affect depression and mood through its connection to the central nervous system[44]. Although it is understood that commensal bacteria are important for a healthy microbiome, there are many open questions about how the

microbiome community forms and how or why the microbiome community becomes dysregulated. It is currently unclear the extent to which QS plays a role in these processes. Thompson et al. showed that AI-2 may play a role in the composition of the gut microbiome[45]. They engineered *E. coli* to either overproduce AI-2 (by eliminating the ability for uptake) or not produce AI-2 (through elimination of the AI-2 synthase) and showed that treatment with these two strains in the antibiotic treated mouse changed the resulting composition of the species in the mouse gut. AI-2 shifted the relative levels between Bacteroidetes and Firmicutes phyla. Another study suggested that probiotic *Bacillus* can interfere with QS systems and prevent pathogen infection[46]. These early investigations show potential for manipulating the microbiome using engineered bacteria that can manipulate QS processes within the gut. Many questions remain however. There is currently not a clear idea of autoinducer levels in the gut, and whether these levels vary drastically spatially, over time or, naturally, from person to person. Potentially, synthetic biology could be used to probe for these signals in order to begin to answer these basic questions.

Synthetic biology can also be used to probe for pathogens or halt infections from pathogens that rely on QS to initiate virulence. *Vibrio cholerae,* for instance, uses multiple QS systems to control production of virulence factors and biofilm formation and dispersal[47, 48]. At low cell density, *V. cholerae* attaches to the intestinal wall and produces virulence factors. At high cell density, *V. cholerae* disperses. Duan et al. engineered a commensal *E. coli* strain, Nissle, to overexpress CAI-1, a *V. cholerae* specific autoinducer[49]. They showed that prophylactic treatment with this Nissle strain reduced *V. cholerae* virulence and cell number in the infant mice model.

More recently, Mao et al. used a probiotic strain that naturally interrupts the *V. cholerae* QS process to prevent infection[50]. They also engineered their strain to report on *V. cholerae* autoinducer CAI-1 as an early detection of *V. cholerae*. Another strategy is to design sense and kill bacteria that detect QS molecules produced by pathogens and then produce molecules (often released by cell lysis) that kill the pathogen[51-53]. Hwang et al. showed their engineered probiotic strain could treat *P. aeruginosa* infections in the mouse gut[51]. A different strategy is to use phage. Silpe et al recently showed that a *V. cholerae* phage encodes a homologous receptor for a *V. cholerae* autoinducer[54]. Interestingly, the phage encoded autoinducer receptor can activate the relevant promoter in both the phage and *V. cholera* genomes. However, the *V. cholerae* receptor cannot activate the promoter in the phage genome. The authors then used this information to design a species-specific kill switch for *V. cholerae*.

Synthetic biologists have also begun to investigate QS for engineering cell-cell signaling in the gut. Kim et al. engineered bacteria that can secrete and respond to AHL molecules within the mouse gut[55]. Sedlmayer et al. engineered mammalian cells that are able to detect autoinducers and interfere with QS controlled processes in microbes[56, 57]. While these studies were completed *in vitro*, they suggest opportunities to use QS for interkingdom communication.

Oral and skin microbiomes

Studies of the human microbiome thus far have predominately focused on the GI tract. However, research shows that the oral and skin microbiomes play a role in

human health as well. QS is important in these communities. *Streptococcus mutans* and *Aggregatibacter actinomycetemcomitans* (*A. act*) are both associated with dental cavities. *A. act* was found to induce the QS regulon of *S. mutans* through an unknown mechanism in dual species biofilms grown on saliva[58]. Further, the authors found this only occurs when the species are co-cultured and does not occur if *A. act* are cultured separately and cell free conditioned medium added *to S. mutans*. Muras et al. studied the effect of exogenously supplied AHL molecules to *in vitro* biofilms resembling the oral microbiome and found that some of the signals changed cell metabolism and shifted the consortia composition[59].

The makeup of the skin microbiome is also thought to be a contributing factor to various diseases including the common skin disease atopic dermatitis, although direct causes are still generally unknown[60, 61]. *Staphylococcus aureus* is often associated with atopic dermatitis[60]. Williams et al. showed that *S. aureus* QS controlled protease production that contributes to skin inflammation could be inhibited by a peptide secreted by *S. epidermidis*[62].

Plant microbiome

Plant microbiomes affect plant health and crop yield[63]. As environmental concerns about pesticide and land use related to crops increase, forward engineering microbiomes that promote plant health is a new and potentially promising approach to reducing the environmental impacts of agriculture[64, 65]. QS plays a role in plant microbiomes, and there is potential to positively impact plant health by monitoring or manipulating QS processes in these communities. In crop microbiomes, some

pathogens rely on QS for virulence factor production, and community interactions can inhibit or aggravate virulence. *Lysinibacillus*, a soil bacterium, can attenuate virulence from the pathogenic species *Pectobacterium carotovorum* by degrading AHL signals and interrupting QS processes of the pathogen[66]. By engineering overexpression of the AHL degrading enzyme, the authors were able to inhibit virulence of the pathogen. In another example, Valente et al. showed that crosstalk between species could actually cause virulence of plant pathogens[67]. That is, they found autoinducers from *P. carotovorum* could induce virulence in the pathogen *P. wasabiae*. Engineers have also begun to use QS to engineer commensal bacteria with desired, density-dependent behavior. Zuniga et al. engineered the rhizobacterium *Cupriavidus pinatubonensis* with autoinducer regulated production of indoleacetic acid[68]. In this way, the bacteria autonomously produced indoleacetic acid at the appropriate time (i.e. a specific bacterial cell density) to promote plant growth.

QS may also be important for facilitating interactions between species in other ecologically important microbiomes. For instance, in the coral microbiome, the microbiome composition is different in communities affected by Blank Band Disease and this may be in part due to differences in QS between communities with and without the disease[69]. Cyanobacteria prevalent in the disease state can produce the metabolite, lyngbic acid, which is able to inhibit QS in *V. harveyi* and may contribute to the disease.

2.4 Creating synthetic consortia using quorum sensing processes

Quorum sensing provides an opportunity to design sophisticated or robust synthetic microbial communities. The synthetic consortia can be used to explore social behavior in complex ecosystems in order to make hypotheses or even draw conclusions about natural consortia[70, 71]. Metabolic engineers are also interested in using co-cultures and multi-population systems for production of molecular products[72, 73]. Often products synthesized from complex pathways cannot be produced in high titers from pure cultures of single strains. This can be due to a high metabolic burden, or sometimes one part of the pathway inhibits a different part of the pathway[74]. Use of co-cultures can alleviate many of these issues, but introduces the additional challenge of regulating the behavior of individual populations and their composition within the consortia. Here, we discuss how engineers can use QS to construct synthetic consortia. Rewired QS circuits can be used to coordinate gene expression between subpopulations, control consortia composition, or enable communication between distant cell populations (**Figure 2.3**).

Controlling and coordinating gene expression

QS can be used to autonomously control or to coordinate gene expression within co-cultures or consortia. For instance, QS can be used to engineer co-cultures where the two populations express target genes only when cultured together[75, 76]. Others have engineered artificial cells that can send and receive signals to and from bacteria[77-79], and others have created Gram-negative *E. coli* that are able to communicate with Gram-positive *Bacillus megaterium*[80]. Terrell et al. engineered a

co-culture made up of two strains that respond to different levels of AI-2[70]. Each strain produced a different fluorescent protein in response to AI-2 and constitutively expressed a magnetic nanoparticle that allowed all of the cells to be collected after surveying a complex environment. Comparison of expression profiles of the two strains after collection resulted in a color "pattern" and information about the environment surveyed by the cells. The cell network was able to detect AI-2 that had been secreted by *Listeria*. This work also demonstrated the close relationship between fundamental research on quorum sensing mechanisms and the potential for synthetic biology to be useful for studying and manipulating quorum sensing phenomena. The engineered design used in the manuscript relies on foundational knowledge of the AI-2 QS process, and the final design allowed for sophisticated interrogation of AI-2 levels in different environments.

A challenge in incorporating greater numbers of members or subpopulations within synthetic consortia is that many of the QS systems are not completely orthogonal. Studies that mix and match the different QS regulators, autoinducers, and promoters in *E. coli* have been conducted to characterize cell responses for a range of constructs[81]. Others have developed computational models to aid in designing systems using multiple QS signals in order to optimize signal to noise ratio and minimize crosstalk[82, 83]. Interestingly, recently Wellington et al. studied QS receptor sensitivity and promiscuity to different AHL signals in the native species and compared to results in *E. coli*. They concluded that QS systems in their native hosts are less promiscuous than experiments in *E. coli*, where the QS receptor is often overexpressed, would indicate[84].

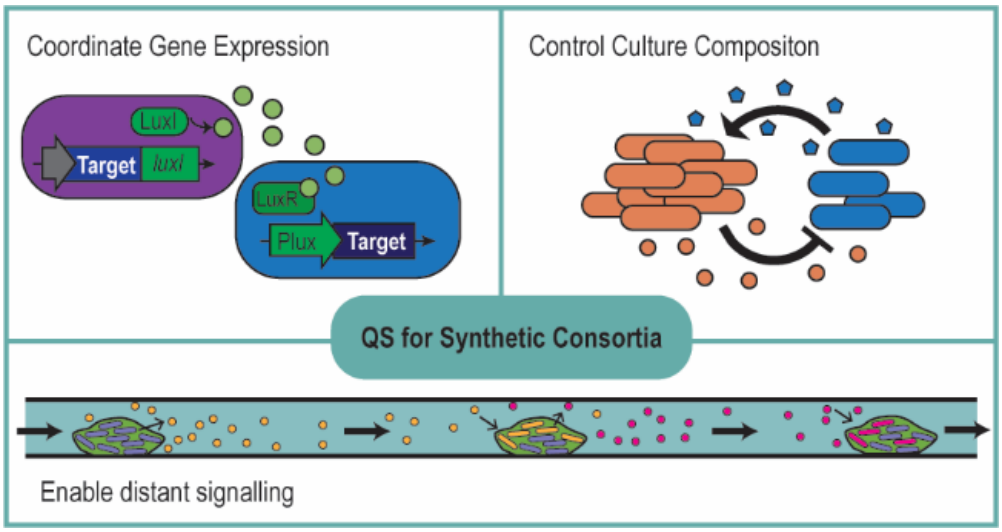

Figure 2.3. Quorum sensing for designing synthetic microbial consortia.

QS is used by synthetic biologists to design synthetic microbial consortia in order to coordinate cell behavior and allow for cell-cell signaling. QS can be used to coordinate gene expression (top left) between subpopulations. It is also used to control consortia composition (top right). This can be accomplished by using autoinducer production as a measure of cell density in one population in combination with autoinducer-regulated synthesis of a molecule that either enhances or inhibits growth in a second population. QS is also used to enable cell-cell communication over a distance (bottom), for instance between two populations located in different places in a microfluidic device.

Controlling consortia composition

Consortia composition is a critical parameter in many synthetic co-culture systems, and methods for controlling composition may be beneficial. Stephens et al. designed a co-culture where the composition of the co-culture varies depending on

the level of AI-2 in the environment[85]. The authors accomplished this through use of rewired quorum sensing pathways and through autoinducer modulated cell growth rate. Growth rate of an individual strain in the co-culture was modulated by controlling transcription of a sugar transport protein, HPr, using a species-specific AHL. Others have controlled cell density of individual populations or strains using autoinducer controlled cell lysis[8, 86, 87] or production of toxins[88]. These strategies have been used to stabilize a co-culture, preventing one population from outgrowing the other[86], and to create oscillating behavior[88]. Kong et al. created co-cultures displaying a range of social behavior using small molecules that accumulate with cell density (as in QS processes) and activate genes that help or hurt growth of specific populations[89]. Wu et al. designed a co-culture using QS that relied on mutualism to survive[90]. They used a model to describe the resulting conditions for survival or population collapse. Many studies have also been conducted using QS-component mutant strains that are able to "cheat" on their wild type counterparts by benefiting from but not producing QS controlled public goods (see review[91]). Recently, Ozkaya et al. studied a *ΔluxR* cheater population of *P. aeruginosa* that causes population collapse when cultured with wild type cells[92]. Interestingly, adding a third *ΔpvdS* population, that was able to cheat on the *ΔluxR* cheaters, resulted in stable cultures.

Thus far, studies on controlling population density in engineered co-cultures has primarily resulted in platforms to control culture composition or systems that mimic social behaviors (mutualism, competition, etc.). Questions remain about whether these strategies could be broadly applied by metabolic engineers. Honjo et al. employed a QS based technique to control a co-culture for production of

isopropanol[93]. The first population produced enzymes required to break down sugars in the extracellular media and then secreted a QS signaling molecule. After accumulation of the autoinducer (at a specific cell density), the autoinducer caused lysis of the first population, releasing the sugar degrading enzymes and decreasing the composition of the first population in the co-culture. A second population then was able to use the digested sugars to produce the target chemical.

Enabling cell-cell communication between localized populations

QS systems are also used to enable cell-cell communication between distant populations. Luo et al. showed in a microfluidic device populations upstream could signal to populations downstream, even as modified by intermediate populations – all by modulating the QS signaling molecule as a function of distance[94]. Alternately, QS can allow for recruitment of one population to a specific location. For instance Wu et al. engineered AI-2 synthases that dock to a specific locale (cancer cell receptor) and recruit a bacterial population to that locale[95]. The synthesized AI-2, which bacteria naturally chemotax towards, served both as a molecular beacon recruiting cells at one concentration and as a QS autoinducer altering gene transcription at another. Others have used QS to control microbial biofilms. Wood et al. engineered bacteria that prevent biofilm formation by other bacteria[96] and Hong et al. engineered bacteria that are able to cause dispersal of specific populations in a biofilm[97].

2.5 Concluding remarks

Currently there is a high level of interest in understanding microbiomes and the interactions and contributions of individual members, along with an interest in forward engineering multi-population systems and consortia. QS likely plays a key role in these consortia, both allowing members within the consortia to act in a population-based manner and by enabling interspecies and even interkingdom communication. However, many questions remain regarding how microbiomes form, how their compositions may shift over time, and how QS contributes to the composition and function of consortia. Synthetic biology provides tools to study and manipulate these processes, including in their native environments. Synbio constructs, if designed using native strains and with minimal alteration, can be used to eavesdrop on native environments and report on their findings. Such efforts represent a new strategy for influencing human health, agriculture, and the environment. At the same time, QS processes are being used by synthetic biologists to design and assemble synthetic consortia composed of discrete subpopulations that communicate amongst each other and work together to achieve a designed objective function. This strategy will surely extend the capabilities of systems currently using single strains. In sum, research on the role of QS within microbiomes and the use of QS to build synthetic consortia are still in the early stages of development with many exciting avenues for exploration and high potential to influence human health and the environment.

Chapter 3: AI-2 quorum sensing is regulated by the PTS transport protein HPr

This chapter was primarily reproduced, with permission, from sections of the publication: Ha, J.H., Hauk, P., Cho, K., Eo, Y., Ma, X., Stephens, K., Cha, S., Jeong, M., Suh, J.Y., Sintim, H.O., Bentley, W.E., Ryu, K.S. "Evidence of link between quorum sensing and sugar metabolism in *Escherichia coli* revealed via cocrystal structures of LsrK and HPr," *Sci Adv*, **2018**, 4, eaar7063. This was a collaboration in which we found, *in vitro*, that HPr binds the protein LsrK and affects LsrK activity. We corroborated this *in vitro* data with *in vivo E. coli* experiments. Chapter 2 presents the *in vivo* experiments, which were my contribution to the work. Due to the narrower focus, the text is slightly modified from the text in the published manuscript.

3.1 Introduction

Bacteria, despite being unicellular organisms, are capable of coordinating population-level behavior through a process termed quorum sensing (QS). In this process, bacteria secrete chemical signaling molecules called autoinducers (AIs) which accumulate as cell density increases. Once the AI level reaches a threshold, signaling a "quorum" of cells, the AI signals are transported intracellularly, where they activate gene expression and enable coordinated phenotypic responses in the population. The importance of QS in biofilm formation and maintenance[98], bacterial persistence[99], and pathogenicity[100] has appeared in many review articles. Further, the interplay between the signaling components that comprise QS systems has been the

subject of many studies in metabolic engineering and synthetic biology, wherein genetic networks have been developed to enable "programmed" design and control of metabolic pathways and bacterial phenotype[101, 102]. For example, researchers have exploited QS circuitry for the design and implementation of "smart" bacteria that target and destroy cancers and pathogens[51, 87]. Some of these systems depend on the "orthogonality" of the signaling system with the metabolic activity of the host organism. For instance, Saeidi *et al*. engineered bacteria that sense acyl-homoserine lactone QS signals produced by *Pseudomonas aeruginosa* and subsequently release toxins to eradicate the pathogen[103]. Other systems rely on the interdependence of QS activity and host metabolism. For example, an autoinduction system was constructed by Tsao *et al.*, in which *Escherichia coli* secrete AI-2 [dihydroxy-pentane-dione (DPD)] and, at the appropriate time for gene expression, self-induce expression of a recombinant protein by amplifying expression from the native *lsr* (LuxS-regulated) promoter using T7 polymerase[36]. Further mechanistic understanding of how the cell regulates QS processes, for example, based on the availability of substrates like glucose, will further enable researchers to exploit these QS systems for the design of synthetic biology systems with new capabilities.

There is evidence that the AI-2 mediated QS system is partially regulated by substrate availability and cell metabolism. LuxS synthesizes AI-2 as a byproduct of the activated methyl cycle[100], after which AI-2 accumulates extracellularly. AI-2 is imported by LsrACDB[32] and phosphorylated by the kinase LsrK, sequestering it within the cell[104] (**Figure 3.1**). Phosphorylated AI-2 relieves LsrR-mediated repression of the *lsr* operon[105], allowing transcription of the *lsr* genes and acceleration

of AI-2 uptake. Several studies suggest that the bidirectional *lsr* operon, in addition to being regulated by LsrK and LsrR, is also subject to carbon catabolite repression (CCR). For instance, activation of the *lsr* promoter does not occur in the presence of glucose[32] or glycerol[106] and requires the global regulators cyclic adenosine monophosphate (cAMP) and cAMP receptor protein (CRP)[32]. Binding sites for cAMP-CRP exist between the *lsrR* and *lsrACDB* promoters[107] and binding of cAMP-CRP likely modulates the promoter activity[108]. Here, we propose a new mechanism linking cell metabolism to the AI-2 QS system. Specifically, we have discovered that the activity of LsrK is regulated by the phosphoenolpyruvate (PEP)-dependent sugar phosphotransferase system (PTS) protein HPr.

The PTS is important for sugar uptake and regulation of carbohydrate metabolism. It comprises three units- EI, HPr, and the EII protein complex- that sequentially transfer a phosphoryl group from PEP to the transported carbohydrate (**Figure 3.1**). The active transport of PTS sugars affects the phosphorylation state of each of the PTS components. Although EI and HPr are general PTS proteins, EII is specific to the carbohydrate being transported, and one of the most commonly studied is a subunit involved in glucose transport, $EIIA^{Glc}$. The phosphorylation state of $EIIA^{Glc}$ regulates the activity of adenylate cyclase, which synthesizes cAMP, a global regulator within the cell[109, 110]. As discussed above, the cAMP-CRP complex regulates transcription from the *lsr* promoter. There is evidence to suggest that the phosphorylation state of the other general PTS proteins also regulate AI-2 quorum sensing activity. Pereira *et al.* demonstrated that phosphorylated EI is required for the initial uptake of AI-2, although the mechanism behind this has not been elucidated[34].

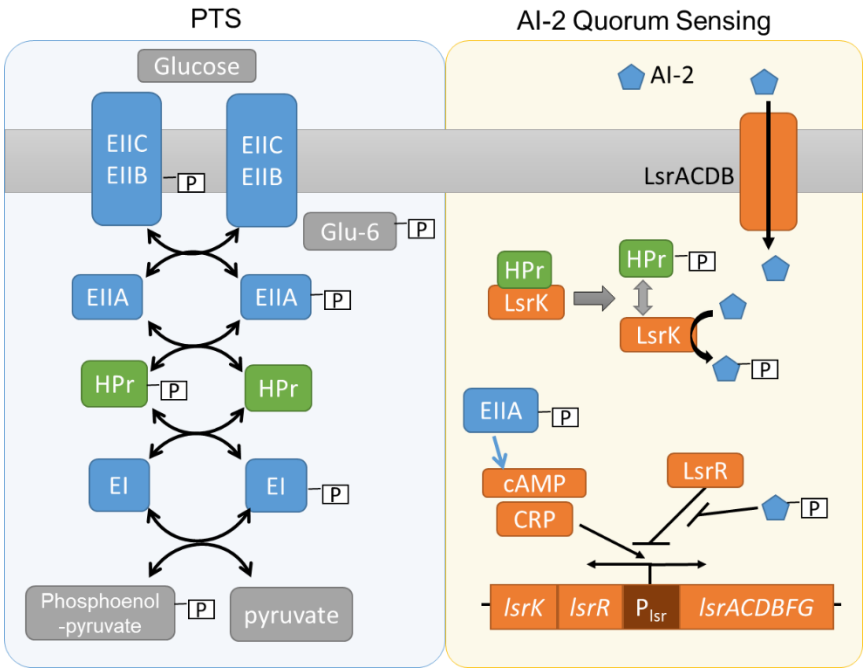

Figure 3.1. Scheme of interactions between PTS and AI-2 QS systems

The PTS uptakes PTS sugars, including glucose, into the cell. In this process, a phosphoryl group is sequentially transferred from phosphoenolpyruvate through the PTS components (EI, HPr, and EII) to glucose. In the AI-2 QS system, LsrACDB uptakes AI-2. LsrK phosphorylates AI-2. Phosphorylated AI-2 binds LsrR and relieves repression of the *lsr* promoter. Phosphorylated $EIIA^{glu}$, which accumulates at low glucose levels, activates the global regulator cAMP. cAMP and CRP positively regulate the *lsr* promoter. HPr binds LsrK and inhibits LsrK activity (negatively regulating the *lsr* promoter). Phosphorylated HPr binds LsrK much less strongly, allowing increased LsrK activity.

Our research demonstrates, *in vitro*, that HPr tightly binds LsrK and directly influences LsrK activity[33]. Here, we demonstrate *in vivo*, that HPr affects AI-2 uptake and *lsr* promoter activity. These results corroborate the *in vitro* conclusions. Together,

these results demonstrate that uptake of PTS carbohydrates has direct involvement in signaling and show for the first time that the PTS regulates AI-2 quorum sensing not only through the global regulator cAMP, but also directly through specific interactions with LsrK. This finding suggests that bacteria have evolved sophisticated mechanisms for incorporating information about substrate availability and cell metabolism into QS processes. This discovery is of fundamental importance as phenomena such as pathogenicity, bacterial persistence, biofilm formation, etc., have previously been shown to be influenced by nutrient availability and QS. Here, we suggest these may be more closely linked than previously thought.

3.2 Results

3.2.1 HPr influences *lsr* promoter activity

To investigate the *in vivo* activity of LsrK in the presence or absence of the wild-type HPr or a mutant HPr^{H15A}, Miller assay experiments were performed. LsrK activity was accessed indirectly via LacZ expression levels in the presence or absence of 40 μM synthetic AI-2. For this experiment, we transformed the mid-copy pSkunk plasmid harboring wild-type HPr, its mutant HPr^{H15A}, or the empty plasmid into PH02, which is a *ptsH* and *luxS* knockout strain (Table S2). A *luxS* knockout strain was used so that the cells would not synthesize AI-2. In addition, a reporter pLW11 plasmid was cotransformed into PH02, because this plasmid carries the *lacZ* reporter gene under the *lsr* operon promoter[32]. Note that LsrK phosphorylates AI-2 and phosphorylated AI-2 activates the *lsr* promoter, so use of the Miller assay here is an

indirect measurement of LsrK activity. In the absence of the wild-type HPr or HPr^{H15A}, we observed an early increase in LacZ expression in the presence of 40 μM AI-2 when compared to the same condition but in the absence of AI-2 (**Figure 3.2A**). Next, the effects of the wild-type HPr and HPr^{H15A} on the *in vivo* activity of LsrK were accessed according to different *E. coli* growth stages. To evaluate whether the wild-type HPr and its mutant HPr^{H15A} affected cell growth, we measured the PH02 growth rate under different conditions. PH02 transformed with pSkunk-HPr grew faster than the same strain carrying pSkunk-HPrH15A or pSkunk-empty (no HPr). That is, the growth rate observed in the absence of HPr (pSkunk-empty) was similar to that of the HPr mutant (pSkunk-HPrH15A) (**Figure 3.2B**). Because HPr is involved in sugar transport, it is probable that the H15 mutation abolishes HPr activity as a phosphocarrier in the PTS, affecting the use of sugars and other carbon sources that affect the phosphorylation state of the PTS. The presence of HPr^{H15A} decreased the *lacZ* activity irrespective of the different growth phases. On the other hand, the *lacZ* activity of the *E. coli* strain carrying pSkunk-HPr was suppressed during exponential growth but was increased at the late stationary growth phase likely due to the increased population of p-HPr (**Figure 3.2A**). These data largely agree with the *in vitro* inhibition assays which showed that HPr inhibits LsrK activity much more than phosphorylated HPr inhibits LsrK activity[33].

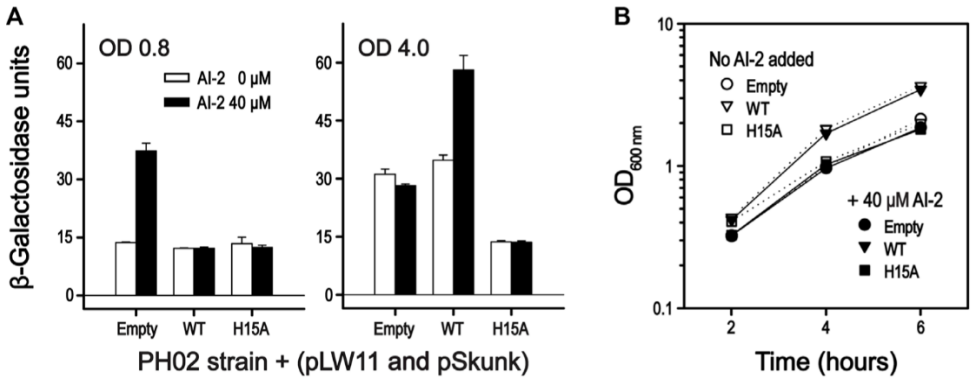

Figure 3.2. *E. coli lsr* promoter activity during cell growth (indirect measurement of LsrK activity).

(a) *E. coli* PH02 strain (Δ*ptsH* and Δ*luxS*) carrying the reporter plasmid pLW11 (*lacZ* gene under *lsr* operon) and the pSkunk-empty, pSkunk-HPr, or pSkunk-HPr^{H15A} plasmid. Cells were cultivated in LB medium in the presence or absence of 40 µM AI-2. The culture aliquots were collected for the measurement of β-galactosidase activity at 0.8 and 4.0 $OD_{600\ nm}$. The data showed representative experiments performed independently. Data are means ± SDs of technical triplicates. **(b)** Growth curves of the *E. coli* PH02 strains cotransformed with pLW11 and pSkunk-empty (circle), pSkunk-HPr (triangle), or pSkunk-HPr^{H15A} (square) were measured in the absence or presence of 40 µM AI-2, as indicated. Aliquots were collected for the measurement of OD at 600 nm at different time points during cell growth. The growth rates of the *E. coli* strains in the absence of AI-2 were only slightly higher than those in the presence of 40 µM AI-2.

3.2.2 HPr influences AI-2 uptake in media with glucose

The apparent HPr mediated inhibition of LsrK was also studied by measuring extracellular AI-2 levels of the PH01 strain, which is a *ptsH* knockout strain that still carries *luxS* (synthesize AI-2). **Figure 3.3** shows the extracellular AI-2 activity of PH01 pLW11 pSkunk and PH01 pLW11 pSkunk-HPr. The cells were grown in LB medium with or without 0.8% added glucose. Uptake of glucose normally decreases *lsr*-mediated expression, significantly reducing AI-2 uptake and resulting in prolonged accumulation of extracellular AI-2. This was seen in the strain with *ptsH*. This is likely partially due to downregulation of cAMP in the presence of glucose, which is required for activation of the *lsr* promoter[32]. However, in the cell line with the empty plasmid, AI-2 uptake is not inhibited even in the presence of glucose, indicating activation of the *lsr* operon was occurring. Given the dependence of *lsr* on cAMP-CRP, one could infer that deleting HPr results in upregulation of cAMP, but a previous study indicates that *ptsH* knockout strains actually have lower levels of cAMP than wild-type strains[111]. Thus, we suggest that these findings further support the hypothesis that HPr inhibits LsrK activity and that LsrK activity is higher in the absence of HPr.

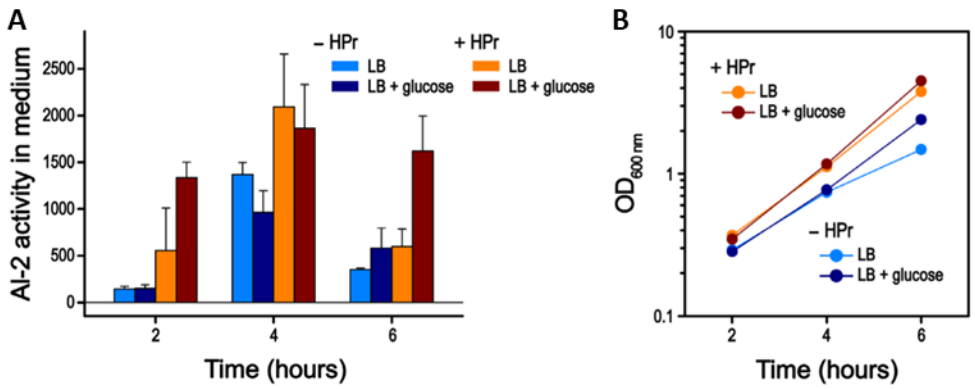

Figure 3.3. AI-2 uptake in *ptsH* mutant strains

(a) *E. coli* PH01 (Δ*ptsH*) strains cotransformed with pLW11 and either pSkunk-empty or pSkunk-HPr were inoculated into LB medium with or without 0.8% glucose at $t = 0$. Samples were taken every 2 hours for the measurement of the extracellular AI-2 activity. Cultures with pSkunk-empty or pSkunk-HPr are indicated as "− HPr" or "+ HPr," respectively. Data are the average of technical duplicates. **(b)** Growth curves of the *E. coli* PH01 strains cotransformed with pLW11 and either pSkunk-empty or pSkunk-HPr in the presence or absence of 0.8% glucose.

3.3 Discussion

Here, we present data that support the hypothesis that HPr lowers LsrK activity. The data shown here compared *lsr* promoter activity and AI-2 uptake in *E. coli* that either express or not HPr. *lsr* promoter activity was increased at earlier stages of growth in HPr knockout strains. Further, HPr knockout strains showed AI-2 uptake in media with glucose, which does not occur in wild type strains. These results supported the *in vitro* data showing that HPr binds Lsrk, inhibits LsrK activity, and that phosphorylated HPr inhibits LsrK to a lesser extent. HPr is part of a major

metabolic process in the cell, the PTS, and the phosphorylation state of PTS proteins are known to regulate many metabolic processes in the cell. The data presented here, along with the *in vitro* data, demonstrate a previously unknown link between metabolism and AI-2 quorum sensing.

3.4 Materials and Methods

Strains and plasmids

Strains, plasmids, and primers are listed in Supplementary Tables 1 and 2. In order to create *E. coli* strains PH01 and PH02, *ptsH* was knocked out from the ZK126 and LW7[32] genomes, respectively, using the one-step replacement method described by Datsenko and Wanner[112]. PCR was performed with ptsHdel-F and ptsHdel-R primers using pKD3 as a template. Deletion of *ptsH* gene was confirmed by PCR using the ptsHout-F and ptsHout-R primers using genomic DNA from recombinant colonies as template. For plasmids used in the study, the wild-type HPr and HPr^{H15A} were cloned into the pSkunk plasmid[113] using the ptsH-BamHI and ptsH-SpeI primers (Table S2).

lsr promoter activity in *ptsH* mutant strains

E. coli PH02 harboring the plasmid pLW11[32], and either empty pSkunk, pSkunk-HPr or pSkunk-HPr^{H15A} were grown overnight in LB media, and then diluted 100-fold (OD_{600} = 0.05) into fresh LB media supplemented with 50 μg/ml ampicillin and 50 μg/ml spectinomycin. Cultures were incubated at 37°C with shaking at 250 rpm in flasks. When the OD_{600} reached approximately 0.2, the cultures were split into multiple 2 ml culture tubes and 40 μM of synthetic AI-2 was added. Cultures grew in

the absence or presence of AI-2, and were samples at OD_{600} = 0.8, 4 for measurement of β-galactosidase activity. β-galactosidase activity was measured using the Miller assay[114]. Specific activity of β-galactosidase is expressed in Miller Units.

Measurement of AI-2 uptake

To perform the AI-2 uptake experiments, PH01 harboring plasmids pLW11 and either empty pSkunk or pSkunk-HPr were grown overnight in LB media, and then diluted 100-fold into fresh LB media or LB media with 0.8% glucose. Cultures were supplemented with 50 μg/ml ampicillin and 25 μg/ml spectinomycin. Every two hours samples were taken and filtered through a 0.2 μm filter. A bioluminescent reporter strain, *Vibrio harveyi* BB170[115], was used to measure AI-2 activity of the conditioned media samples. BB170 was grown at 30°C for 16 hours in AB media and then diluted 5,000-fold into fresh AB media supplemented with 10 μg/ml kanamycin. 20 μl of the experimental samples were added to 180 μl of the diluted BB170 cells. Luminescence of cultures were recorded and presented as a fold change relative to a negative control, where fresh media was added in place of an experimental sample.

Chapter 4: Engineering *Escherichia coli* for enhanced sensitivity to the autoinducer-2 quorum sensing signal

This chapter was reproduced, with permission, from the publication: Stephens, K.*, Zargar, A.*, Emaminan, M., Abutableb, N., Choi, E., Quan, D.N., Payne, G., Bentley, W.E. "Engineering Escherichia coli for enhanced sensitivity to the autoinducer-2 quorum sensing signal," *Biotechnol Prog*, **2019**, 35, e2881. *Authors contributed equally

4.1 Introduction

The "universal" quorum sensing signal autoinducer-2 (AI-2) is produced and recognized by many species of bacteria and influences important cell processes including biofilm formation, persistence, and virulence.[25, 100, 116, 117] AI-2 is likely also important in the GI tract, as the AI-2 signal can influence mammalian cell gene expression,[118] and manipulation of AI-2 signaling influences the microbiome composition of the mouse GI tract after antibiotic treatment.[45] As the fields of synthetic biology and metabolic engineering have advanced, an emerging area of focus is on engineering cell-cell communication, both amongst a single population (intra-) of bacteria or between communities (inter-).[72, 119] Developing strains of *E. coli* able to sense and respond to a range of AI-2 concentrations could be useful both for interrogating and manipulating native populations of bacteria and as tools for regulating communication in engineered ecosystems.

Previously, we developed inducible AI-2 controller cells with enhanced ability to uptake and respond to AI-2 by manipulating the AI-2 quorum sensing network through overexpression of proteins responsible for uptake and phosphorylation of AI-2, specifically LsrACDB and LsrK.[28, 35, 39] We have also engineered cells that autonomously activate protein expression based on accumulation of AI-2[36] and demonstrated that deleting genes responsible for degrading and altering AI-2, *lsrF* and *lsrG*, results in activation of protein expression at lower AI-2 levels.[27, 70] In this paper, we demonstrate that combining these two strategies, use of an enhanced feedback loop through overexpression of LsrK and LsrACDB and deletion of *lsrF* and *lsrG* from the genome, can be used to engineer *E. coli* cells with enhanced sensitivity and ability to uptake and report on the presence of biologically relevant extracellular AI-2 concentrations. We envision these cells could be further engineered to genetically actuate "programmed" responses based on AI-2 level, enabling their activation at lower levels or with less delay than possible based on current AI-2 sensing capabilities.

4.2 Results

4.2.1 Design of enhanced AI-2 reporter cell

The native *E. coli* response to AI-2 and the enhanced AI-2 reporter cell design are illustrated in **Scheme 4.1**. In the native system, AI-2 is imported by the transporter, LsrACDB, and phosphorylated by the kinase, LsrK. Phosphorylated AI-2 relieves repression of the *lsr* operon resulting in additional transcription of the AI-2

uptake and processing genes. In our previously designed system, phosphorylated AI-2 also activates transcription of the florescent reporter sfGFP encoded on amplifier plasmid pET-sfGFP using a two plasmid system wherein the first transducer plasmid (pCT6) uses the *lsr* promoter to express T7 polymerase, which then directs sfGFP expression from the second – the net result being significant amplification of the native *lsr*-mediated signal.[36] In a *luxS* knockout (cells lacking the ability to produce AI-2) host strain such as MDAI2, this systems allows for uptake and reporting of AI-2 in the extracellular environment.[27] For the design of the "enhanced" cells, we build on this system by manipulating the response and sensitivity to AI-2 by also overexpressing LsrK or LsrACDB in addition to sfGFP in response to AI-2 (using plasmids pET-sfGFP-LsrK or pET-sfGFP-LsrACDB), and by using a host strain CT104 that lacks the AI-2 degrading proteins, LsrF and LsrG.

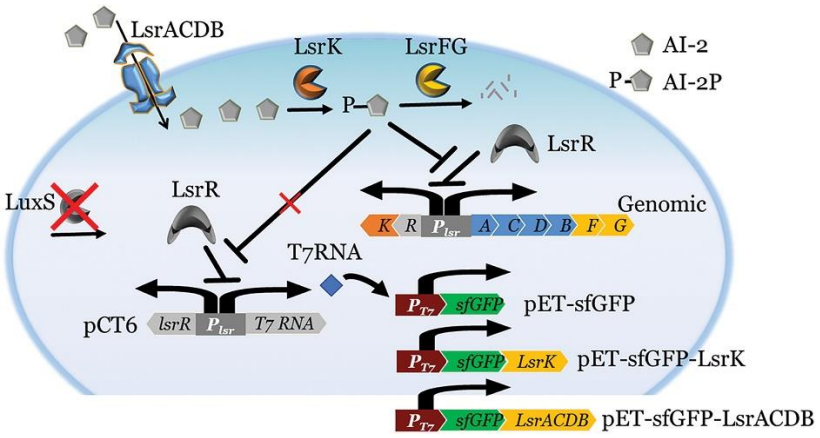

Scheme 4.1 Enhanced *E. coli* Al-2 sensor.

Al-2 is imported by LsrACDB and phosphorylated by the kinase LsrK. Al-2P activates expression of the native *lsr* operon causing production of additional LsrACDB and LsrK. Al-2P also activates transcription of T7 RNA polymerase on plasmid pCT6 followed by transcription of the reporter gene on plasmid pET-sfGFP. On plasmids pET-sfGFP-LsrK and pET-sfGFP-LsrACDB, Al-2P activates additional production of LsrK or LsrACDB resulting in an enhanced feedback loop and further uptake and processing of Al-2. The Al-2 degrading units LsrF and LsrG are deleted from the genome. AI-2, autoinducer-2; AI-2P, phosphorylated AI-2

4.2.2 Enhanced feedback loop in MDAI2 results in accelerated AI-2 uptake and increased AI-2 driven transcription

We first tested the enhanced feedback loop in host stain MDAI2. Plasmids pET-LsrK or pET-LsrACDB were tested and compared to the control plasmid pET in MDAI2 pCT6 (**Figure 4.1**). AI-2 concentrations of 40 µM and 4 µM were exogenously added and extracellular AI-2 levels and pET transgene transcription

levels were observed over six hours. Use of plasmids pET-LsrK and pET-LsrACDB resulted in accelerated AI-2 uptake over the control plasmid (**Figure 4.1A**). When 40 µM AI-2 was added, it was rapidly cleared within 3 hours using either enhanced feedback plasmid. Using the control plasmid, AI-2 was more slowly removed over the course of 6 hours. When a lower concentration of 4 µM AI-2 was added, the control population was unable to clear the AI-2 within the time tested, while the cells with the enhanced feedback plasmids still cleared the AI-2 within 3 hours, illustrating that these cells have an increased sensitivity to AI-2. qPCR results also indicated that the enhanced plasmids result in greater expression of the pET transgene at both AI-2 concentrations (**Figure 4.1B)**. This effect is seen within 3 hours of addition of AI-2, in agreement with the AI-2 uptake data. Growth rates were similar in all strains (**Figure S1**).

We note here that the use of either of the enhanced feedback loops (pET-LsrK or pET-LsrACDB) significantly increased AI-2 uptake over the control strain and that the LsrK+ strain appeared to have a slightly increased uptake rate compared to the LsrACDB+ strain. This suggests that LsrK is the bottleneck in the AI-2 uptake process in this experimental setup. That is, phosphorylation and sequestration of AI-2 within the cell is the limiting step in comparison to AI-2 uptake from the extracellular environment by the LsrACDB transporter. There is likely an ideal balance between LsrK and LsrACDB levels that maximizes AI-2 uptake and this balance may change over time or at different stages of growth. For instance, we have previously seen that overexpression of LsrACDB results in increased AI-2 uptake compared to overexpression of LsrK when expressed via an IPTG inducible promoter (as opposed

to induction from the *lsr* promoter as illustrated here).[39] It may be that early expression of LsrACDB has a disproportionately significant effect, reflecting the fact that LsrK acts downstream of LsrACDB in the AI-2 signal transduction pathway. For instance, in the IPTG inducible system, LsrACDB can be expressed prior to the cell taking up any AI-2 in order to jump start the process. In the autonomous induction system used here, the cell would have already taken up some AI-2 in order to activate the *lsr* promoter and subsequent overexpression of either LsrACDB or LsrK. Overexpression of LsrACDB may be less important (relative to overexpression of LsrK) at that point. Also, the activity of LsrK can be inhibited based on the phosphorylation state of the phosphotransferase protein HPr,[33] which is involved in sugar transport. The state of HPr likely changes over the course of the growth curve and may necessitate the need for more or less LsrK for optimal AI-2 uptake.

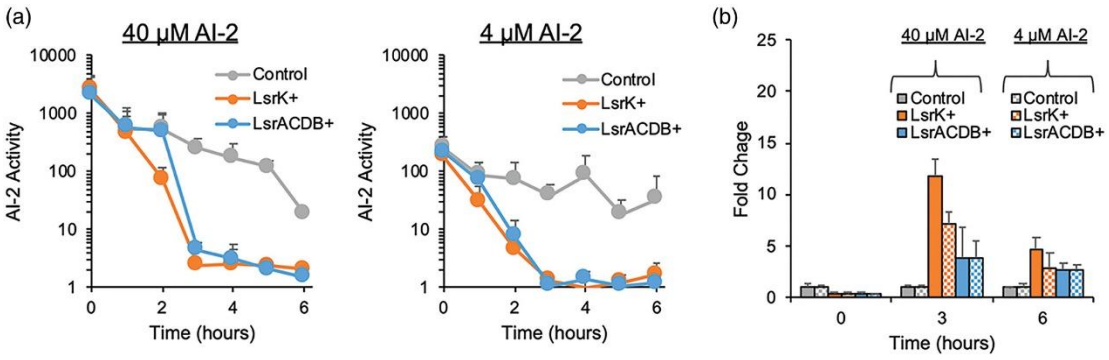

Figure 4.1. Al-2 uptake profiles and transgene expression for MDAl2 pCT6 transformed with either pET (control), pET-LsrK (LsrK+), or pET-LsrACDB (LsrACDB+).

Each culture was grown to approximately OD600 0.4 at which time cultures were supplemented with 4 or 40 μM Al-2 (t = 0 hr). **(a)** Al-2 activity in the extracellular media for cultures, with 4 μM(left panel) or 0.4 μM(right panel) added Al-2 is shown over time. **(b)** qPCR was used to measure pET transgene mRNA levels for each culture at 0, 3, and 6 hr from Al-2 addition. Fold change is shown relative to "Control" levels. Error bars represent SD of biological triplicates.

4.2.3 Enhanced feedback loop in CT104 further increases sensitivity to AI-2

We next tested the enhanced feedback loop in host strain CT104. CT104 has previously been shown to be more sensitive to AI-2 than MDAI2.[27, 70] Here, we tested whether use of the enhanced feedback loop could further increase AI-2 sensitivity in these cells. We tested AI-2 concentrations of 4 μM and 0.4 μM and observed results over three hours. When 4 μM AI-2 was added, AI-2 was rapidly cleared within two hours using either enhanced feedback plasmid (**Figure 4.2A**). We note that this is a shorter time for AI-2 clearance than observed in the MDAI2 cells with the enhanced

plasmids at the same AI-2 concentration (**Figure 4.1A**). Experiments with both cell lines were started at cell densities of approximately 0.4 (MDAI2 and CT104 starting densities ranged from 0.40 to 0.60 and 0.36 to 0.46, respectively) and growth curves were similar between the two strains (**Figure S1**). Therefore, the increased rate of AI-2 clearance in the CT104 strain is not an artifact of using more cells in the culture. Using the control plasmid in CT104, AI-2 was removed over the course of three hours (**Figure 4.2A**). When adding 0.4 μM AI-2, AI-2 uptake was difficult to observe for both the control and enhanced cell lines, likely due to the sensitivity of the assay. The qPCR results largely agree with the AI-2 uptake data (**Figure 4.2B**). The enhanced plasmids result in an increase in transgene levels over the control plasmid when 4 μM AI-2 was added. This effect was especially significant when using the enhanced LsrK plasmid, and could be observed 1.5 hours after addition of AI-2. Growth rates were similar in all CT104 strains (**Figure S1**).

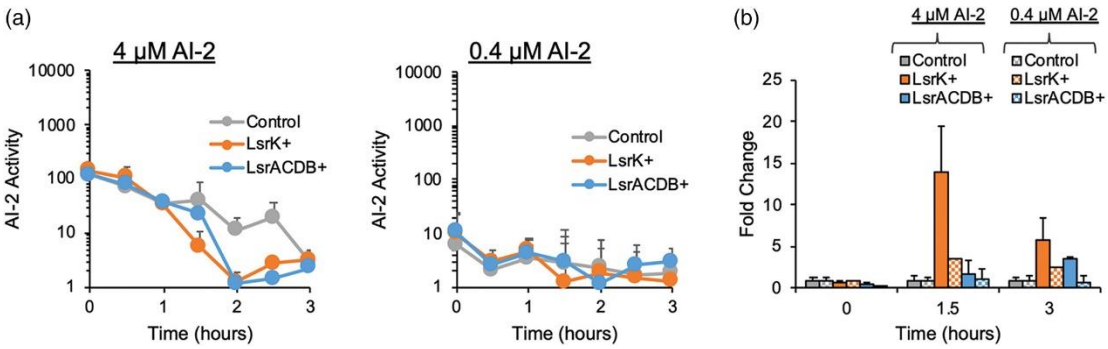

Figure 4.2. Al-2 uptake profiles and transgene expression for CT104 pCT6 transformed with either pET (control), pET-LsrK (LsrK+), or pET-LsrACDB (LsrACDB+).

Each culture was grown to approximately OD600 0.4 at which time cultures were supplemented with 4 or 0.4 μMAl-2 (t = 0 hr). (a) Al-2 activity in the extracellular media for cultures with 4 μM (left panel) or 0.4 μM (right panel) added Al-2 is shown over time. **(b)** qPCR was used to measure pET transgene mRNA levels for each culture at 0, 1.5, and 3 hr from Al-2 addition. Fold change is shown relative to "Control" levels. Error bars represent SD of biological triplicates.

4.2.4 Enhanced feedback loops in MDAI2 and CT104 result in greater expression of reporter genes

We then tested whether the enhanced feedback loops could improve expression of a fluorescent reporter protein in response to AI-2. sfGFP expression was tested in both MDAI2 and CT104 containing plasmid pCT6 and either pET-sfGFP, pET-sfGFP-LsrK, or pET-sfGFP-LsrACDB for AI-2 concentrations ranging from 0 – 40 μM (**Figure 4.3**). As expected, both the number of fluorescing cells and the intensity of fluorescence were generally higher in CT104 than MDAI2.[27, 70] The

lack of AI-2 degrading proteins likely allows prolonged activation of the *lsr* promoter resulting in measurable levels of sfGFP even in cells with low intracellular AI-2 levels. MDAI2 cells with the enhanced feedback loops showed a trend towards higher fractions of fluorescing cells over the controls across all tested AI-2 concentrations, although an increase in fluorescence intensity (per cell) was not observed (**Figure 3.3A**). The control cells showed a noticeable increase in fluorescent population only when adding 40 μM AI-2, the highest concentration tested. Even at this high AI-2 concentration, the fluorescent population reached a maximum of less than 20%. In contrast, in the cells with enhanced expression of LsrK or LsrACDB, 40 μM AI-2 addition resulted in a fluorescent population of over 40%. We note that distributed responses to AI-2 and other signaling or inducer molecules is common[27, 28, 120] and can be controlled.[28, 121]

For example, here, using the enhanced plasmids in the host strain CT104 resulted in an increase in fluorescence over use of the control plasmids at AI-2 concentrations of 4 μM or higher (**Figure 4.3B**). At the 4 μM AI-2 concentration, the fluorescent population was about twice as high in the cells with the enhanced feedback loops. An increase in the fluorescent population was not seen at the 40 μM AI-2 concentration, but the percentages were already high (~ 90%) across all cells including the control strain. We note, however, that the intensity of fluorescence was significantly higher in these cells with the enhanced feedback plasmids.

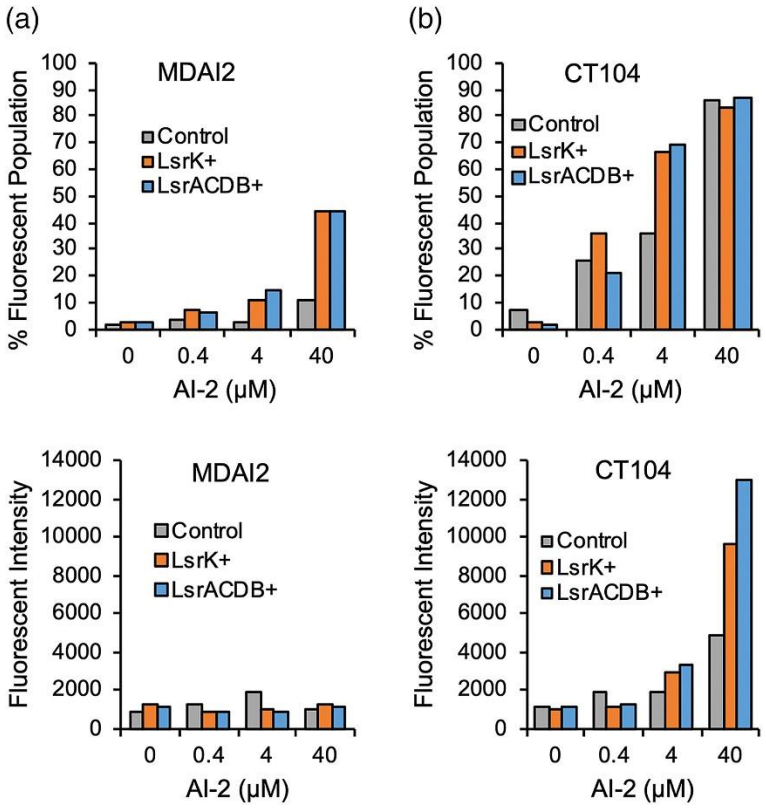

Figure 4.3. sfGFP expression in MDAI2 and CT104.

Fluorescent population percentage and average fluorescence intensity for MDAl2 (a) and CT104 (b) containing pCT6 and either pET-sfGFP (control), pET-sfGFP-LsrK (LsrK+), or pET-sfGFP-LsrACDB (LsrACDB+). Each culture was grown to approximately OD600 0.4 and supplemented with Al-2 ranging from 0 to 40 μM. Samples were taken 4 hr after Al-2 addition for flow cytometry analysis.

4.3 Discussion

In conclusion, we developed an *E. coli* strain that consumes AI-2 more rapidly and responds with higher protein output to physiological ranges of AI-2 by combining two previous strategies. We overexpressed the AI-2 uptake and phosphorylation units,

LsrK or LsrACDB (using the enhanced feedback loop plasmids), to increase uptake of AI-2, and we deleted the AI-2 degrading units LsrF and LsrG (through use of host strain CT104), to increase sensitivity to AI-2. We show that these cells uptake AI-2 at an accelerated rate and respond with increased protein expression when biologically relevant concentrations of 4 μM AI-2 or higher are added. We envision these cells will allow for more precise interrogation of and response to AI-2 in natural environments, such as the GI tract.

4.4 Materials and Methods

Bacterial strains and growth conditions

The bacterial strains and plasmids used in this study are listed in **Table S1**. Unless otherwise noted, all cultures were inoculated from single colonies grown on LB-agar plates into LB media with 50 μg/mL ampicillin and 50 μg/mL kanamycin at 37ºC with 250 rpm shaking and grown to approximately OD 0.4, at which time AI-2 was added (ranging from 0 – 40 μM AI-2). Chemically synthesized AI-2 was kindly provided by Dr. Herman Sintim (Purdue University).[122]

qPCR analysis

RNA was extracted with the RNAqueous kit (Invitrogen). qPCR was performed using SensiFAST SYBR Hi-ROX One-Step Kit (Bioline, Taunton, MA). Analysis was performed using an Applied Biosystems HT7900. The transgene immediately following the T7 promoter on the pET plasmid and various plasmid derivatives as well as 16sRNA (e.g. reference gene) were quantified. Results are shown as a fold change relative to the control samples (either MDAI2 pCT6 pET or

CT104 pCT6 pET) for each AI-2 concentration. Each sample was performed in triplicate. Averages are reported.

AI-2 analysis

To measure AI-2 activity, *V. harveyi* BB170 cells were used in a reporter assay.[115] Briefly, conditioned media (CM) samples were collected from experimental cultures by filtration through a 0.2 µm filter and frozen until they were made ready for analysis. BB170 cultures were inoculated into AB medium with 10 µg/mL kanamycin and grown overnight for 16 hours at 30ºC with 250 rpm shaking. The overnight BB170 cultures were diluted 5,000 times into fresh AB medium with 10 µg/mL kanamycin. To measure AI-2 activity, CM samples were added to dilute BB170 cultures in a 1:9 ratio and grown at 30ºC and 250 rpm shaking. For a negative control, fresh LB media was added in place of the CM. Luminescence was recorded using a luminometer (EG&G Berthold LB 9509 Jr) and values were normalized to the negative control. Each sample was tested in triplicate.

sfGFP protein expression

Flow cytometry was used to analyze sfGFP expression. A BD FACSCanto II flow cytometer with a 488 nm laser and 530/30 green filter was used to measure both the percent of fluorescing cells and the average intensity of the fluorescence of each cell.

Chapter 5: Bacterial co-culture with cell signaling translator and growth controller module for autonomously regulated culture composition

This chapter was reproduced, with permission, from the publication: Stephens, K., Pozo, M., Tsao, C.Y., Hauk, P., Bentley, W.E. “Bacterial co-culture with cell signaling translator and growth controller modules for autonomously regulated culture composition,” *Nat Commun*, **2019**, 10, 4129

5.1 Introduction

Advances in synthetic biology and metabolic engineering have expanded the potential for engineered cell-based systems[7, 102, 123]. Engineered microbes enable environmentally friendly manufacture of valuable molecular products[2]. Also, smart bacteria have appeared that sense their environments and execute desired functions such as the synthesis and delivery of therapeutics[95, 102, 103, 124, 125]. It is well recognized, however, that engineering cells to carry out multiple functions or produce products through extensive interconnected pathways leads to new challenges. These include bottlenecks, inefficient use of cell resources, and increased metabolic burden on individual cells. An emerging area of focus has been on the use of cell co-cultures or small consortia wherein individual populations work together to accomplish a desired output in cooperation with the rest of the consortia[72, 73, 119, 126-129]. There are many potential advantages to using multi-cell systems over traditional clonal populations including the potential for division of labor and reduced metabolic

burden on individual strains, ability for specialization and ease of optimization, and options for plug and play[72, 119, 126]. While promising, the use of co-cultures requires not only regulation of gene transcription within each population, but also regulation of each cell population within the consortia.

Relatively few studies have been devoted to developing devices or systems that regulate the compositions of subpopulations within consortia. Often, studies that use multi-cell populations to carry out a coordinated task, such as producing biofuels or chemicals, rely on specific inoculation ratios or similar manual strategies to optimize the ratio of each population[130-132]. Alternatively, microfluidic and other devices can modulate the relative contributions of subpopulations by providing means to sequester or retain one population relative to another (e.g., using immobilization strategies) or by fluidically, but not physically, connecting populations (e.g., via porous membranes or 3D-printed microenvironments[94]). A potentially more powerful approach that does not rely on equipment is to reengineer native cell-cell signaling systems in such a way as to enable the *autonomous* coordination of subpopulation densities. We and others have previously exploited quorum sensing (QS), a bacterial form of cell-cell communication, to engineer communication circuits amongst and between bacterial strains to coordinate behaviors[70, 75, 82, 133, 134] or enable density dependent activation of desired behavior[19, 36]. QS circuits and signals have also been used to alter cell densities by, for instance, activating production of toxins or lysis genes in order to program stationary phase cell density of a monoculture[8] and to create co-cultures with defined behavior[86, 88]. Similar strategies have been used to design co-cultures with a range of social interactions[89].

Here, we develop a platform for autonomous and targeted regulation of consortia composition based on the prevailing level of an environmental cue, autoinducer-2 (AI-2) (**Figure 5.1a**). The universal QS signal, AI-2, which is recognized and produced by many species of bacteria[31, 135], broadly indicates cell population density and is also likely to be an important signal in natural consortia or microbiomes[45]. Therefore, our synthetic system can be modulated based on an important signal often present in bacterial environments, AI-2, that is not easily measured on-line by users, either in fermentation reactions or in natural consortia. We achieve this by rewiring bacterial QS systems so that the growth rate of communicating consortia members is controlled by interspecies signaling. Thus, we present development of a signaling and control system that imparts trans-species communication and growth rate control. Our synthetic co-culture consists of an *E. coli* translator strain that senses AI-2 and translates this into an orthogonal QS signal (AI-1). This translator strain's output, in turn, mediates the growth rate of the second strain. That is, a second engineered *E. coli* controller strain has signal-mediated tunable growth rate, regulated by the level of the second, species-specific autoinducer signal, AI-1. Thus, the translator population produces AI-1 after sensing AI-2, in turn regulating the growth rate of the AI-1 responsive controller strain and subsequently the composition of the synthetic consortia based on the prevailing AI-2 level (**Figure 5.1b)**.

There are two important and innovative aspects to our design. First, QS-mediated communication between subpopulations enables composition adjustment to occur autonomously. Importantly, the system is based on the prevailing concentration of a

common naturally occurring autoinducer (AI-2) and the controller signal is based on an orthogonal species-specific autoinducer (AI-1) that has no function beyond its native host (*Pseudomonas aeruginosa*), a strain either included or not, based on system design. The second aspect of our design is signal-mediated tunable growth rate of bacteria via positive feedback. This is made possible by regulation of HPr, a phosphotransferase system (PTS) protein[109], important for sugar (including glucose) transport in bacteria. We recently discovered that transgene expression of HPr in isogenic null mutants enables accelerated growth[33]. By controlling HPr expression via QS signaling, we enable autonomous subpopulation control. Importantly, our strategy positively modulates cell growth rate, preserving enhanced metabolic function, rather than increasing cell death (e.g., through expression of toxins or lysis genes), a strategy previously used by others[8, 86, 88]. Regulating expression of a critical gene for methionine synthesis has also been used to regulate cell growth, although this strategy requires use of dropout media[136].

In this paper, we develop and characterize each construct of the synthetic co-culture and then demonstrate autonomous regulation of co-culture composition based on initial AI-2 levels in batch and extended batch conditions. We create a simple mathematical model of the autonomous consortia regulator and show that the model can be used to either target a specific population composition or predict co-culture behavior given specific inputs. The model can then be used to explore parameter ranges and synthetic biology designs for future applications.

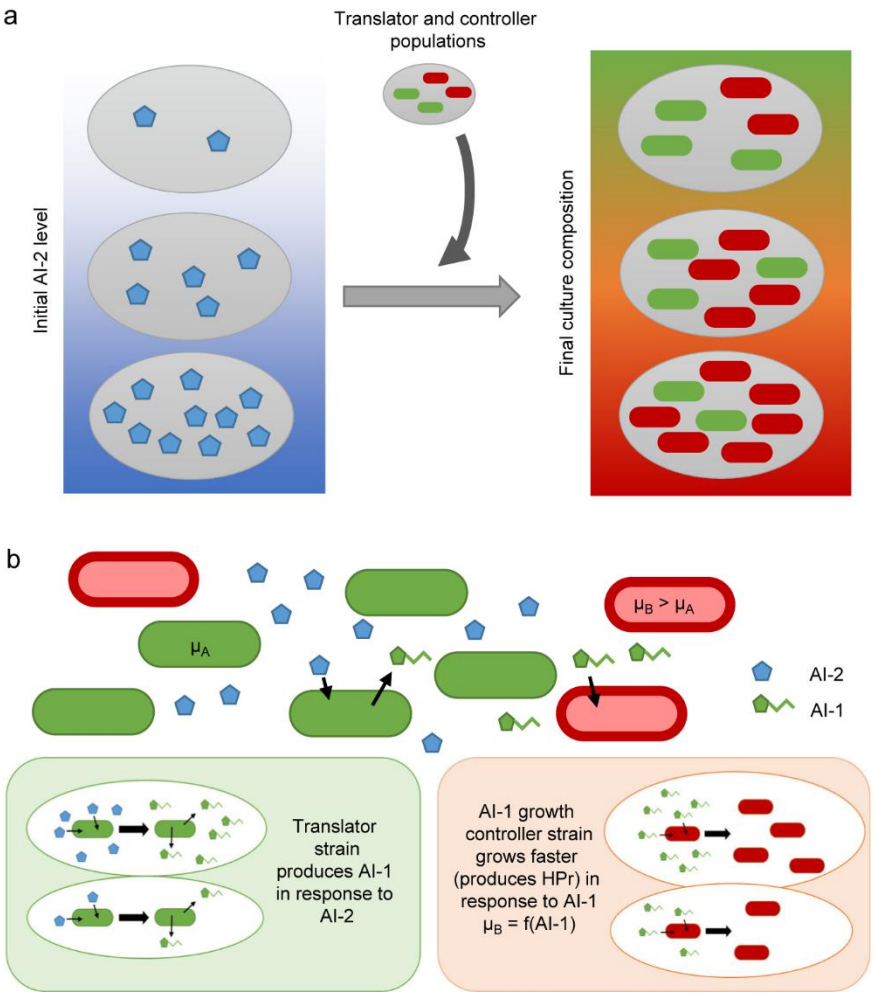

Figure 5.1. Design of autonomously regulated co-culture.

(a) Engineered co-culture with AI-2 regulated composition. When the translator and controller populations are added to environments with AI-2, the resulting culture composition varies based on the AI-2 level. **(b)** Depiction of each strain in engineered co-culture. The translator strain senses AI-2 level and produces AI-1. The AI-1 growth controller strain produces HPr in response to AI-1, which alters cell growth rate and changes the culture composition.

5.2 Results

5.2.1 AI-1 signal controlled cell growth rate

We first tested *E. coli* cell growth rate control through transcriptional regulation of *ptsH*, a gene involved in sugar transport. HPr (encoded by *ptsH*) is widely recognized as one of a series of proteins (e.g., E1, HPr, EII) that sequentially transfers a phosphoryl group from phosphoenolpyruvate (PEP) to glucose (or other PTS carbohydrate)[109]. HPr is highly conserved[137]. We recently discovered that HPr interacts with the AI-2 kinase LsrK, influencing AI-2 uptake. We leveraged the AI-2 modulating functionality later when constructing the AI-2 sensing cell. Here, we demonstrated that *ptsH* mutant strains grow more slowly than wild type strains in minimal media containing glucose (**Supplementary Figure 1a**). When *ptsH* was placed under an IPTG inducible promoter in a *ptsH* mutant, growth rate could be controlled based on IPTG addition (**Supplementary Figure 1b**). Importantly, we demonstrated that inducing expression of *ptsH* results in an increase in cell growth rate. Equally importantly, this behavior is irrespective of whether or not the media contains glucose as the principal carbon source (**Supplementary Figure 1c**).

Based on this proof of concept, we next engineered QS signal controlled growth rate. To construct the controller strain, *ptsH* was placed under control of the AI-1 *lasI* QS promoter on the plasmid pAHL-HPr (**Figure 5.2a**) in a *ptsH* mutant strain PH04. Elsewhere on the plasmid both dsRedExpress2, for cell visualization, and LasR, required for *lasI* promoter activation, were expressed under a constitutive T5 promoter. Addition of AI-1 to the controller strain increased cell growth rate up to 1.8 times the baseline growth rate in a dose dependent manner (**Figure 5.2b**). The

measured specific growth rate (between 1 and 4 hours after AI-1 addition) served as the basis for a Monod-type model of growth rate based on the AI-1 level (**Fig. 5.2c**).

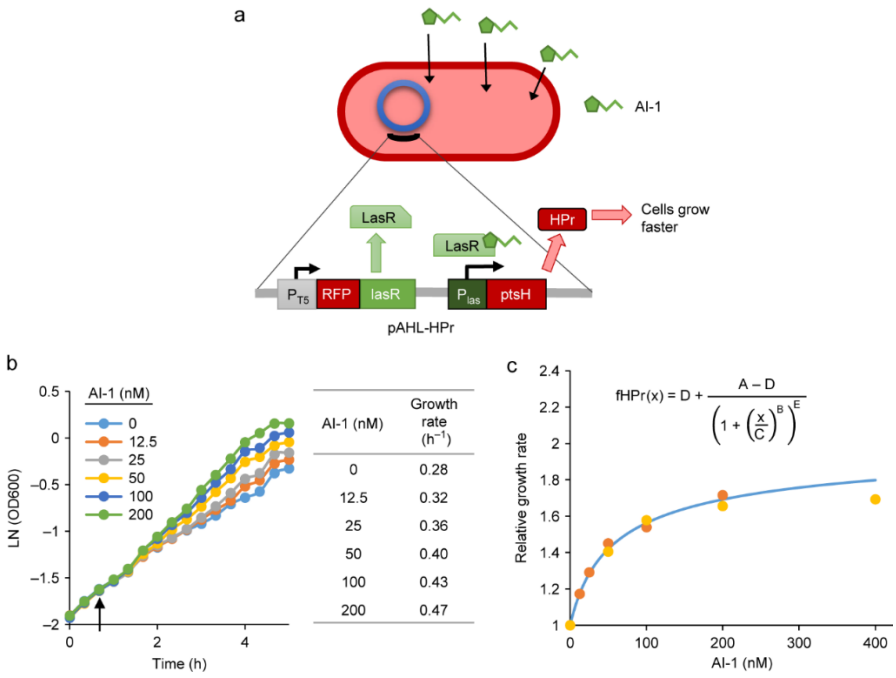

Figure 5.2. AI-1 quorum sensing signal controlled growth rate through expression of HPr.

(**a**) Schematic of AI-1 growth responsive controller cells (PH04 pAHL-HPr). AI-1 binds LasR (constitutively expressed) and activates the *las* promoter resulting in expression of HPr which increases cell growth rate. (**b**) Growth curves of PH04 pAHL-HPr cultures grown with varying levels of AI-1. Cultures were grown to OD 0.15 (t = 0) and AI-1 was supplemented at 40 min (indicated by arrow). Table shows the average growth rate from 1 to 4 hours after AI-1 addition. (**c**) Growth rate relative to basal growth rate (either 0.28 hr^{-1} or 0.32 hr^{-1}) for different AI-1 concentrations is plotted for two separate experiments (yellow and orange dots). Function *fHPr* describing relative growth rate as a function of AI-1 is plotted (blue line). A = 1, B = 1, C = 29, D = 2.1, E = 0.48.

5.2.2 AI-1 modulates composition in controller cell co-cultures

The AI-1 regulated controller cells were then co-cultured with other strains to verify that addition of AI-1 altered the composition of the co-culture. Growth controller cells expressing a red fluorescent protein (PH04 pAHL-ptsH) were co-cultured with either PH04 pCT6 or TOP10 pT5G[125]. PH04 pCT6 has a similar baseline growth rate to PH04 pAHL-ptsH, while TOP10 pT5G grows significantly faster. Cultures were inoculated at approximately equal cell densities and supplemented with varied AI-1 levels. After 8 hr, samples were taken for analysis using fluorescence microscopy and quantified using ImageJ. As expected, when controller cells were cultured with PH04, culture composition of the controller cells increased with increasing AI-1 concentration (**Figure 5.3a)**. A similar trend was seen when cells were cultured with TOP10, despite the faster growth rate of TOP10 (**Figure 5.3b**). That is, in co-cultures without AI-1, the fraction of the controller cells in the TOP10 co-cultures actually dropped significantly from the initial ~0.5 to ~0.09 during the ensuing 8 hours. Addition of AI-1 counteracted that growth rate difference and resulted in a higher level of controller cells during the same 8 hr period. These results demonstrate that irrespective of other strains in the culture and their respective growth rates, AI-1 (which is not an *E. coli* QS signaling molecule) modulates the growth rate of the engineered controller strain and the change occurred sufficiently rapidly so as to enable an observable change in culture composition - notably even under relatively short term batch conditions (as opposed to fed-batch, repeated batch or continuous cultures).

Next, the AI-1 regulated controller strain was co-cultured with cells that produce AI-1 when induced. PH04 pSox-LasI and PH04 pAHL-HPr were co-cultured together. Plasmid pSox-LasI contains *lasI*, which synthesizes AI-1, under the pyocyanin inducible *soxS* promoter[125]. In this experiment, the controller strain receives a signal from a translater strain that, in turn, produced AI-1 in response to pyocyanin. In this way, the co-culture control scheme is shown to respond to a particular molecular cue. Here, each culture was inoculated at approximately equal starting densities and co-cultures were either exposed or not, to pyocyanin. Exposed cultures showed increased production of AI-1 and corresponding increased composition of PH04 pAHL-HPr within five hours (**Figure 5.3c**). These results demonstrate that AI-1 produced from an alternate strain can modulate growth rate of the controller strain, and that this can occur on timescales required to affect change in a batch process. In addition, this demonstrates potential feasibility of a user regulated co-culture based on a user-specific application of a molecule or inducer, in this case pyocyanin. We next engineered the translator strain to create an autonomously regulated co-culture based on the pervasive AI-2 signaling molecule.

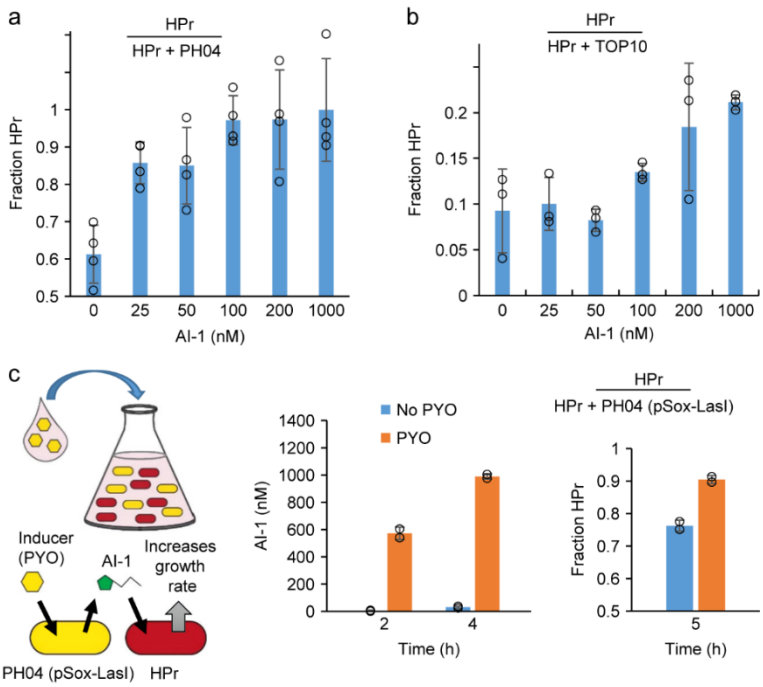

Figure 5.3. AI-1 regulates cell growth rate in co-cultures.

(**a**) PH04 pAHL-HPr (abbreviated as HPr) co-cultured with PH04 pCT6 (abbreviated PH04). Each culture was inoculated 0.5% for an initial HPr fraction of approximately 0.5. Indicated AI-1 level was added during inoculation. Samples were collected for analysis of co-culture composition after eight hours. Error bars represent s.d. of technical quadruplicates. (**b**) PH04 pAHL-HPr (abbreviated as HPr) co-cultured with TOP10 pT5G (abbreviated as TOP10). Each culture was inoculated 0.5% for an initial HPr fraction of approximately 0.5. Indicated AI-1 level was added during inoculation. Samples were collected for analysis of co-culture composition after eight hours. Error bars represent s.d. of technical triplicates. (**c**) PH04 pAHL-HPr (abbreviated as HPr) co-cultured with PH04 pSox-LasI with or without 1 µM PYO induction. Initial fraction HPr in co-culture was approximately 0.5. Samples collected for AI-1 measurement after 2 and 4 hours and co-culture composition analysis after 5 hours. Error bars represent s.d. of biological duplicates.

5.2.3 Design of AI-2 sensing translator cells

To construct cell lines that sense AI-2 and produce AI-1, we engineered strains to activate expression of LasI, which synthesizes AI-1, when the AI-2 *lsr* promoter is activated. We used a two plasmid system to amplify expression from the weak *lsr* promoter[36] (**Figure 5.4a**). Briefly, AI-2 is phosphorylated by LsrK and phosphorylated AI-2 relieves repression of the promoter by LsrR, increasing transcription of the *lsr* transporter genes and accelerating AI-2 uptake. At the same time, AI-2-mediated activation of the *l*sr promoter results in transcription of T7 RNA polymerase from plasmid pCT6 and subsequent transcription of *lasI* from plasmid pET-LasI.

The system was first constructed in the *E. coli* host strain CT104, which is a *luxS* mutant (e.g., incapable of producing AI-2). CT104 also lacks *lsrFG*, responsible for degrading the phosphorylated AI-2 signal, increasing sensitivity of the cell to AI-2[27]. We verified this cell line, CT104 pCT6 pET-LasI, produced AI-1 when cultured in conditioned media (CM) from AI-2 producing BL21 (**Supplementary Figure 2**). BL21 were grown to varying cell densities, CM was collected, and CT104 cells were grown in the collected CM. Importantly, AI-1 produced by the CT104 cells correlated with the density of the AI-2 producing BL21 cells (**Supplementary Figure 2a**). We also tested whether translator cells added to consortia with varying fractions of AI-2 producing cells could produce the AI-1 signal based on the consortia composition. CT104 cells were added to cultures of varying ratios of BL21 (*luxS*$^{+}$) to BL21 Δ*luxS*. After six hours, the level of the AI-1 signal in the extracellular media was indicative

of the culture composition, which, in turn, is based primarily on the initial fraction of *luxS*$^{+}$ cells[36] (**Supplementary Figure 2b**).

The above experiments demonstrated that a cell line could be constructed to produce AI-1 in response to AI-2 from AI-2 producing cells. These experiments were performed in LB media and not in media with glucose. The presence of glucose inhibits AI-2 uptake and *lsr* promoter activity[32] and the use of the CT104 cells could potentially be limited to media without glucose (see **Supplementary Figure 3** for scheme of AI-2 QS pathway). Based on knowledge of the AI-2 QS system, we attempted to engineer a strain that was capable of AI-2 uptake and *lsr* promoter activation in glucose containing media. In this way, our results could be more generally applied. Previously, we demonstrated that HPr (encoded by *ptsH*) interacts with LsrK, inhibiting LsrK kinase activity, and that *ptsH* mutants have been shown to uptake AI-2 even in media containing glucose[33]. Hence, we hypothesized, use of PH04 (Δ*ptsH* Δ*luxS*) as a host strain would allow for AI-2 based production of AI-1 in media containing glucose. We tested the translator cells using both host strains in LB and M9 glucose media with and without AI-2. The level of AI-1 produced was dependent on addition of AI-2, but also on the host strain and the media (**Figure 5.4b**). Both strains produced AI-1 when cells were added to LB media with AI-2. As expected, in M9 media, using the CT104 host strain resulted in a small or insignificant fold change in AI-1 activity when comparing cultures with and without AI-2. Importantly, the PH04 translator cells however showed AI-2 activated production of AI-1 in M9 + glucose media. In this way, the engineered system could be used in glucose-containing media.

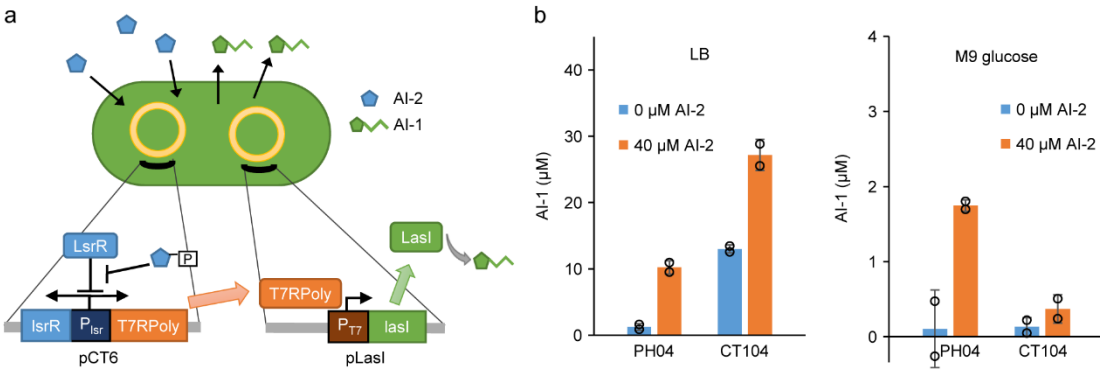

Figure 5.4. Engineered translator cells produce AI-1 in response to AI-2.

(**a**) Translator cells couple the AI-2 and AI-1 quorum sensing circuits using a dual plasmid system. Phosphorylated AI-2 activates expression of T7 RNA polymerase and subsequent expression of LasI which synthesizes AI-1. (**b**) AI-1 produced by CT104 pCT6 pLasI or PH04 pCT6 pLasI grown in different media with and without AI-2 addition. AI-2 was added as indicated at approximately OD 0.1 and samples for AI-1 measurement were taken six hours later. Error bars represent s.d. between technical duplicates.

5.2.4 Characterization of PH04 translator cells

PH04 translator cells uptake the AI-2 signal molecule, transduce the signal by activating expression of LasI and synthesize and secrete AI-1. The desired AI-1 output is then a function of the AI-2 input. We characterized AI-2 signaled production of AI-1 in the PH04 translator strain over time and for a range of biologically relevant AI-2 concentrations. The rate of AI-1 production by PH04 translator cells was found to be dose dependent on AI-2 (**Figure 5.5a**). We note that under these and similar

conditions, AI-2 is mostly consumed within four hours (**Figure 5.5b**). Addition of AI-2 or AI-2 based production of AI-1 in these batch cultures resulted in no observable decrease in cell growth (**Figure 5.5c**). We then characterized the rate of AI-1 production on a per cell basis over time for each tested AI-2 concentration by plotting a logistic function through the AI-1 data, determining the derivative of this equation over time, and dividing the derivative by the cell density over time (**Supplementary Table 1**) yielding a time-dependent specific production rate. The resulting plots (**Figure 5.5d**) show the estimated per cell rate of AI-1 production as a function of added AI-2 and time from AI-2 addition. As will be shown later, this aligns with an underlying observation we have observed that the trajectory of gene expression in response to an initial cue is fairly robust[27, 70, 138].

Next, the effect of AI-1 produced by the PH04 translator cells on the growth rate of the AI-1 responsive controller cells was tested. That is, growth responsive cells were added to CM containing AI-1 from translator cells that had been exposed to varying levels of AI-2 and cultivated for ~3 hrs (**Supplementary Figure 4a**). Beyond what was shown in **Figure 5.5** where AI-1 is generated from direct exposure to AI-2, this experiment demonstrates that the cell translation of AI-2 into AI-1 can be done with the necessary expression and cell culture dynamics so as to influence the growth rate of the second population (**Supplementary Figure 4b**). We note also, that the dynamic growth rate of the controller cells was shown to decrease in time over the ensuing 3 hr. This observation was made more dramatic in later co-culture experiments.

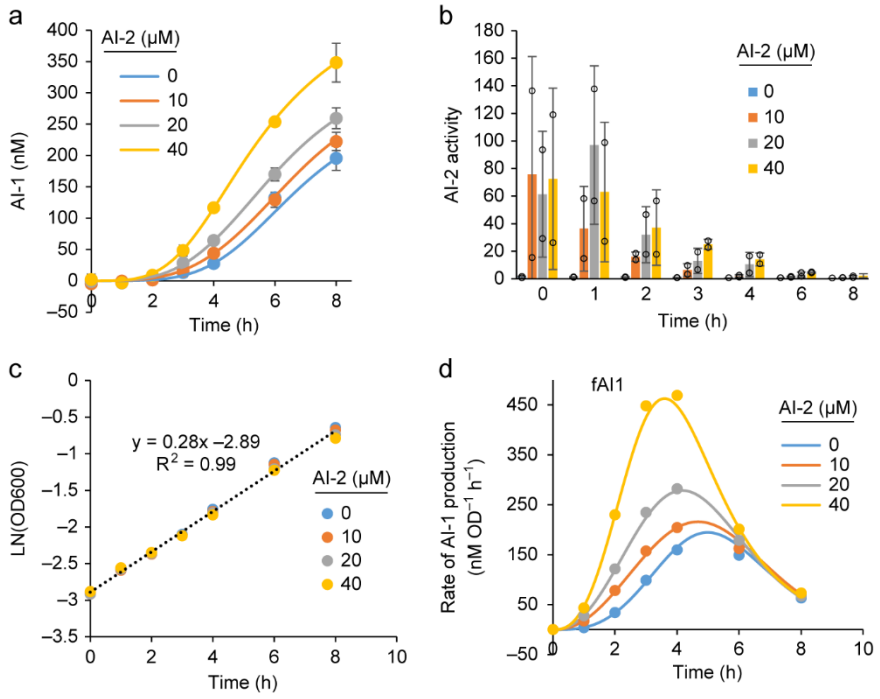

Figure 5.5. Characterization of AI-1 production in translator cells.

PH04 translator cells cultured in M9 glucose media with varying concentrations of AI-2. Cells were inoculated from overnight cultures and AI-2 was added as indicated at t = 0. (**a**) Extracellular AI-1 levels over time. Error bars represent s.d. of technical duplicates. (**b**) Extracellular AI-2 activity over time. Error bars represent s.d. of technical duplicates. (**c**) Cell density over time. (**d**) Functions for AI-1 production rate, *fAI1*, for different AI-2 concentrations (solid lines) and AI-1 production rates calculated with experimental data (dots).

5.2.5 Autonomous regulation of co-culture composition

We next added the translator cells (referred to as Population A) and the AI-1 responsive controller cells (Population B) to solutions having a range of initial AI-2 concentrations. In co-cultures of translator cells and controller cells, the translator

cells autonomously regulate consortia composition based on initial AI-2 level. In **Supplementary Figure 5**, the co-cultures with increased initial AI-2 levels resulted in an increase in AI-1 (**Supplementary Figure 5b**) and a corresponding increase in relative abundance of Population B (**Supplementary Figure 5a**). These results demonstrated the concept of signal-mediated autonomous control of consortia population. Importantly, estimates of growth rate for Population A and Population B agreed with expected growth rate values measured during monoculture experiments (**Supplementary Figure 5c**).

Then, having demonstrated that translator cells could regulate consortia composition based on exposure to AI-2, we developed a mathematical model to characterize the system dynamics. In this way, one may predict co-culture behavior given specific initial conditions, growth rate designs, etc., in order to determine parameters required to target a desired output. This conceptually simple mathematical model was created to predict co-culture behavior using data from the individual strains. The model consists of four ordinary differential equations, one for each population density, substrate concentration, and AI-1 concentration (**Supplementary Tables 2, 3**). Monod growth kinetics with a constant yield coefficient were used to model cell growth and substrate concentration, with additional functions accounting for the production and/or effects of the QS molecules. The AI-1 produced by Population A is based both on the level of AI-2 exposure and time (*fAI1*). In previous work[27] we found that time-dependent trajectories of cell behavior were a consequence of initial exposure to autoinducer so that time-dependent functions of AI-1 production would be plausible here. The growth rate of Population B was formulated based on

the prevailing level of AI-1 (*fHPr*). Maximum specific growth rates were measured using experimental data, yields were estimated based on experimentally observed stationary phase density and known initial substrate concentrations, and K_1 and K_2 values were chosen based on literature values for glucose. The MATLAB (Version R2016a) ode45 solver was used to solve the system of ODEs. The model can be used to show how a co-culture population is predicted to change with time given these simple phenomenological rate equations and best-fit constants. As noted, this provides the basis for determining whether a co-culture can even be predicted to evolve over the limited times available in a batch culture. Importantly, our results from monocultures are used to simulate experimental results from co-cultures.

That is, we next evaluated autonomously-programmed co-culture control via model predictions. Co-cultures of Populations A and B were placed together for a range of initial cell populations and were then added to media with prescribed levels of AI-2 in order to set in motion a population trajectory. In our system, the initial composition is selected based on the ratio of cells supplied in the co-culture and then the culture composition is autonomously adjusted over time based on the AI-2 level in the media. We compared results to our model. In **Figure 5.6**, the co-culture composition and AI-1 level after five hours is shown for a variety of conditions including varied initial A:B ratios and AI-2 level. In these tests, we used one initial population cell density. Importantly, we found that our model predicted well the experimental results of both the AI-1 level and co-culture composition. We note also that the model can be used to select initial conditions that give a desired output. For instance, to target a Population B with relative cell density of 55% at 5 hours, the co-

culture could be started with an initial A:B ratio of 60:40 and AI-2 concentration of 40 μM. Other scenarios were tested and validated, as depicted. These results clearly demonstrate that the initial condition of cell composition (e.g., ratio of A:B) and the exposure to different levels of AI-2 both influence the trajectory of the co-culture population. Equally important, however, is that the orthogonal signal molecule, AI-1, behaved as modeled. We anticipate that, by extension, inclusion of this and other translator signals will enable further, varied or more complicated consortia to be designed and/or controlled.

That is, we tested the co-culture controller system by exposure to an AI-2 concentration, 80 μM, that was higher than the AI-2 concentrations used to characterize the translator cells, and for which we had no model. We used results of the co-culture (**Figure 5.6**) to estimate behavior of translator cells in a monoculture at this AI-2 concentration. We then performed monoculture experiments by adding 80 μM AI-2 to translator cells and showed that we were able to predict monoculture behavior using the co-culture data and the model. **Supplementary Figure 6a** shows the rate of AI-1 production predicted from the co-culture data and model (line) and the actual rate of AI-1 production during the monoculture experiment (data points). **Supplementary Figure 6b** shows the predicted AI-1 levels in the monoculture over time compared to the actual measured AI-1 levels. The predicted AI-1 level was determined using the model, inputting in the estimated AI-1 production rate and the initial cell density of the monoculture.

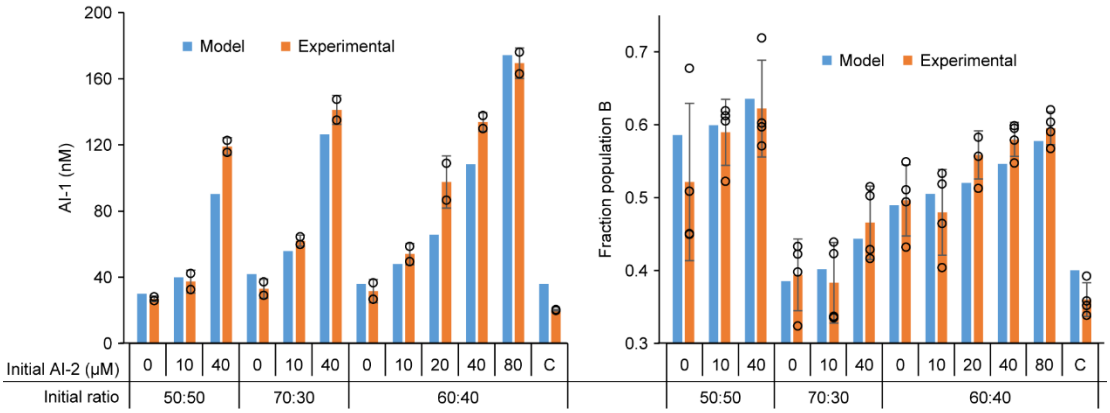

Figure 5.6. Predicting co-culture behavior using mathematical model.

Co-cultures of A and B were added to media containing varied AI-2 concentrations and samples for AI-1 and co-culture composition measurement were collected after 5 hours. Both cell lines were inoculated from overnight cultures to a combined initial OD of 0.05. The initial ratio of A:B is indicated. The control "C" used PH04 pAHL-sfGFP instead of PH04 pAHL-HPr as Population B and used media with 0 μM AI-2. Both model results and experimental results are shown. Error bars represent s.d. between technical duplicates (AI-1 measurements) and technical quadruplicates (composition measurements).

Lastly, we tested our co-culture system over a more extended time period using repeated batch feeding with multiple AI-2 additions (**Figures 5.7**). Here, our objective was to extend the population trajectory beyond that obtained by varying the initial composition and exposure to a fixed AI-2 level in a simple batch culture. In this way, we test the robustness of the control scheme. For example, in **Figure 5.6**, for cultures initially at ~40% population B, we found we could only achieve levels of Population B that approached 60% and only by exposure to high levels (>80 μM) of

AI-2. By testing a repeated batch system, we thought we could drive the B population to over 80% by simply resuspending and extending the system in time. We added our co-culture to media with varied levels of AI-2 and every three hours we resuspended the cells in fresh media with additional AI-2. Immediately prior to each resuspension, samples were taken for analysis of AI-1 concentration and cell culture composition (**Figure 5.7a, 5.7b**). Cell density and AI-2 activity were also measured (**Supplementary Figure 7**). We found that in this more complex experimental set-up, the system generally worked as designed. We found that by exposure to lesser quantities of AI-2 (20 & 40 μM), we could reach nearly 80% population B. During this test, however, we found that our experimental results diverged from the results predicted by our mathematical model. We looked more closely at the AI-1 produced and the growth rate of the cultures during each three hour segment in order to glean an understanding of the culture dynamics based on the observed divergence with the simple model. For instance, the AI-1 produced during the second and third three hour cycles was higher than predicted by the model. In hindsight, this made sense because the cells, after the first batch cycle, had already produced LasI (which synthesizes AI-1), and the additional AI-2 was likely inducing further production of LasI (we did not include a degradation tag on LasI, so its maintenance should have been anticipated). We then adjusted the model so that the AI-1 production rate at the beginning of each subsequent resuspension in new media was the same as at the end of the previous cycle (**Figure 5.7c**, solid lines). Incorporating these new functions for AI-1 production into the model resulted in values for AI-1 that closely fit the experimental AI-1 data (**Figure 5.7a**, model in solid lines). Similarly, we estimated the growth rate

of the controller cells (see **Supplementary Note 1**) and found that the growth rate in combination with the AI-1 concentrations did not fit our earlier *fAI1* function (**Figure 5.7d**). We note that to calculate the growth rate of the controller cells we assumed the growth rate of the translator cells remained constant, although they may have decreased slightly as a result of repeated AI-2 additions. While the controller growth rate seemed to initially increase as a function of AI-1, with subsequent resuspensions in fresh media the overall growth rate decreased. We had earlier noted a dynamic decrease in growth rate upon overexpression of HPr and LasI (**Supplementary Figures 4, 5**). Here, we suspect that either a metabolic burden placed on the cells from repeated exposure to high levels of AI-1 or reduced substrate or nutrient levels could have been causes for decreased growth during the later cycles. Importantly, by adjusting our model so that the effect of AI-1 on growth rate decreased with time (see **Supplementary Note 2**), we were able to fit our experimental data (**Figure 5.7b**, adjusted model in solid lines) without adding model complexity.

In sum, our co-culture system responded as designed whether it was placed in media without AI-2 or with a high level of AI-2. Moreover, our results showed controllable population densities that spanned 40 to 80% of the controller cells. Also, comparison to our original model gave insight into how the system behaved in this more complex experimental set-up; the translator cells appeared to produce higher levels of AI-1 over time while the controller cells seemed to have reduced AI-1 regulated changes in growth rate over time.

Finally, the model might provide a basis to explore *in silico* how the strategies used here for autonomously-regulated cultures (marked by signal-regulated growth

rate and native cell-cell signaling) could be extended to other systems, including user-regulated or programmable systems that could be dynamically controlled. For example, chemostat cultures are distinguished from the current autonomous system in that their outputs are directed by user-specified inputs, such as the dilution rate. As a first pass, we performed simulations of chemostat grown co-cultures by the addition of the standard flow terms to the batch model (**Supplementary Figure 8**, **Supplementary Tables 4, 5**). We found in some cases, that the dilution rate defines a steady-state culture composition which, in turn, can subsequently be "tuned" within a range constrained by the dilution rate. The "tuning" can be achieved by externally modulating the cell-cell signaling, for example, by exogeneous addition of signal molecules. These cases illustrate how the interplay between our autonomous system and other user-controlled systems might lead to more complex population trajectories. Our simulation results here serve as a conceptual framework for controlling consortia composition in more complex, user-guided systems. Further discussion of the chemostat simulations are in **Supplementary Note 3**.

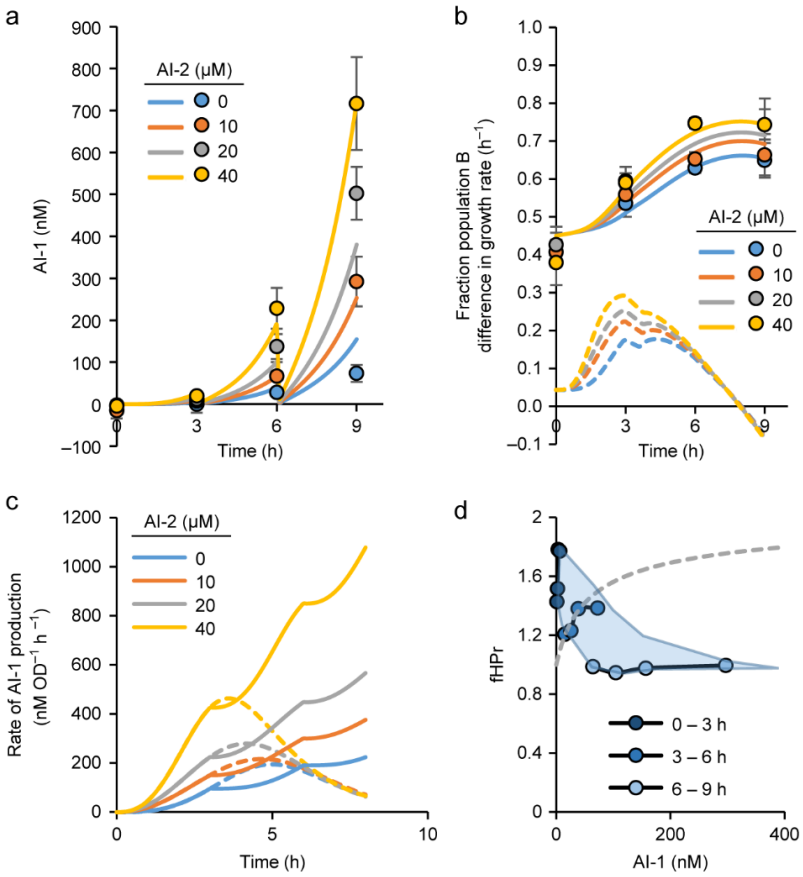

Figure 5.7. Co-culture system in repeated batch set-up.

Co-cultures of A and B were inoculated to a total starting OD of approximately 0.05 in media with the indicated level of AI-2. Every three hours, cultures were spun down and resuspended in fresh media with AI-2. Prior to resuspension samples were collected for AI-1 level and co-culture composition analysis. (**a**) AI-1 level in the cultures at inoculation (t = 0) and at the end of each three hour segment. Data points show experimental data and lines represent adjusted model. Error bars represent s.d. between biological duplicates. (**b**) Fraction of Population B at inoculation (t = 0) and at the end of each three hour segment. Data points show experimental data. Solid lines represent Fraction Population B predicted by adjusted model. Dashed lines represent the difference in growth rate between Populations A and B predicted by

adjusted model. Error bars represent s.d. between biological duplicates. (**c**) Rate of AI-1 production over time for each AI-2 level (*fAI*) used in the original model (dashed lines) and the adjusted model (solid lines). (**d**) Data points are time averaged growth rate (Population B) versus time averaged AI-1 concentration for each three hour segment and each AI-2 concentration. See Supplementary Note 1 for details on estimation of growth rate and AI-1. Dashed line shows original *fHPr* function.

5.3 Discussion

Rapid advances in recombinant DNA technologies have greatly improved the ease of constructing engineered cells for applications ranging from bioprocessing (for production of valuable products) to smart bacteria capable of carrying out a multitude of functions. The bottleneck to further advancing these systems is typically not re-engineering genomes or their regulation, but optimizing cells to efficiently overproduce many proteins or carry out many functions without becoming metabolically overburdened. To work around this, many have proposed using consortia, where tasks can be divided and cells can be specialized. We and others have designed systems using QS circuits to regulate or coordinate gene expression amongst populations or between subpopulations in small consortia. However, by designing QS signal-regulated growth rate and an orthogonal translator controller, we create a tool for an additional layer of control. That is, we enable regulation of composition of the co-culture or small consortia.

In our co-culture system, the composition of each subpopulation is autonomously regulated based on the level of AI-2 in the environment. The translator

cells detect the level of AI-2 and produce the species specific signal molecule AI-1. The AI-1 regulated controller cells then adjust their growth rate based on the AI-1 signal level, which is a function of the initial AI-2 level. The result is an altered co-culture composition based on a native environmental cue, AI-2. We envision our system could be further engineered so that each population carries out part of a concerted effort or function that is autonomously fine-tuned when cells are placed into a particular environment. For example, we had previously reported on sensing cell networks in which the fractional level of responder cells indicates the previous environment they had surveyed[70]. Importantly, because of the partitioning of metabolic functions among subpopulations, our system reduces the potential metabolic burden on the cells – this done through use of QS to enable crosstalk between cells. Equally importantly, we have designed the system so that the AI-1 increases cell growth rate of the translator cells through increased transcription of a sugar transport protein *ptsH*, instead of by causing a reduced cell growth rate – the latter which may strain other engineered functions. We further believe using *ptsH* to regulate growth rate is likely a generalizable strategy due to its being well-conserved[137]. To estimate the behavior of a system using different strains or species, we suggest that prior to implementing the genetic circuit for growth control, one quantifies independently the growth characteristics of the individual strains. This information could be integrated into a simple model such as the one shown here, providing a range of culture dynamics that might be achieved. That is, a co-culture where the maximum growth rates are similar will be dramatically different than if they are very different, irrespective of our cell-based growth-controller module.

In summary, we believe this system can easily be adjusted for further application. In this work, we described a scenario where the system is used to respond to external levels of AI-2 produced by cells in an environment of interest. As an alternative, the system could be rewired so that either population produces AI-2. In this case, both populations would grow naturally until a certain time when a threshold of AI-2 has been reached, at which time the growth rate of Population B would be signaled to change. That is, we believe the autonomous platform shown here, which functions independently and is accompanied by a simple model, could be used to design co-culture systems that allow for self-regulation of the composition of each subpopulation in multiple ways with regulation that requires no user or device intervention. Also by extension, our simple chemostat model predictions suggest we could maintain co-culture compositions at various steady states, but this would occur only with the interjection of well-defined user input (e.g., dilution rate, autoinducer addition, etc.). With such systems, or by inclusion as a subsystem within more complex environments, we expect to enable more widespread use of co-cultures – and the realization of the advantages that come with co-cultures or consortia in synthetic biology or metabolic engineering applications.

5.4 Methods

Strains and plasmids

All strains, plasmids, and primers used are listed in **Supplementary Tables 6 and 7**. pTac-HPr was cloned for IPTG inducible expression of *ptsH*. The *tac* promoter with *ptsH* was amplified from pSkunk-HPr[33] using primers TacProm-PvuI-

F and HPr-SpeI-R to add PvuI and SpeI restriction digestion sites upstream of the promoter and downstream of the stop codon respectively. The fragment was inserted into pLSR[37], a vector containing the repressor for the *tac* promoter *lacI*, using restriction digestion with SpeI and PvuI.

To clone pAHL-HPr, sfGFP was replaced with *ptsH* in a previously cloned AI-1 fluorescent reporter plasmid (pAHL-Reporter_Red-Green) with constitutive expression of dsRedExpress2[139]. Primers HPr-SpeI-F and HPr-SacI-R were used to amplify *ptsH* while adding SpeI and SacI restriction digestion sites upstream and downstream of the start and stop codons respectively. Restriction digestion of both the fragment and reporter plasmid followed by ligation were used to insert *ptsH* under the *lasI* promoter.

pSox-LasI, for PYO induced AI-1 production, was cloned by inserting the *lasI* gene with an ssRA degradation tag (AANDENYALAA) in place of the reporter *philov* in plasmid pTT01[125] using Gibson Assembly (New England Biolabs).

For the translator strain, pLasI was cloned using the Invitrogen Champion™ pET200 Directional TOPO® Expression Kit to insert *lasI* under the T7 promoter. Primers LasI_F and LasI_R were used to amplify *lasI* from the genome of PA01. Constitutive eGFP expression was added elsewhere on the plasmid, at the NruI restriction digestion site, although eGFP expression was not measured during experiments due to low intensity.

Strains PH03 and PH04 were derived from PH01 and PH02[33], respectively. Briefly, the antibiotic resistance cassettes in PH01 and PH02 were removed using plasmid pCP20[140] to create PH03 and PH04.

Cell culture conditions

For all experiments, cells were cultured at 37ºC and 250 rpm shaking. M9 media was prepared with 0.8% glucose and 0.2% casamino acids. Either M9 media or LB media was used for experiments as indicated. LB media was also used for cloning and to grow overnight cultures. Antibiotics were added based on resistance in plasmids. Concentrations used were 50 μg mL^{-1} kanamycin (pLasI), 50 μg mL^{-1} ampicillin (pCT6, pAHL-HPr, pSox-LasI), or 32 μg mL^{-1} chloramphenicol (pTac-HPr). For multi-population experiments, antibiotics were added only if all populations contained genes for resistance. For instance, co-cultures of Population A and Population B contained ampicillin and not kanamycin. AI-1 (N-3-oxo-dodecanoyl-L-homoserine lactone) was purchased from Cayman Chemicals. AI-2 was chemically synthesized and generously provided by Dr. Sintim[122].

Quorum sensing signal activity assays

Bioluminescent reporter assays were used to determine AI-1 and AI-2 activity. Experimental CM samples were prepared by filtering supernatant through a 0.2 μM filter and storing at -20ºC until needed for activity assays. For the AI-1 activity assay[139], *E. coli* luminescent reporter cells containing plasmid pAL105[141] were grown in LB media overnight. In the morning they were diluted 2500 fold in LB media with 50 μg mL^{-1} tetracycline and 50 μg mL^{-1} kanamycin. Experimental samples were diluted in LB in order to be within the linear range of the assay. Samples for a standard curve of known AI-1 concentrations ranging from 0 – 60 nM AI-1 in LB were also prepared. 10 μL of the experimental or standard curve samples were added to 90 μL of the reporter cells. Cultures were grown at 30ºC and 250 rpm

shaking, and luminescent values were recorded after three hours using a GloMax®-Multi Jr (Promega, Madison, WI, USA). Values were normalized to the negative control (fresh LB media with 0 µM AI-1). Each sample was performed in duplicate. The resulting standard curve along with the dilution factor of the sample were used to estimate AI-1 concentration in the original sample.

Vibrio harveyi BB170 was used to measure AI-2 activity.[115] *Vibrio harveyi* BB170 were grown overnight at 30ºC in AB media and diluted the next morning 5000 times in AB media with 10 µg mL^{-1} kanamycin. 20 µL of CM experimental samples were added to 180 µL reporter cells and cultured at 30ºC and 250 rpm shaking. At 3 hours and every half hour thereafter, luminescence values were recorded until the negative control reached a minimum luminescent value. Values were normalized to the negative control (fresh media with 0 µM AI-2). Each sample was performed in duplicate.

Microscopy image analysis

Microscopy images and ImageJ software were used to estimate fractions of each population within the co-cultures. An Olympus BX60 fluorescence microscope with a 20x objective lens and CellSans software were used for imaging cultures. For each sample, at four different locations or frames on the slide a bright field image and image with the fluorescent dsRed filter were taken. Fiji ImageJ software was used to count the cell numbers for each picture. For bright field images, the background was first subtracted using the "subtract rolling background" feature. Thresholds were set for each image type (bright field or fluorescent) and kept consistent for each day's experiment. For each frame, the red cell count was divided by the total cell count. For

each sample, the values calculated for each of the four frames were averaged. Finally, a standard curve, where known amounts of each cell type were mixed directly before taking microscopy images was used to calculate the reported “Fraction Population B” value (**Supplementary Figure 9**).

Chapter 6: Dual-input genetic controller for modulating quorum sensing (QS)-mediated protein expression

This chapter was primarily reproduced from the unpublished manuscript: Hauk, P., Stephens, K., Virgile, C., VandArsdale, E., Schardt, J., Pottash, E., Jay, S.M., Sintim, H., Bentley, W.E. "Dual-input genetic controller for modulating quorum sensing (QS)-mediated protein expression." My contribution to this work was the conceptualization and generation of a mathematical model that is used to interpret the data presented in this chapter regarding the new dual-input controller. Importantly, this model, which describes the AI-2 regulated expression of both a marker protein and a biotherapeutic of mammalian origin, can provide the basis for new controllable genetic designs.

6.1 Introduction

Reprogramming metabolic and biosynthetic functions within microorganisms enables both new routes for biopharmaceuticals production[142], and more recently, for the diagnosis and treatment of disease[51, 124, 143-152]. The terms "smart bacteria" or "smart probiotics" have been used to describe the latter, reprogrammed bacteria that make decisions based on prevailing molecular cues and that subsequently take action, including expressing a marker protein as an indicator of disease, and/or a small molecule or protein-based therapeutic for treatment[17, 49, 50, 152-156]. Several environmental conditions such pH, oxygen tension, and host inflammatory conditions, or even the absence of an important nutrient, have the potential to be used

for signaling these bacteria[70, 124, 157-160]. That is, because there is now an extensive network of signal/receptor pairs that enable tight exogenous control of gene regulation[101], many gene circuits have appeared that ensure high signaling fidelity and precise control of the intended bacterial program. For example, bacterial community size has served as a factor, wherein a quorum sensing (QS) signal molecule, indicating the presence of a number of pathogens, was used to signal the synthesis and delivery of a pathogen-specific toxin from an engineered commensal strain[51]. Indeed, QS systems and their components are widely exploited for building circuits that help to detect metabolic diseases, fight bacterial infections, or serve as biosensors. QS component libraries have served in this capacity as repositories for subsequent assembly of a variety of useful circuits[19, 49, 103, 161].

The autoinducer-1 (AI-1) family of autoinducers, also called acyl-homoserine lactones (AHL), mediate intraspecies communication, including signaling among pathogenic strains enabling their detection in native environments. AI-1 systems have also been assembled into heterologous synthetic circuits. Because there are no AI-1 receptor/synthase pair homologs in *E. coli*, these bacteria do not natively respond to AI-1. Thus, there are few off target responses that might otherwise alter phenotype in unintended directions. When paired with the knowledge that AI-1 freely diffuses through *E. coli* membranes, this attribute enables the incorporation of a variety of pathogen-specific components that provide for sophisticated engineered circuits and pathogen-targeting functions[103].

On the other hand, autoinducer-2 (AI-2) is an interkingdom signaling molecule[118] produced and/or sensed by many bacterial species, including Gram

positive species and commensal Gram negative strains[49], as well as pathogens[31]. In *E. coli,* QS is regulated by the *lsr* promoter via AI-2 (signal) and its cognate repressor, LsrR. Because the native *lsr* promoter is subject to interference by several *E. coli* global regulators (e.g., CRP and σ^s) and is a relatively weak promoter[32, 36, 104, 106, 162, 163] , its use in synthetic systems has been limited. Instead, AI-2 QS circuitry enables native signaling processes to be coopted for specific user-intended purposes wherein the endogenous phenotypes are meant to be exploited or augmented (e.g., autoinduction of heterologous proteins[36], or programmed chemotaxis[95]).

Seeking to expand the use of native bacterial communication within the biotechnology arena, our group focused here on the development of an homologous synthetic circuit based on *E. coli* AI-2 QS. We had previously evolved the native LsrR transcriptional regulator to enable tuned responses based on altered repression[164]. We have also evolved the *lsr* promoter, creating a library containing stronger *lsr* promoter variants, EP01rec and EP14rec[37]. These two mutated promoters were 8-fold stronger than the wild type and yet retained the native LsrR repressor function when the promoters were provided in low copy vectors (~1-2 copies). In this work, we have employed these variants in dual-input genetic controllers for modulating quorum-sensing (QS) networks wherein the wildtype LsrR expression level is augmented by the arabinose-activated pBAD promoter. In addition, LsrK kinase was incorporated into the system to maintain heightened levels of phosphorylated AI-2. The system thus consists of two plasmids, pPHT01 or pPHT14, and pSkunk-LsrK. The pPHT01 and pPHT14 plasmids carry the evolved *lsr* promoters, EP01rec and EP14rec, respectively, for driving a gene-of-interest and *lsrR*

expression placed under the pBAD promoter (**Figure 6.1**). This controller exhibits tunable repression owing to arabinose-inducible LsrR under the pBAD promoter, and induction by AI-2 using the evolved *lsr* promoters, EP01rec and EP14rec. The circuit also shows efficient constitutive expression in the absence of arabinose. We also created a mathematical model that incorporates both the inducible LsrR expression and AI-2-mediated induction to predict protein expression over a range of arabinose and AI-2 concentrations.

This new system, denoted the "homologous quorum sensing regulatory circuit" (hQSRC), is based on native *E. coli* quorum sensing and has the potential for a variety of metabolic engineering and synthetic biology applications, especially where native interspecies communication is envisioned. For example, biomolecule conversion or production using co-cultures[129, 165-167] or consortia[168, 169] may benefit from such a system. Additionally, cell constructs intentionally deployed in complex environments where exogenous control may be difficult, such as smart probiotics or those that are based on interkingdom signaling, may benefit. We anticipate a variety of applications in a variety of settings.

6.2 Results

6.2.1 AI-2 synthetic circuit - parts and strain engineering

Figure 6.1 depicts the dual-input QS regulator for controlling homologous quorum sensing that is comprised of three parts: (i) an *lsr* or *lsr*-derived promoter (EP01rec or EP14rec); (ii) the LsrR repressor expressed via a non-QS signaling

modality (e.g., under pBAD promoter) and (iii) the Lsr kinase, LsrK, which enables enhanced sensitivity to AI-2[28, 170] (e.g., expressed via pSkunk-*lsrK* which has a p15a origin of replication and expresses LsrK kinase under the uninduced *tac* promoter). These components provide for tunable control of heterologous gene expression via native AI-2 QS signaling. We refer to this system as an homologous quorum sensing regulatory circuit (hSQRC) and have constructed two testable examples. The pPHT01 and pPHT14 plasmids each contain two parts of our system (Fig. 1B), the evolved *lsr* promoters (EP01rec or EP14rec) and the pBAD controlled *lsrR* repressor sub-circuit. The third component (LsrK background) is enabled by pSkunk-*lsrK* (**Fig. 6.1B**) which maintains an elevated LsrK kinase level that ensures uptake and phosphorylation of AI-2, allowing LsrR to release the *lsr* promoter via de-repression. Our decision to incorporate the *pBAD* promoter was based on its tight regulation and facile modulation via arabinose addition[171]. When envisioning future applications, this feature retains homologous QS (hQS) regulation for *in vivo* purposes such as "smart" probiotic use in drug-delivery and diagnosis applications. That is, the extra control is enabled by simple carbohydrate (arabinose) addition. Importantly, the third component, LsrK, maintains circuit sensitivity to the prevailing AI-2 level. Here, the hybrid *tac* promoter was used because it has a high background level of *uninduced* LsrK so that the prevailing AI-2 level is rapidly converted into viable genetic signal[28, 39, 170]. While not described thus far, our *E. coli* host strains were also engineered to achieve better control of protein expression levels. Notably, because our focus is on the homologous QS circuitry and the *lsr* promoter of *E. coli*, which is a component of native *E. coli* quorum sensing, our host cell has additional mutations (e.g., Δ*ptsH*) that

ensure our host functions with advanced sensitivity to AI-2 and for a variety of environmental niches[33]. The *luxS* gene was also deleted. LuxS is a S-ribosylhomocysteinase that catalyzes the last committed step in the biosynthetic pathway of AI-2, which is the autoinducer in our system. Thus, the engineered cells respond to the prevailing AI-2 level, rather than contribute to it. Our tested systems include *E. coli* Nissle 1917 (a commensal host) and *E. coli* PH04 (see Table S1). We previously discovered that deletion of *ptsH* enables homologous AI-2 QS in the presence of glucose[33]. That is, *ptsH* encodes HPr, which is involved in the central phosphotransferase system (PTS) for sugar uptake; we found HPr forms dimers with LsrK, inhibiting its activity and altering native QS. The extent of inhibition is dependent on the phosphorylation state of HPr, which varies depending on whether glucose is being transported into the cell. Additionally, Lsr is directly regulated by CRP owing to the CRP binding site located in the lsrR / lsrA intergenic region[32, 162]. These functions all serve to diminish QS signaling among *E. coli* and other genera[31] in the presence of glucose. Manipulation or removal of these controls in the host cells enables QS modulation in the presence of glucose and a variety of other conditions[33, 37, 85, 106]. In **Supplementary Figure 1**, we found no growth impairment in PH04 due to AI-2 and arabinose addition.

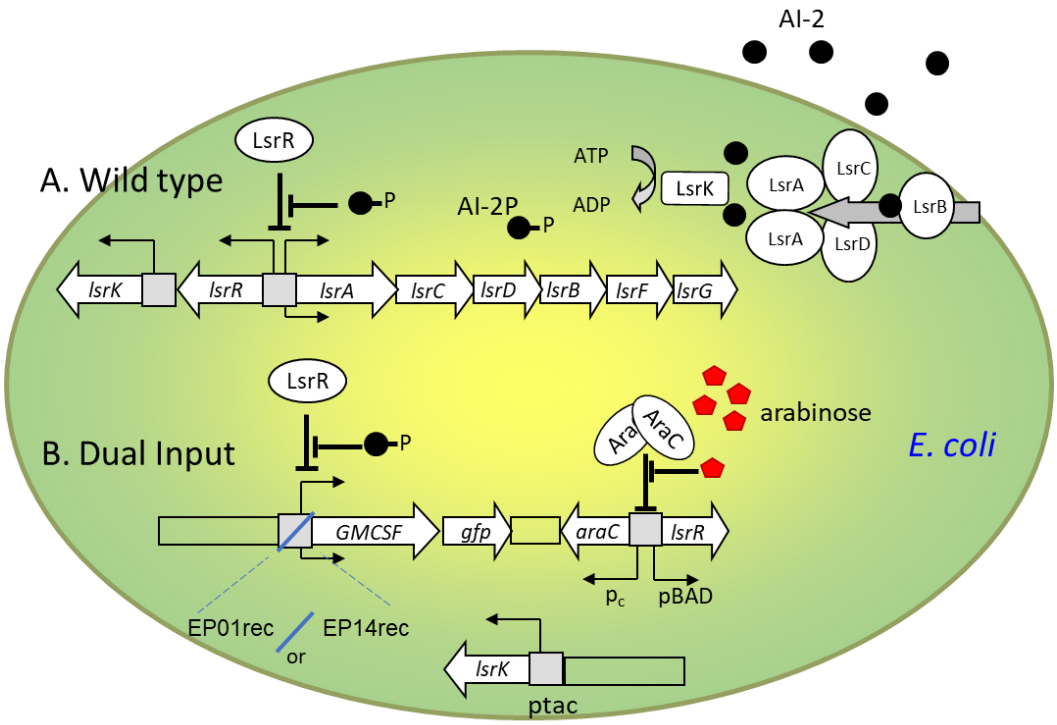

Figure 6.1. Schematic of dual-input genetic controller for modulating quorum-sensing (QS) -mediated protein expression.

(A) QS genetic regulation in *E. coli*. Lsr operon is regulated by the LsrR (repressor), LsrK (AI-2 kinase), and AI-2 (inducer, produced via LuxS) (B) Homologous Quorum Sensing Regulatory Circuit (hQSRC). The hQSRC system consists of two parts: pPHT01 or pPHT14 (Plasmid #1) and pSkunk-*lsrK* (Plasmid #2). pPHT01 and pPHT14 harbor evolved *lsr* promoters, EP01rec and EP14rec[37], respectively. The *araC-pBAD-lsrR* sequence was introduced to provide extra LsrR repression by arabinose addition. The second plasmid is a p15a origin plasmid expressing LsrK under the *tac* promoter w/out induction.

6.2.2 Ara-mediated QS repression via LsrR

In our semisynthetic QS regulator, we make use of the native QS repressor, LsrR, In **Fig. 6.2**, we measured the level of GFP expressed via the EP01rec and EP14rec promoters and repressed by the araC-induced overexpression of LsrR. *E. coli* PH04 cells (Δ*luxS* Δ*ptsH*) carrying pSkunk-lsrK and pPHT01 or pPHT14 were either grown in LB media to OD_{600} ~0.2 and then supplemented with arabinose at 0.002% or were grown from inoculation (e.g., OD_{600} ~0.02) in the presence of 0.02% and 0.2% arabinose. We measured GFP fluorescence via flow cytometry at OD_{600} ~0.2 at 2 and 4 hr. These experiments enable elucidation of both the extent of repression and its transient nature. In all cases the addition of more than 0.02% arabinose resulted in a tightly repressed state and this was maintained throughout. Interestingly, in the experiments where arabinose was added at OD_{600} ~0.2, even 0.002% arabinose prevented the subsequent induction of GFP (the levels at OD_{600} ~0.2 were maintained at 2 and 4 hrs). We further note that the absence of arabinose enabled the native-like (e.g. leaky) expression of GFP previously observed in EP01rec and EP14rec[37]. The PH04 strain used to perform the experiment is not an AI-2 producer (Δ*luxS*), and AI-2 was not added to these cultures. We note that the EP01rec promoter was previously shown to exhibit more leaky expression than the EP14rec promoter,[37] which is likely the cause for relatively higher GFP levels shown here.

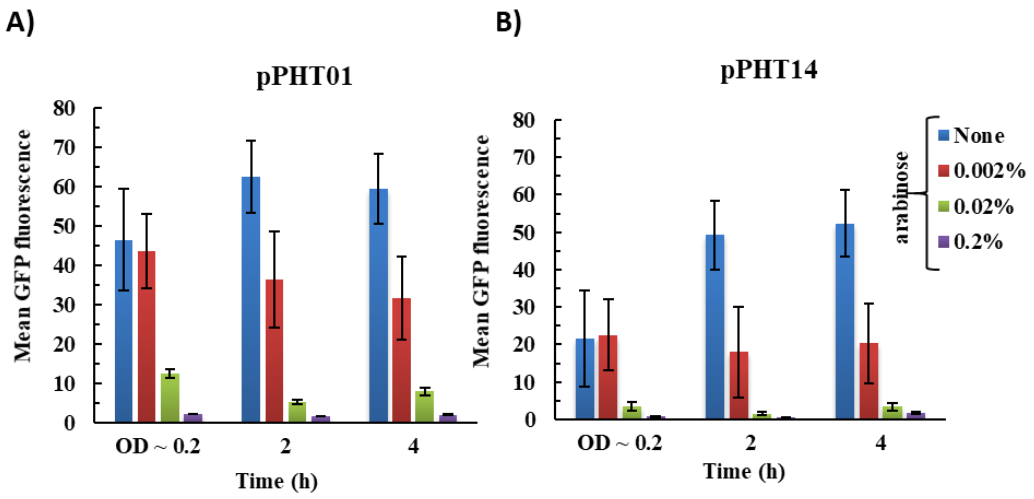

Figure 6.2. GFP fluorescence based on arabinose addition.

Representative FACS histograms show the mean GFP fluorescence from *E. coli* PH04 (Δ*luxS* Δ*ptsH*) cells transformed with either pPHT01 (A) or pPHT14 (B) and pSkunk (see Figure 1). Panels (A) and (B) show arabinose dose-dependent repression. PH04 were grown in LB media until OD_{600nm}~ 0.2 and then supplemented with 0, 0.002, 0.02 and 0.2% arabinose and shaken at 37°C for 2 and 4 h. GFP expression was measured at three different points, OD_{600nm} of 0.2 (starting point), 1.0 (2 h) and ~ 2.5 (4 h). Data are plotted as means ± standard deviations of technical triplicates.

6.2.3 Dual input control of homologous QS signaling

Having demonstrated that even low levels of arabinose provide for repression of the genetic circuit, we wanted to test the release of this repression by the addition of the native QS signal molecule, AI-2. In this way, the genetic circuit would exhibit low or no expression of the encoded transgene unless AI-2 was present. Experiments were performed combining arabinose (repressor) and AI-2 (inducer). For this,

cultures were grown in LB media prepared with 0, 0.005 and 0.01% arabinose, and then at OD_{600nm} ~ 0.2, different concentrations of AI-2 (0, 40 or 80 µM AI-2) were added to cell cultures. Based on our previous results (**Fig. 6.2**), we determined 0.005 and 0.01% arabinose would correspond to a minimal and maximal repression condition, over which we could test AI-2 mediated de-repression. That is, with higher levels of arabinose (e.g., 0.02%, **Fig. 6.2**), we suspect that subsequent AI-2 addition would have minimal impact. GFP fluorescence was measured at OD_{600nm} ~ 0.2, which is the induction point, and after 2, 4, 6 and 9 h. In **Fig. 6.3**, we found expression levels in both systems (hQSRC01 and hQSRC14) were reduced by at least ~ 50% in the presence of 0.005 and 0.01% arabinose, when compared to expression in the absence of arabinose, as expected. Then, both hQSRC01 and hQSRC14 were switched ON in the presence of 40 or 80 µM AI-2 (inducer), even in the presence of 0.005 or 0.01% arabinose. hQSRC01 showed higher expression levels (**Fig. 6A**) in comparison to hQSRC14 (**Fig. 6.3B**), but as noted earlier, this is likely due to more constitutive expression in the absence of repressor or inducer (see OD_{600} ~ 0.2 controls). Also shown at the right are the $hLSR_{WT}$ and $hQSRC_{WT}$ controls, which are just the wildtype *lsr* promoter driving GFP and the same circuit as hSQRC01 and hSQRC14 systems but with the native *lsr* promoter, respectively. These data are from the 9 hr samples, but the low expression levels shown clearly demonstrate the advantages of using the evolved EP01rec and EP14rec promoters in this homologous circuit. Importantly, both of the new constructs function in a similar manner, which was anticipated. Also, in all cases, arabinose-mediated repression was sustained or

de-repressed (by AI-2 addition) and the resulting expression levels were maintained while the cells grew from 0.2 to the final OD (~ OD_{600} = 4).

Our results suggest that the dual input hQSRC system, which makes use of an added carbohydrate and the homologous AI-2 QS signal could be "operated" in three different modes: (1) there is a well-defined constitutive expression mode when neither the arabinose nor AI-2 are present (e.g., no repression and no induction), (2) a controllable repression mode in which tight LsrR repression is rapidly induced by the addition of arabinose, and (3) a repression/induction mode via native AI-2 signaling with levels that are tuned by the prevailing AI-2 level. Both of the systems made use of evolved promoter regions of the native *lsr* promoter which had advantageous characteristics (e.g., higher expression and more amplification relative to the wild type).

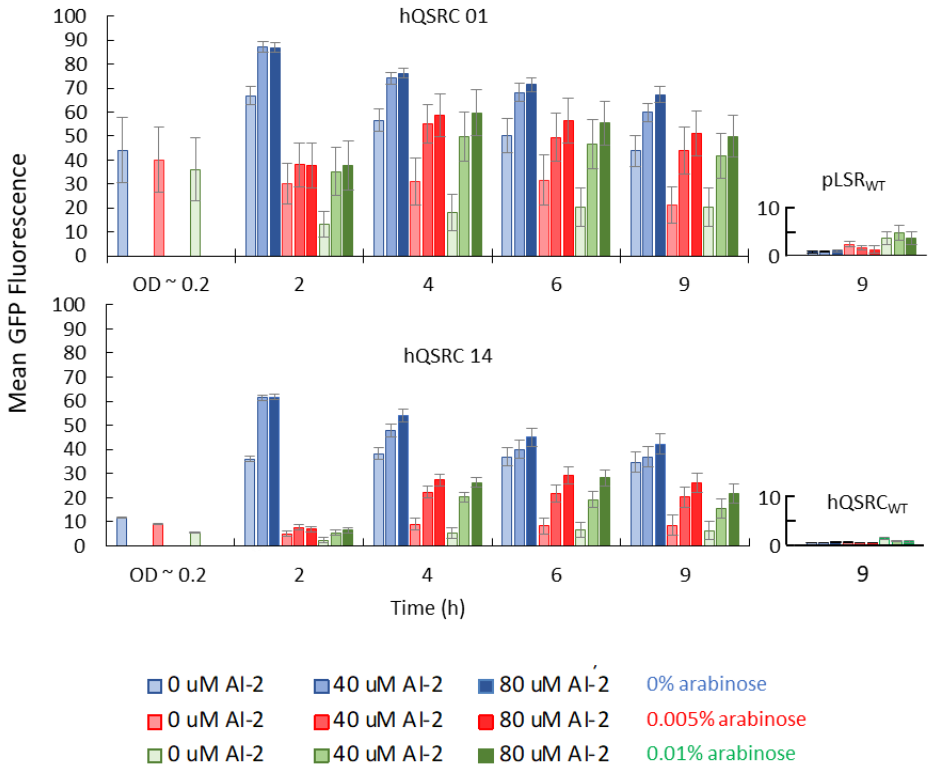

Figure 6.3. Transcriptional regulation of hQSRC01 and hQSRC14 in the presence or absence of arabinose (repressor) and/or AI-2 (inducer).

PH04 cells carry hQSRC01 or hQSRC14 system expressing GFP. At different time points during cell growth (2, 4, 6 and 9 h); samples were collected for measurement of GFP fluorescence. Bar color (blue, red, or green) indicates whether arabinose was added; color intensity (faded to strong) indicate the level of AI-2 supplemented, as indicated. On the right are two sets of controls: pLSR$_{WT}$ represents native *lsr*-mediated expression with no AraC controller sequences. hQSRC$_{WT}$ represents the same control vectors as hQSRC01 and hQSRC14, but with the native *lsr* promoter. Extra repression is clearly visible. Data are plotted as means ± standard deviations of technical triplicates.

In **Supplemental Tables 3** and **4** and **Supplemental Note 1**, we describe a simple mathematical model that enables dynamic simulation of gene expression using these circuits. In particular, the model equations employ standard forms of repression and activation (as mediated by a single transcriptional regulator). The model was developed to accommodate arabinose-induced LsrR, as well as LsrR and AI-2-mediated regulation of *lsr* promoter activity. Its utility is in its discriminatory ability to tease out the relative amplification (fold change) that is obtained by having the extra repression enabled by overexpressed LsrR. That is, a central purpose for designing this system was to first provide low background expression but then develop autoinduced amplification that responds strongly to AI-2. This is an alternative motivation to that of our previous work in which we sought only amplification of *lsr*-mediated expression by using a T7 amplification scheme[36, 121]. We simulated the experiment carried out in **Figure 6.3A** (hQSRC01) using the model, adjusting the unknown model parameters (e.g., repressor binding, K_{LsrR}, transcription rate, β_{GFP}) so the model and experimental results were in reasonable agreement. In Supplemental Figures S2 & S3, cell growth and expression results predicted by the model for all levels of arabinose and AI-2 are depicted. For simplicity, **Fig 6.4A** shows the strong agreement between the model and the data for the 0.01% arabinose cases of hQSRC01. This agreement suggests that the general model formalism and constants are reasonable. We subsequently altered the GFP transcription rate constant, β_{GFP}, to simulate the hQSRC14 system, anticipating that this should be the only altered parameter between the two systems (the host and remaining genetic control components are identical). To do this, we simply halved the

rate constant based on our previous data showing mRNA and the expression levels of two transgenes[37] using the EP14rec promoter were at about half the levels of the EP01rec promoter. The simulated GFP levels were again within experimental error. Again, this result confirms that the genetic circuit as modeled by a set of ODEs reasonably reflects the level of gene expression from this dual-input controller.

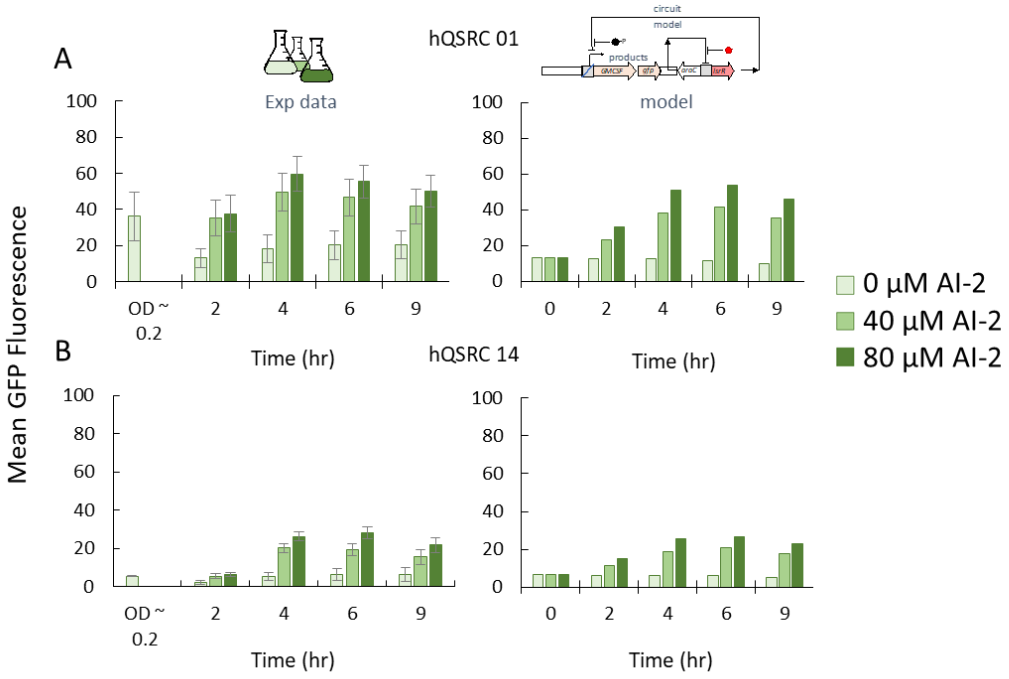

Figure 6.4. Comparison of Experimental Data to Model Simulations

(A) hQSRC01 data (left) were used to ensure reasonable agreement with model (right). (B) Based on previous measurements of promoter strength[37], one model parameter, β_{GFP} (Supplemental Table 4), was adjusted to predict behavior of hQSRC14. Model equations, parameters, and assumptions along with other simulations are provided in Supplemental Tables 3, 4 and Supplemental Note 1.

6.3.4 Engineered probiotic bacteria secrete active recombinant human GM-CSF via hQSRC system

Armed with a predictive model, especially one that characterizes the control that is enabled by arabinose controlled LsrR-repression and AI-2 de-repression, one can use this formalism to design expression characteristics for therapeutic proteins, ultimately enabling a base model for "smart probiotic" delivery systems for complex *in vivo* environments. *E. coli* Nissle 1917 (EcN) is a commensal *E. coli* strain that has been widely used in many studies involving probiotics and the production of biotherapeutics[145, 172-175]. We engineered EcN to create *E. coli* PH08 which is a *luxS* and *ptsH* double knockout of the isogenic parent. In this way, alterations of the genetic background used to construct PH04 with results from **Fig. 6.3** were maintained. Naturally, the rest of the genetic backgrounds for the two strains were different. Next, pPHT01 and pPHT14 were modified to express a granulocyte macrophage colony stimulating factor (GM-CSF), a model gastrointestinal (GI) tract therapeutic.[121, 124] Here, we express a chimeric protein consisting of a secretion mediator, YebF, an enterokinase cleavage site, and a C-terminal hexahistidine tag for purification via immobilized metal ion affinity chromatography (IMAC). The YebF-EK-rhGM-CSF-His6 fusion construct was placed in front of the *gfpmut2* gene, both under EP01rec or EP14rec control, thus creating pPHT01-*yebF*-rhGM-CSF-His6 and pPHT14-*yebF*-hGM-CSF-His6, respectively.

The *E. coli* PH08 strain expressing YebF-EK-hGM-CSF-His6 fusion via hQSRC01 or hQSRC14 were cultivated in various conditions including (or not) the repressor signal (arabinose) or inducer signal (AI-2). Subsequently, we expected

GM-CSF would be expressed and secreted into the extracellular media at various levels according to the signaling conditions. After 4 h of induction or repression, supernatants from each culture were collected and precipitated using a TCA protocol as described in Materials and Methods followed by Western blot. In **Fig. 6.5A**, the YebF-EK-rhGM-CSF-His6 fusion was detected in the positive control (denoted "C"), where the pAES plasmid was used to express the fusion under the *tac* promoter via IPTG addition. For hQSRC01, rhGM-CSF expression was significantly lower due to the added presence of 0.01% arabinose (repressor signal, Lane 1). We note that the YebF-EK-rhGM-CSF-His6 fusion was observed in both conditions in which AI-2 was added to the culture, 40 µM AI-2 and 40 µM AI-2 plus 0.01% arabinose (Lanes 2 and 3). Importantly, in the condition that both inducer and repressor were added (Lane 3), rhGM-CSF levels were higher with AI-2 only (**Fig. 6.5A**, Lane 2). Analogously, the hQSRC14 system showed similar protein expression profiles to hQSRC01; however, since EP14rec is a weaker promoter compared to EP01rec, protein expression levels were somewhat lower in comparison. Both systems exhibited the repressible and inducible phenotype shown dynamically and at more conditions for the GFP experiments. In **Figure 6.5b**, we compared repression and induction of GFP (**Fig. 6.3**) to the repression and induction of YebF-EK-rhGM-CSF-His6 estimated from the gel images (**Fig. 6.5a**, gel image quantification illustrated in **Supplementary Figure 4**). We also show the results predicted by the mathematical model. That is, we previously demonstrated that the model was in agreement with the GFP data (**Fig. 6.4**), and here we used the model to predict outcomes using GM-CSF as a product. We compare conditions with or without arabinose or AI-2 as a means to

normalize the data. While the model can provide a molar concentration of GM-CSF, it is the fold-change and tunability that we are most interested in capturing. By describing fold change, the stochiometric constants that convert transcript level to concentration of protein are factored out. Without altering transcription rate constants, the four hour time points after AI-2 addition were used to compare to the YebF-EK-rhGM-CSF-His6 expression experiments. Here, the effect of arabinose was evaluated from Western data in A, where the intensity of blots from Lane 3 data were divided by Lane 2. The effect of AI-2 is shown as the expression level with 0.01% arabinose and 40 µM AI-2 addition relative to the same experimental setup without AI-2 (Lane 3 divided by Lane 1 in (A)). Note that the model predicts the same fold changes for both hQSRC01 and hQSRC14. The expression model correlated extremely well with the repression and subsequent AI-2-mediated de-repression, illustrating that for GMCSF, a secreted protein of mammalian origin, the model was still viable. This suggests that the model may have potential for future designs and more importantly, it corroborates the mechanistic relationships between the promoter and repressor designs in the model equations. Thus, the expression and secretion of human GM-CSF (i.e., rhGM-CSF) using an engineered commensal *E. coli* strain (PH08) may serve as a step towards a viable "smart" probiotic delivery system. While not shown here, the extra benefit enabled by the tight arabinose-mediated repression is that potentially cell toxins (e.g., cancer therapeutics) could be delivered in a more spatially or temporally controlled manner. Our data also suggest the expression of a protein or other molecule could potentially be stopped by the exogenous (or otherwise) addition of arabinose. That is, the YebF-EK-hGM-CSF-His6 fusion could

be constitutively expressed and then stopped. There might be advantages to all three modes of expression and control (i.e., switched from one mode to the other).

To ascertain whether the GM-CSF expressed and secreted was biologically active, supernatants collected after 4 h of protein expression were passed through a Ni^{2+}-sepharose column, purified, and evaluated using a human TF-1 cell line, wherein proliferation is stimulated by rhGM-CSF[176]. Since LPS interacts directly with a TLR4/MD-2 complex on hematopoietic progenitor cells[177], we also depyrogenated the purified chimera by incubating with polymyxin B sulfate to remove possible LPS contamination from the host *E. coli* cells. In **Fig. 6.5C**, TF-1 cell proliferation was higher for the GM-CSF purchased from Preptotech™ than the rhGM-CSF chimera expressed via hQSRC01 in PH08 host cells at most concentrations tested. However, the *E. coli* expressed protein was also quite active; differences could be due to many factors including potential effects from fusion with translocation and purification tags. We also note that the samples treated with polymyxin B showed further decreased TF-1 cell proliferation when compared with the other samples (Fig. 5C), indicating a possible activation effect by LPS. Perhaps more importantly, a 250 ml culture of PH08 cells carrying the hQSRC01 GM-CSF expression system yielded ~100 µg/ml of active YebF-EK-hGM-CSF-His6 fusion, which is appreciable.

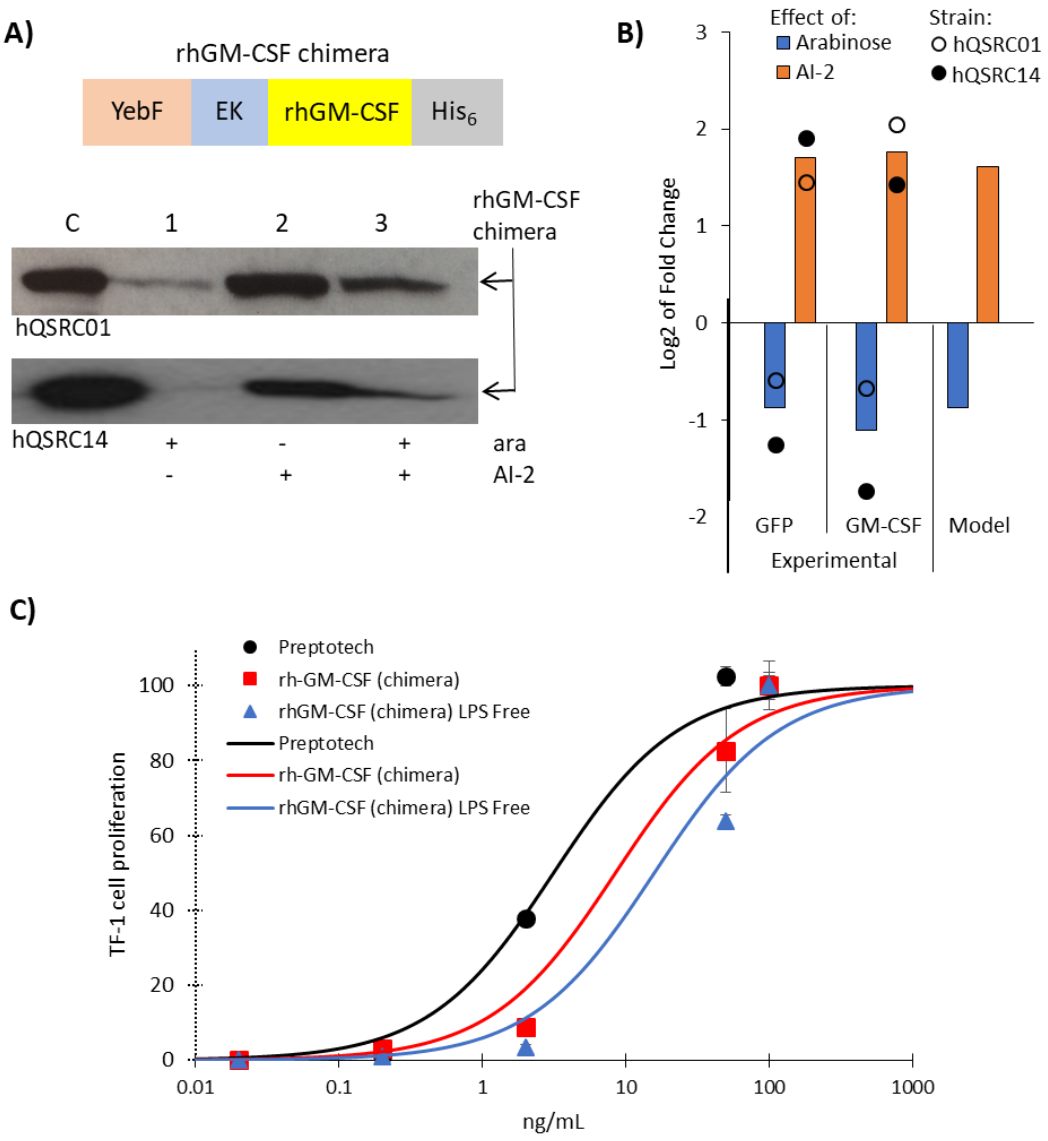

Figure 6.5. Dual-input controlled expression of rhGM-CSF

(A) Recombinant human GM-CSF chimera (rhGM-CSF chimera) expression and secretion in *E. coli* Nissle *ΔluxS ΔptsH* strain (PH08). PH08 cells were grown in LB media and supplemented with 0.01% arabinose and/or 40μM AI-2. The rhGM-CSF chimera exported to LB culture media was analyzed using Western blots. Samples from different growth conditions were precipitated using a TCA protocol. Lanes indicated were: (1) A positive control (pAES40-GM-CSF induced via IPTG), (2)

0.01% arabinose, (3) 40 μM AI-2 and (4) 40 μM AI-2 plus 0.01% arabinose. (B) AI-2 and arabinose-mediated fold change in expression of GFP and rhGM-CSF chimera after 4 hours growth in the presence of 0.01% arabinose and after AI-2 addition (40 μM). Here, the effect of arabinose was evaluated from Western data in A, where the intensity of blots from Lane 3 data were divided by Lane 2. AI-2 mediated fold change is shown as expression levels with 0.01% arabinose and 40 μM AI-2 addition relative to the same experimental setup without AI-2 (Lane 3 divided by Lane 1 in (A)). Note that the model predicts the same fold changes for both hQSRC01 and hQSRC14. (C) Purified and depyrogenated (LPS free) rhGM-CSF chimera expressed by PH08 strain was bioactive as noted by proliferation of TF-1 cells. Activity was also compared to the commercially available rhGM-CSF (Preptotech).

6.3 Conclusions

We created a semisynthetic QS regulator that enables both external and endogenous control of gene expression based on native AI-2 signaling. This was built upon our previous directed evolution efforts of the *lsr* promoters[37]; key features of the new system are due to the rewiring and adjusting of the AI-2 QS regulatory components, LsrK and LsrR. Here, we enabled tighter than native repression by the addition of the heterologous arabinose repressor/actuator system and more sensitive AI-2 mediated activation by the incorporation of additional levels of LsrK[170]. To transition this system towards *in vivo* application, we added these constructs to *luxS* and *ptsH* deletion mutants enabling their function in the presence of glucose and precluding extraneous signaling by AI-2 synthesis. Further, we built a mathematical

model that can be used to estimate protein production based on both the native and external cues. We believe the novelty and value of this system is that it builds tunable control onto the homologous (AI-2) signaling processes native to *E. coli* and many other bacteria, both Gram positive and Gram negative, as well as by the addition of a simple digestible sugar. Its tight repression until AI-2 accumulates for de-repression is attractive for industrial biotechnological settings and its two-cue processing logic should enable robust use in complex environments.

6.4 Materials and Methods

Strains and media

DH5α (NEB), PH04 and PH08 strains (**Supplementary Table 1**) were grown in Luria-Bertani (LB) medium at 37°C for DNA manipulation or expression experiments. Media were supplemented with chloramphenicol (34 μg/ml) to maintain pPHT, pPHT01, pPHT14, pPHT01-YebF-rhGM-CSF and pPHT14-YebF-rhGM-CSF, kanamycin (25 μg/ml) for pBAD-*lsrR*, spectomycin (25 μg/ml) for pSkunk-*lsrK*, and ampicillin (50 μg/ml) to maintain pAES40, pAES40-GM-CSF or pGM29OmpA plasmids (**Supplementary Table 1**).

E. coli knockouts

PH04 and PH08 are derived from *E. coli* LW7 and *E. coli* Nissle (EcN), respectively. The *ptsH* gene was deleted from both LW7 and EcN. The *luxS* gene was also knocked out from the EcN genome. Homologous recombination facilitated by λ Red recombinase was used to construct knockouts[112]. The pKD3 plasmid was used as

template for PCR, and the ptsHd_Fw and ptsHd_Rv primers were used to create the PH04 strain, while luxSEcN_Fw,luxSEcN_Rv, HprEcN_Fw and HprEcN_Rv were used to create the PH08 strain. Deletion of *ptsH* and *luxS* genes was confirmed by PCR using primers ptsHout_Fw, ptsHout_Rv, ptsHd_Rv, luxSEcNout_Fw, LuxSEcNout_Rv, HprEcNout_Fw, and HprEcNout_Rv. The pCP20 plasmid was used for removing the antibiotic cassettes from the genome[140].

Plasmid construction

pPHT, pPHT01 and pPHT14 are derived from plasmids pLSR, pLSR01 and pLSR14, respectively. pLSR, pLSR01, and pLSR14 contain *gfpmut2* under an *lsr* promoter variant, either wild type, EP01rec, or EP14rec, respectively[37]. pPHT, pPHT01, and pPHT14 also contain *araC*-pBAD-*lsrR*. To construct these plasmids, *lsrR* was first cloned into pBAD/HisA (Invitrogen) to create pBAD-*lsrR*. The *araC*-pBAD-*lsrR* sequence (2264 bp) was then amplified through PCR using pBAD-*lsrR* as a template. pLSR, pLSR01 and pLSR14 were digested using the restriction enzyme, XhoI, and then dephosphorylated via alkaline phosphatase (Calf intestinal, New England BioLabs) as described by the manufacturer. The *araC*-pBAD-*lsrR* fragment was digested using XhoI, and ligated into pLSR, pLSR01 and pLSR14, creating plasmids pPHT, pPHT01 and pPHT14.

pPHT01-*yebF*-hGM-CSF and pPHT14-*yebF*-hGM-CSF are derived from pPHT01 and pPHT14 and contain the *yebF*-hGM-CSF-Histag sequence downstream of the *lsr* promoter (either EP01rec or EP14rec) and upstream of *gfpmut2*. To construct the *yebF*-hGM-CSF-Histag sequence, pGM29OmpA[178] was used as a template for amplifying the hGM-CSF sequence. This was then cloned into pAES40

(AthenaES) containing *yebF*. pAES40-GM-CSF was then used as a template to amplify the *yebF*-hGM-CSF-Histag fragment for cloning into pPHT01 and pPHT14. Vectors pPHT01 and pPHT14, and the *yebF*-hGM-CSF-Histag fragment were digested using SpeI. Alkaline phosphatase (Calf intestinal, New England BioLabs) was used to prevent vector self-ligation during cloning. The *yebF*-hGM-CSF-Histag insert was ligated into pPHT01 and pPHT14.

The pSkunk-LsrK plasmid was constructed using the restriction sites NcoI and SpeI. Plasmid information and primer sequences are also available in Supplementary Table S1 and Supplementary Table S2, respectively.

Repression and induction experiments

PH04 harboring pSkunk-*lsrK* and pPHT, pPHT01 or pPHT14 were grown overnight at 37ºC in 2 mL of LB medium supplemented with 25 μg/mL of spectinomycin and 34 μg/mL of chloramphenicol. Bacterial suspensions were then re-inoculated into 10 mL of fresh LB medium with chloramphenicol and spectinomycin in order to have initial optical densities ($OD_{600\ nm}$) of 0.05.

To evaluate the pBAD-*lsrR* system repression range over the wild-type *lsr* promoter, EP01rec and EP14rec promoters[37], 0.002, 0.02 and 0.2 % arabinose were added to the cultures. Cells were allowed to grow at 37ºC with shaking at 250 rpm. Bacterial cell samples (200 μL, technical triplicate) were collected at optical density ($OD_{600\ nm}$) ~ 0.2 and 2 and 4 hour thereafter.

To analyze the de-repression caused by AI-2 over the wild-type *lsr* promoter and its variants, experiments were conducted adding synthetic AI-2 in the absence or presence of 0.005 and 0.01% arabinose. At $OD_{600\ nm}$ ~ 0.2 cultured cells were induced

by adding 0, 40 or 80 μM of synthetic AI-2. Cells were collected at $OD_{600\ nm}$ ~ 0.2 (induction start point) and after 2, 4, 6 and 9 h.

To prepare samples for analysis of GFP expression, samples were centrifuged (1,000 *g*, 5 minutes), washed, resuspended in 1X PBS and kept on ice until flow cytometry.

GFP expression

Flow cytometry analyses were performed using a FACSCanto II flow cytometer equipped with 488 nm, 633 nm, and 405 nm lasers (BD Biosciences, San Jose, CA) and all flow cytometry data were analyzed with FACSDiva software (BD Biosciences). Side and forward scatter of bacterial suspensions were determined using semi-log scale SSC/FSC plots with a threshold of 5,000. Voltage settings for the SSC, FSC and FITC channels were kept constant for all flow cytometry experiments. Bacterial suspensions were analyzed at a medium flow rate with a maximum of 1,000 events per second for 75 seconds and a minimum of 50,000 events. Positive cells for GFP fluorescence were compared with negative controls (LW6 pLSR14 and *E. coli* W3110).

Human GM-CSF (hGM-CSF) expression experiments

E. coli Nissle PH08 harboring pSkunk-*lsrK* and pPHT01-*yebF*-hGM-CSF or pPHT14-*yebF*-hGM-CSF were grown overnight at 37ºC in 2 mL of LB medium supplemented with 25 μg/mL of spectinomycin and 34 μg/mL of chloramphenicol. Cells were re-inoculated into 15 mL of fresh LB medium supplemented with antibiotics mentioned above in the same concentrations. Repression and induction were evaluated based on the presence or absence of either 0.01% arabinose and/or 40

μM synthetic AI-2. Cells were grown at 37ºC with shaking at 250 rpm for 4 h. Cultures were then centrifuged (5,000 *g*, 10 min). Cell-free supernatant fractions were precipitated overnight with 10% TCA at 4ºC. After centrifugation at 10,000 rpm for 10 min the pellet was washed once with ice-cold 100% acetone. All samples were resuspended in 70 μl of 2X SDS-PAGE buffer to be analyzed by Western Blot.

Western blot analysis

To detect rhGM-CSF chimera excreted into the PH08 culture media, supernatant from different conditions were precipitated using the TCA method as described above. After that, samples were loaded in equal volumes of 2X SDS-buffer for separation on 15% SDS-PAGE gel and then transferred to a PVDF membrane for western blot analysis. To detect YebF-hGM-CSF-Histag fusion a polyclonal rabbit anti-YebF (1:20,000, AthenaES) was used. Membranes were developed using SuperSignal™ West Femto Maximum Sensitivity Substrate according to the manufacturer's instructions.

Protein purification

YebF-hGM-CSF-His6 (rhGM-CSF chimera) was expressed under the constitutive expression mode (in absence of both arabinose and AI-2) and purified from PH08 cell-free supernatant after 4 h of growth. Supernatant was absorbed to HiTrap Chelating HP filled with 1 ml of Ni2+-charged chelating Sepharose (GE Healthcare) previously equilibrated with PBS 1X, pH 7.4 buffer. After absorption of rhGM-CSF, the resin was washed with 5 volumes of PBS 1X, pH 7.4 containing 5mM imidazole, following protein elution with 5 volumes of PBS 1X, pH 7.4 containing 150 mM imidazole. The purified YebF-hGM-CSF-Histag fusion was

dialyzed against PBS 1X, pH7.4 buffer and then concentrated to 100 μg/ml to have its activity tested in the human erythroleukaemia cell line (TF-1).

Recombinant hGM-CSF activity

Cell lines and reagents — The TF-1 cell line was obtained from Dr. David Stroncek (National Cancer Institute). TF-1 cells were maintained in RPMI 1640 (ATCC) with 10% FBS, 1% Pen-Strep, and 2 ng/ml recombinant human GM-CSF (Peprotech). *Cell proliferation assays*— TF-1 cells were seeded at 20,000 cells per well, in media supplemented with 10% FBS, 1% Penicillin-Streptomycin, in a 24 well plate (VWR 10062-900), treated with the indicated factor or control, incubated in 5% CO_2 at 37ºC for 4 days, and analyzed using Alamar Blue (Bio-Rad) following the manufacturer's protocol.

Chapter 7: Electrochemical control of bacterial cell growth rate and culture composition

7.1 Introduction

Synthetic biologists have engineered microbes for wide-ranging functions for an array of applications[7]. Examples include microbes that detect hazardous molecules in environmental samples[179-181], seek out a specific locale[182], and synthesize and secrete pathogen-specific toxins or disease-specific therapeutics[51, 124]. The power of these systems often lies in their ability to synthesize a wide range of biological molecules, and to do so as programmed (at specific times, in response to specific environmental conditions, etc). Recently, synthetic biologists have begun to engineer electronic control of target gene expression using redox active molecules[125, 183]. This is potentially a powerful step forward, one that could allow electronic access to the vast number of biological molecules or functions that can be synthesized or carried out by cells. That is, it could expand the capabilities of electronic systems, which are ubiquitous in modern society.

Electronic control of target gene expression is still its infancy, with few examples. Weber et al. electrochemically oxidized ethanol to acetaldehyde to regulate expression from an acetaldehyde-inducible promoter in mammalian cells[183]. To engineer electronic actuation of gene expression in bacteria, Tschirchart et al. coopted the SoxRS system[125], which natively regulates the cell oxidative stress response[184]. The authors found that by using the redox-active molecule pyocyanin[185] and the

mediator ferricyaninde, *soxS* promoter activity could be controlled electrically. They demonstrated electronic control of QS signaling and chemotaxis. More recently, Terrell et al. generated hydrogen peroxide at an electrode surface to regulate a gene of interest from the *oxyS* promoter (unpublished). The OxyRS system is sensitive to hydrogen peroxide[157, 186], which can be generated at a gold electrode surface through reduction of oxygen[187, 188]. Terrell et al. demonstrated electronic control of cell-cell signaling and synthesis and release of a GI tract biotherapeutic using the OxyRS system.

Here, we use the OxyRS system to engineer electronic control of a fundamental cellular process – cell growth. The use of microbial communities have gained traction recently in synthetic biology and metabolic engineering[3], and tools for modulating the cell growth of subpopulations in order to control the community composition would be beneficial. To electrically modulate cell growth rate, we built off of our previous system for electrogenetic gene regulation using the OxyRS system. We developed a "relay" strain that responds to the hydrogen peroxide generated electrically and produces a quorum sensing molecule, AI-1. The AI-1 signals a second population, the "controller" strain, to grow faster (**Figure 7.1**). We previously developed the controller strain for AI-1 modulated cell growth through regulation of the phosphotransferase system (PTS) protein HPr[85], which is important in uptake of PTS sugars (such as glucose) into the cell[189]. Importantly, the "relay" strain converts the hydrogen peroxide signal that is generated at the electrode surface, into a relatively more stable AI-1 signal. That is, *E. coli* rapidly consume hydrogen peroxide[157], which is not the case with AI-1. The AI-1 signal is dispersed throughout

the bulk media (through stirring or shaking), where it regulates the growth of the "controller" strain. We used a *ptsH* knockout strain for the relay strain, so that this population would grow slowly. In this way, the population relays the signal generated by the electrode to the main population of interest (the controller strain), without overtaking the culture or consuming unnecessary levels of nutrients in the media.

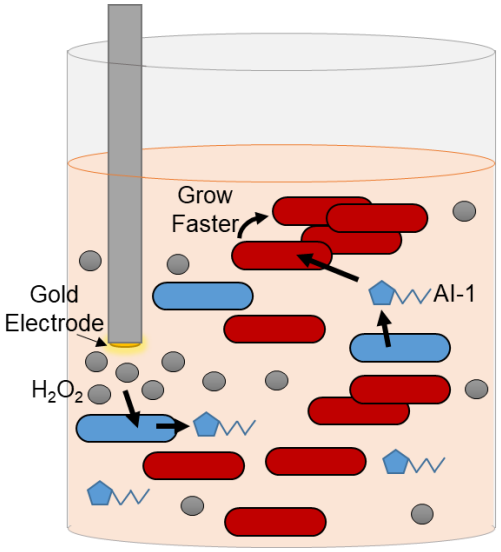

Figure 7.1. Scheme for electronic control of cell growth rate through hydrogen peroxide generation.

Hydrogen peroxide is generated at the surface of a gold electrode. The relay cells (blue) detect hydrogen peroxide and synthesize AI-1 in response. The control cells (red) detect AI-1 which causes transcription of *ptsH* causing the cells to grow faster. Note that counter and reference electrodes are not shown here for simplicity.

In this work, we design and characterize the relay strain. Then, we co-culture the relay and controller strains, and we demonstrate the ability to increase cell growth

rate of the controller strain by applying an electric potential using a gold electrode. In doing so, we also demonstrate electrical alteration of the resulting co-culture composition.

7.2 Results

7.2.1 Design and characterization of the "relay" cell

The relay population was designed to detect hydrogen peroxide and respond by synthesizing AI-1. Plasmid pOxyRS-LasI contains *lasI*, which synthesizes AI-1, under the hydrogen peroxide-sensitive *oxyS* promoter (**Figure 7.2a**). A second construct contained *lasI-ssrA* in place of *lasI*. We hypothesized that the addition of an ssrA degradation tag[190], for increased cellular degradation of LasI, would allow the strain to be turned on or off. To test the construct, NEB10β with plasmid pOxyRS-LasI (or LasI-ssrA) were inoculated to a starting OD of 0.025 in M9 media with or without 25 μM hydrogen peroxide (**Figure 7.2b**). Every thirty minutes, samples were collected to measure extracellular AI-1 levels. The construct that did not contain the degradation tag, showed high background levels of AI-1 resulting in a low signal to noise ratio. However, the construct with the degradation tag showed no detectable background AI-1 levels and still showed high levels of AI-1 synthesis when induced. Synthesis of AI-1 appeared to decrease around 60 min, likely due to consumption of the hydrogen peroxide and degradation of LasI. Moving forward we used only the construct with the degradation tag.

We tested whether or not the relay cells could be turned on, off, and back on again. NEB10β containing plasmid pOxyRS-LasI-ssrA were inoculated to OD 0.025 in media with or without 25 μM hydrogen peroxide (**Figure 7.2c**). Each hour, samples were collected for AI-1 measurement, and then the cultures were resuspended in fresh media with or without 25 μM hydrogen peroxide. This was repeated for three hours. The results show that the cells were able to be turned on or off each hour based on hydrogen peroxide addition. For instance, the culture that received no hydrogen peroxide (indicated by a downward red arrow) at the start of each of the three hours did not produce AI-1. The culture that received hydrogen peroxide at the start of the hour (upward green arrow) on each cycle, produced AI-1 during every cycle. Importantly, the culture where the addition or not of hydrogen peroxide was alternated every hour showed an on/off/on response. This also indicates that LasI decreases to negligible levels in less than 60 min with the degradation tag, supporting the data in **Figure 7.2b**.

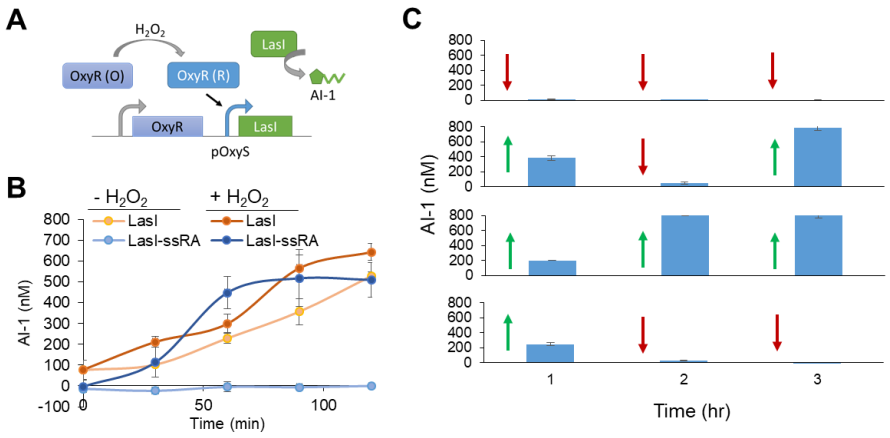

Figure 7.2. Peroxide activates synthesis of AI-1 in relay cells.

a) Scheme of peroxide-induce AI-1 from plasmid pOxyRS-LasI. Hydrogen peroxide reduces OxyR, which then activates the *oxyS* promoter and initiates transcription of *lasI* and subsequent synthesis of AI-1. **b**) AI-1 synthesis in response to hydrogen peroxide was tested in NEB10β with and without an ssrA degradation tag on LasI. NEB10β with plasmid pOxyRS-LasI or pOxyRS-LasI-ssrA were inoculated to a starting OD of 0.025. 0 or 25 µM H_2O_2 were added to cultures as indicated (t = 0). Samples were collected for measurement of extracellular AI-1 every 30 min. Error bars represent s.d. of technical duplicates. **c**) The ability of AI-1 synthesis in the relay strain to be turned on or off was tested by repeatedly resuspending cultures in fresh media with or without hydrogen peroxide. NEB10β pOxyRS-LasI-ssrA were inoculated to OD 0.025, with or without 25 µM hydrogen peroxide. After 1 hour, samples were collected for analysis of AI-1, and then cultures were resuspended in fresh media with or without hydrogen peroxide. One hour later, the cycle was repeated. The red arrows indicate no hydrogen peroxide was added at the beginning of the hour. The green arrows indicates hydrogen peroxide was added at the beginning of the hour. Error bars represent s.d. of technical duplicates.

We next tested our construct in a slow growing strain PH04. PH04 is a *ptsH* knockout, and is deficient in glucose uptake. We hypothesized that by using PH04 as the host, the relay strain would not compete well with other populations for nutrients in the media and would be less likely to overtake the culture if cultured with other populations. Here, we tested whether PH04 pOxyRS-LasI-ssrA could synthesize sufficient levels of AI-1. We compared AI-1 synthesis and cell density overtime in the PH04 and NEB10β hosts (**Figure 7.3**). NEB10β is a commonly used cloning strain and grows more similarly to wild type strains than PH04. Cultures were inoculated to a starting OD of 0.01 and 0 to 50 μM hydrogen peroxide was added. After approximately 5.5 hours, cell density was measured and conditioned media samples were collected for analysis of extracellular AI-1. Hydrogen peroxide resulted in significant synthesis of AI-1 (as expected). PH04 cultures produced less AI-1 than NEB10β cultures. However, both strains produced sufficient AI-1 for signaling to a second population (previous results show that around 100 nM AI-1 produces the maximum response in the controller cells[85]). Importantly, the PH04 relay cells grew to significantly lower cell densities over the 5.5 hours than the NEB10β cells. PH04 densities ranged from OD 0.036 (0 μM H_2O_2) to 0.020 (50 μM H_2O_2), while NEB10β densities ranged from OD 0.946 to 0.098. Hydrogen peroxide addition caused a drop in cell densities. This is contrary to previous results showing that 50 μM hydrogen peroxide addition does not affect cell growth[157]. However, in this study, the authors used a much higher starting cell density, approximately OD 0.5. The difference is

likely due to the low initial cell density of OD 0.01 used here, which will affect the rate that the hydrogen peroxide is consumed and depleted from the media[157].

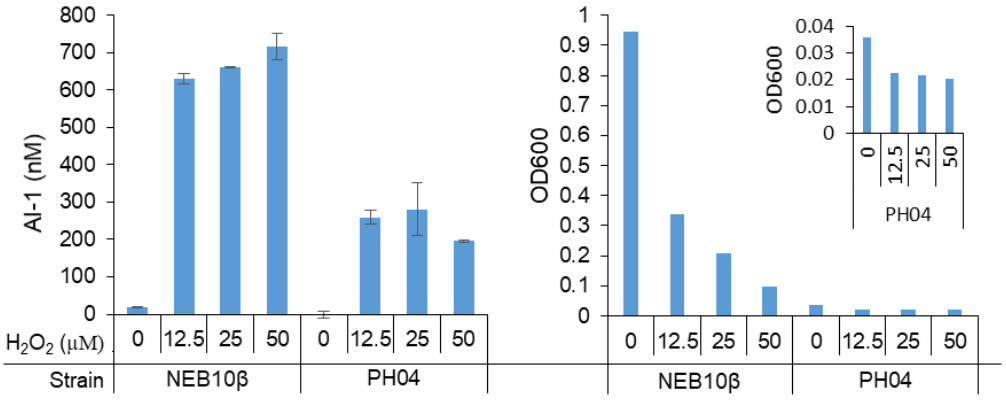

Figure 7.3. Comparison of relay cell behavior in different host strains. NEB10β pOxyRS-LasI-ssrA and PH04 pOxyRS-LasI-ssrA were inoculated to a starting OD of 0.01. Hydrogen peroxide, ranging from 0 – 50 μM, was added to each culture as indicated. After 5.5 hours of growth, samples were collected for measurement of AI-1 levels and cell density (OD600).

7.2.2 Electronic control of cell growth through peroxide generation

To demonstrate electronic control of cell growth rate, we co-cultured the relay cells, PH04 pOxyRS-LasI-ssrA with the growth controller cells, PH04 pAHL-HPr[85] (**Figure 7.4**). We previously showed that the growth rate of this strain increases with increasing AI-1 (up to about 100 nM AI-1). PH04 pAHL-HPr and PH04 pOxyRS-LasI-ssrA were started at initial cell densities of OD 0.01 and 0.04, respectively. The cultures were electrically induced by applying a fixed voltage for a set amount of time. During the electrical induction, a stir bar was used to continuously mix cultures.

An experimental condition with 25 μM hydrogen peroxide instead of an applied charge was used as a control. After induction, all cultures were transferred to an incubator. After 5 hours of growth, samples were collected for measurement of AI-1 levels (**Figure 7.4a**). As expected, applying a charge increased AI-1 levels in the culture. The difference in AI-1 levels between a 900 s and 450 s applied charged was nearly two fold, while increasing the charge length to 1800 s did not have a significant impact.

We expected that the AI-1 would lead to an increased growth rate in the controller strain. We collected samples of the co-cultures 5 hours and 8 hours after induction for measurement of cell density (**Figure 7.4b**) and dsRed fluorescence expression (**Figure 7.4c**). The controller strain constitutively expresses dsRed, so comparison of relative fluorescence (measured with a plate reader) across the cultures should be an indication of higher levels of the controller cells within the co-culture. At 5 hours, induced cultures had increased cell density and dsRed expression relative to uninduced cultures. This trend increased after 8 hours. For the conditions tested, the results appeared to be "on" or "off" rather than a gradient of response; all induced cultures synthesized sufficient AI-1 to fully activate the controller cells. Additional experimental controls were used to test the effect of hydrogen peroxide or application of a charge on cell growth and culture composition independent of AI-1 generation (**Figure 7.4b**, **7.4c**, green bars). In these cultures PH04 pCT6 was used in place of PH04 pOxyRS-LasI-ssrA. In this way, no AI-1 could be generated (due to a lack of *lasI*) and any detrimental effects of hydrogen peroxide or electronic charge on cell growth could be assessed. Neither hydrogen peroxide nor electronic charge had a

significant effect on cell growth. This is contrary to **Figure 7.3**, where similar hydrogen peroxide conditions decreased cell growth rate. However, the total starting density in the co-culture experiment was five times higher than the starting density in the monoculture experiments (**Figure 7.3**), which likely decreased the effect of hydrogen peroxide on cell growth.

After 24 hours of culture, we collected samples and used microscopy and ImageJ analysis to estimate the culture composition. Increases electrical charge resulted in a high fraction of controller cells (expressing dsRed) compared to cultures where no charge was applied (**Figure 7.4d**). This further confirms that the bulk fluorescence measurements obtained with the plate reader are indicative of the fraction of the controller cells in the culture.

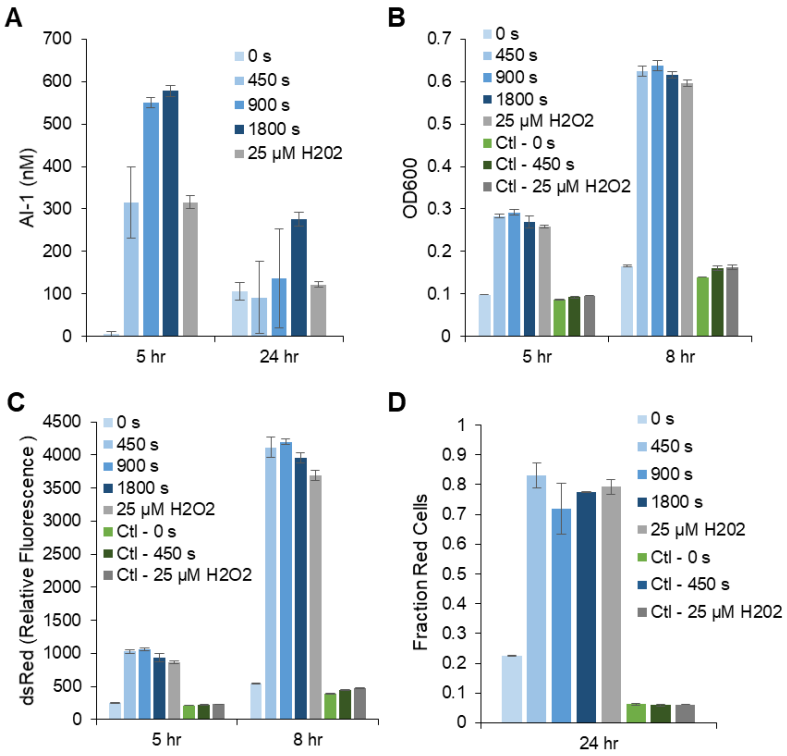

Figure 7.4. Electronic control of cell growth rate.

PH04 pOxyRS-LasI-ssrA (relay cells) and PH04 pAHL-HPr (controller cells) were co-cultured together. The relay and controller cells were inoculated to starting densities of 0.04 and 0.01, respectively. A fixed voltage was applied to the cultures for the amount of time indicated (in seconds). As a positive control, 25 µM hydrogen peroxide was added in place of electric charge. The controls labeled "Ctl" indicate that strain PH04 pCT6 (which cannot synthesize AI-1) was used instead of PH04 pOxyRS-LasI-ssrA to test the effect of charge application or peroxide addition on the cells (independent of AI-1). Time (x-axis) represents the length of time the cultures grew after induction. AI-1 levels (**a**), cell density (**b**), fluorescence measured via a plate reader (**c**), and the fraction of the controller cells measured via microscopy and ImageJ analysis (**d**) are shown. Note that the controller cells constitutively express the fluorescent protein dsRedExpress2. Error bars represent s.d. of biological triplicates.

7.3 Discussion

Electronic modulation of gene expression provides a new avenue for programming and controlling synthetic biology systems. Here, we demonstrate application of a technique for electronic modulation of target gene expression to control cell growth rate. The relay population detects the hydrogen peroxide generated by the electrode and produces a more stable AI-1 signal. This signal alters the growth rate of the controller strain. We saw a significant effect. Electrically induced cultures grew to more than 3 times higher cell density after five hours compared to cultures that were not induced.

The relay population was able to produce sufficient AI-1 to activate the controller cells, even when constructed in a slow-growing host strain and started at a low OD. Importantly, this prevented the relay population from overtaking the culture. It is also possible that the relay cells, by producing AI-1 which could diffuse throughout the culture may allow the controller cells to be activated more uniformly than if *ptsH* was directly modulated by hydrogen peroxide. Currently, whether or not there is a gradient of hydrogen peroxide with the culture (which is stirred during induction) is unclear. However, the AI-1 signal will persist much longer in the culture than the hydrogen peroxide, which may contribute to the significant changes observed in cell growth rate.

We believe this strategy for modulating cell growth rate electrically may be of interest to synthetic biologists. Modulating cell growth rate may provide more control over the level of overexpressed proteins that are produced in synthetic systems. This

strategy also allows for user-modulation of cell growth rate of a *specific* strain within a microbial community. Synthetic biology systems are increasingly made up of multiple populations each performing specific tasks, and the method developed here provides a tool for modulating specific populations within a microbial community. Further, remotely controlled miniature devices for diagnostics and disease treatment have recently generated interest in the field of synthetic biology[191]. The electronic aspect of the system could allow for remote modulation of cell growth rate.

7.4 Materials and Methods

Strains and plasmids

Strains, plasmids, and primers used in this study are listed in Supplementary Tables 1 and 2. Plasmid pOxyRS-LasI and pOxyRS-LasI-ssrA are derived from pOxyRS-LacZ-ssrA (Terrell et al, unpublished). Gibson Assembly (New England Biolabs) was used to insert LasI or LasI-ssrA in place of LacZ-ssrA. Primers OxySv2Assem-R, OxySAssem-F, OxySv2-LasI-F, and LasI-oxyS-R were used to amplify the vector and insert for pOxyRS-LasI. Primers OxySv2Assem-R, ssrA-F, OxySv2-LasI-F, and LasI-ssrA-R were used to amplify the vector and insert for pOxyRS-LasI-ssrA.

Cell culture conditions

Cultures were incubated at 37ºC with 250 rpm shaking. Prior to each experiment, strains were inoculated into LB media from glycerol stocks. After overnight growth, cultures were then re-inoculated into in M9 minimal media (1x M9 salts, 2mM $MgSO_4$, 0.1 mM $CaCl_2$, 0.2%, 0.4% glucose) and grown for at least one

hour. Then, cultures or co-cultures were re-inoculated into M9 minimal media at the desired starting cells densities for the experiments. During electronic induction, cultures remained at room temperature. After induction, cultures were moved to incubator. All media contained 50 μg/mL ampicillin to maintain plasmids.

Electrochemical setup for hydrogen peroxide generation

For electrochemical induction of cultures, 1 mL cultures were placed in a closed glass vial (17x60 mm, Fisher Scientific). The gold standard electrode (1 mm radius, CH Instruments), counter plantinum wire (Alfa Aesar), and Ag/AgCl reference electrode (BASi) were secured by punctured holes in the vial cap. To begin the reaction, the electrodes were positioned near the surface of the liquid culture and biased to -0.5 V vs. Ag/AgCl for variable times. The oxygen reduction current was measured over time to monitor the reaction (generation of hydrogen peroxide). Each sample was continuously stirred using a stir bar. After completion of induction, the culture was transferred to a 2 mL culture tube before being moved to a 37ºC shaker.

Measurement of AI-1

Cell-free experimental conditioned media samples were collected by filtering samples through a 0.2 μM filter. Samples were stored at -20ºC until ready for AI-1 analysis. AI-1 was measured using a fluorescent reporter assay. *E. coli* reporter cells containing plasmid pAL105[141] were grown overnight in LB media. The next day, the reporter cells were diluted 2500x in LB media. The experimental samples were thawed and diluted 5 fold in LB media. Standard curve samples consisting of 0, 12, 24, 36, 48, and 60 nM AI-1 in LB media were generated. 10 μL of experimental or standard curve sample were added to 90 μL of reporter cells. After three hours of

growth at 30ºC, 250 rpm shaking, luminescence values were recorded (Promega GloMAX luminometer). The standard curve was used to calculate the AI-1 level in the assay, and then this number was multiplied by 5 (due to the dilution of sample) to estimate the AI-1 concentration in the original experimental sample.

Measurement of dsRed fluorescence

A SpectraMax M2e plate reader was used to measure bulk dsRed fluorescence in the experimental samples. 200 µL samples were collected from experimental cultures and added to a black wall, clear bottom, 96-well plate. 550 nm and 579 nm were used for the excitation and emission wave lengths, respectively, with a cutoff of 570 nm.

Microscopy and ImageJ were used to estimate the fraction of dsRed-expressing cells in the cultures, using a previously developed method[85]. Briefly, for each sample, bright field images and fluorescent images were taken at four different locations. ImageJ was used to count the cells in the bright field images and the cells in the fluorescent images. The reported fraction is the fluorescent image cell count divided by the bright field image cell count, multiplied by a factor of 1.18 based on the previously developed standard curve.

Chapter 8: Controlling product synthesis in cooperative co-culture with user-modulated culture composition

8.1 Introduction

Metabolic engineers and synthetic biologists are currently investigating novel strategies to expand the repertoire of molecular products synthesized in microbial systems or to control the production of established products[192]. One strategy that continues to gain traction is the use of microbial co-cultures or consortia, where the tasks required to produce a molecular product are divided amongst multiple populations, rather than being carried out by a single population[3, 72]. This allows for division of labor between populations and modularity[193]. Host strains can be optimized for specific tasks. Partitioning a product pathway by splitting it among different populations also provides opportunities to control synthesis of each section of the pathway by controlling culture composition. Importantly, this provides an additional layer of control (as opposed to transcriptional or translational regulation) in increasingly complex synthetic biology and metabolic engineering systems. However, the composition of the culture is a key factor in the behavior of the whole culture and growth differences between populations can be a challenge to using a co-culture strategy. Generally, these co-culture systems could benefit from methods that allow for robust regulation and coordination of subpopulations within the co-culture in order to control the function of the whole consortia.

Previously, we developed a genetic "growth control" module that allowed for autonomous modulation of cell growth rate and culture composition in response to a quorum sensing signal[85]. In our system, upregulation of HPr, a protein involved in sugar transport, in a *ptsH* (encoding HPr) mutant host strain resulted in increased cell growth rate. Similarly, others have regulated the composition of subpopulations in a microbial community by regulating production of lysis proteins or toxins[87, 88]. These strategies have only just begun to be applied by metabolic engineers to co-culture systems that are cooperatively synthesizing a molecular product. That is, there are now many examples of co-cultures being used to synthesize products[73, 129-131, 194, 195], but there are few examples of researchers applying techniques for dynamically modulating the culture composition within these systems despite evidence that the composition is critical to the system behavior. In a recent example, Dinh et al. developed a co-culture for the production of naringenin, where the growth rate of the population responsible for the earlier part of the pathway autonomously decreased after reaching a certain cell density[74].

Here, we show that the growth control module we developed, based on regulation of HPr, can be applied to an *E. coli* co-culture that is cooperatively producing the redox molecule pyocyanin (PYO). Our engineered co-culture is comprised of two cell populations. Population A produces the intermediate phenazine-1-carboxylic acid (PCA) and Population B converts PCA into PYO (**Figure 8.1**). An externally added molecule, autoinducer-1 (AI-1), increases the cell growth rate of the strain containing the growth control module by regulating transcription of *ptsH*. The significance of our design is two-fold. First, we show that a

user-applied signal changes the growth rate of the strain containing the growth control module and subsequently changes the rate of synthesis of the co-culture product PYO. The second significant aspect of our design is that we show that PYO produced by the co-cultures activates a PYO responsive promoter in a third strain, Population C. In this way, PYO can be used as a molecular signal for cell-cell communication in addition to the quorum sensing signals that are already regularly used by synthetic biologists. The lack of orthogonal quorum sensing systems is frequently cited as a limiting factor in engineering synthetic microbial consortia[82]. Further, because the pathway for pyocyanin synthesis requires several genes, we were able to split the pathway between two strains so that the behavior of the PYO responsive strain is dependent on the combined activity and relative levels of both Population A and Population B. This is a new strategy for coordinating cell behavior in multi-population systems.

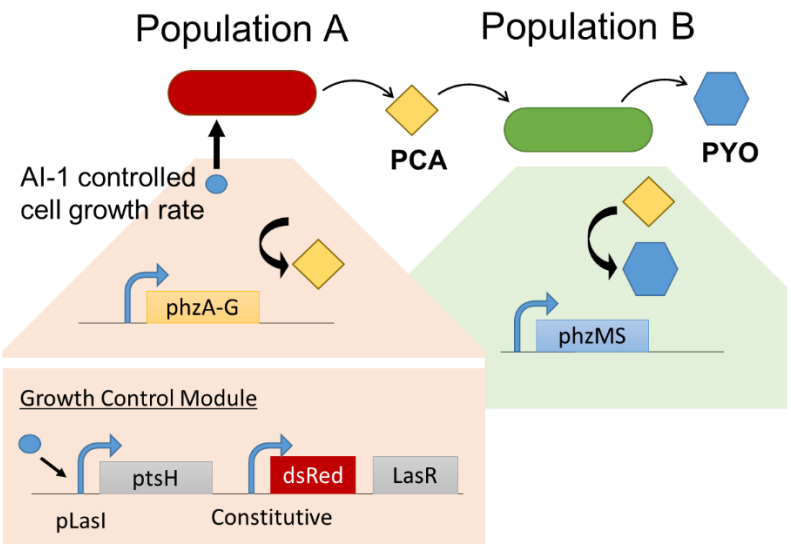

Figure 8.1 Scheme of pyocyanin producing co-culture with growth control module.

Co-culture cooperatively produces PYO. Population A synthesizes the intermediate PCA, using genes *phzA-G*. Population B converts PCA to PYO using genes *phzMS*. The growth control module allows for AI-1 modulation of cell growth rate, allowing for tuning of culture composition between Populations A and B and of the rate of PCA synthesis to the rate of PCA to PYO conversion.

8.2 Results

8.2.1 *E. coli* strains expressing *phzMS* (Population B) convert PCA to PYO

To engineer a co-culture that cooperatively synthesizes pyocyanin, we split the pathway for pyocyanin between two populations. *Pseudomonas aeruginosa* genes *phzA-G* were expressed in Population A and genes *phzMS* were expressed in Population B. This was accomplished previously in *E. coli* in order to assist with

determining the genetic pathway for pyocyanin synthesis[196]. The authors showed that the co-culture synthesized pyocyanin (verified by HPLC), but they did not investigate the dynamics of the co-culture system or the effect of culture composition on pyocyanin synthesis.

We first investigated the ability of Population B to convert PCA to PYO. High copy plasmid pZE-*phzMS* containing *phzMS* under a LacO-1 promoter was transformed into several host strains. 30 μM PCA was added to cultures and, after overnight growth, cell-free conditioned media (CM) samples were collected (**Figure 8.2a**). The CM samples were added to pyocyanin reporter cells to determine the presence of pyocyanin. The reporter cells express the fluorescent protein dsRed regulated by the *soxS* promoter, which responds to pyocyanin. All strains containing *phzMS* converted PCA to PYO. Importantly, reporter cells did not respond to CM from strains that did not express *phzMS*, but were cultured with PCA. We then tested the ability of strain PH04 pZE-phzMS to convert varying levels of PCA to PYO. We grew PH04 pZE-phzMS in media with 0 to 40 μM PCA, and after overnight growth, collected CM. We used the fluorescent reporter cells to determine relative PYO activity (**Figure 8.2b**). Increasing PCA levels resulted in increasing PYO synthesis. At the concentrations tested, there did not seem to be a factor limiting PCA conversion, even at the higher concentrations tested.

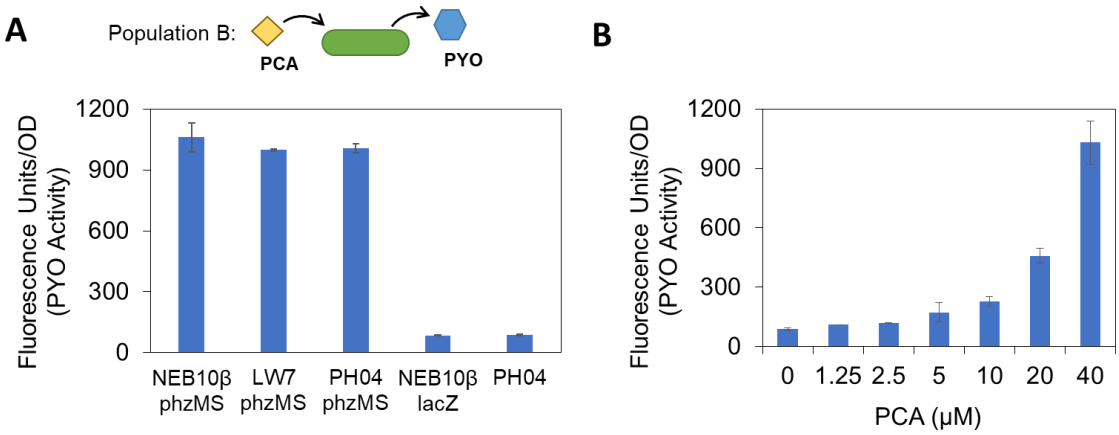

Figure 8.2 Population B converts PCA to PYO.

a) NEB10β, LW7, and PH04 host strains containing pZE-phzMS, pZE-lacZ, or no plasmid (as indicated) were grown in M9 media with 30 μM PCA. Cultures were inoculated 1% (to approximately 0.05 OD) from overnight cultures and PCA was added during inoculation. After overnight growth, CM was collected and tested in a PYO reporter assay using fluorescent reporter cells. **b**) PH04 pZE-phzMS was inoculated 1% from overnight cultures. One hour after inoculation, varying amounts of PCA (ranging from 0 to 40 μM) were added to the cultures. After overnight growth, CM samples were collected. Samples were diluted 5x in LB media, and PYO activity in the diluted samples was measured using the reporter bioassay. The values reporter are the relative fluorescence units divided by the cell density (OD600) of the reporter cells. Error bars represent s.d. of technical duplicates.

8.2.2 Co-cultures of Populations A and B produce PYO and modulate behavior of PYO sensitive strain

Next, we investigated whether co-culturing Population A strains with Population B strains resulted in PYO production. Population A strains contained plasmid pZE-phzAG comprising *phzAG* under a LacO-1 promoter. We cultured NEB10β pZE-phzAG and NEB10β pZE-phzMS, alone or together. (**Figure 8.3A**). Similarly, we grew PH04 pZE-phzAG and PH04 pZE-phzMS, alone or together. PH04 is a *ptsH* knockout strain, which facilitated later addition of the growth control module. After overnight growth, we took cell-free CM from the cultures and tested for extracellular PYO using the fluorescent reporter cell assay. The co-cultures resulted in high levels of fluorescence while the monocultures did not, indicting only the co-cultures were able to produce PYO.

Next, we tested adding a pyocyanin-responsive strain, Population C, directly to co-cultures producing PYO. Here, we sought to illustrate the use of pyocyanin as a tool for cell-cell signaling in synthetic biology systems. We grew NEB10β pZE-phzAG (Population A) and NEB10β pZE-phzMS (Population B) in LB media. We started with different initial ratios of Population A to Population B. After 5 hours of growth, we added a third population (PH04 pSox-LasI, Population C). This population produces AI-1 in response to PYO. One hour after adding Population C, we took samples and measured AI-1 activity in the extracellular media using a previously developed AI-1 reporter bioassay. The results (**Figure 8.3B**) show that Population C responded to PYO in the co-cultures by producing AI-1. Cultures without either Population A or Population B resulted in no AI-1 production in

Population C. Thus, we demonstrate that PYO has potential to be used for cell-cell signaling in synthetic biology systems in addition to frequently used quorum sensing molecules. PYO has several roles in its native host, *P. aeuroginosa*, including as a potential signaling molecule[197]. However, here we show that PYO producing sender and PYO responding receiver cells can be developed in the common laboratory *E. coli* strains. The data also shows that the level of AI-1 produced in the culture varied based on the initial ratio of Population A to Population B. This demonstrates that the culture composition affects the rate of PYO synthesis. Further, the relative levels of Population A and B affected the behavior of Population C. Interestingly, we were able to achieve this by using PYO as a signaling molecule, because the synthesis pathway is multi-step and could be split between two different populations.

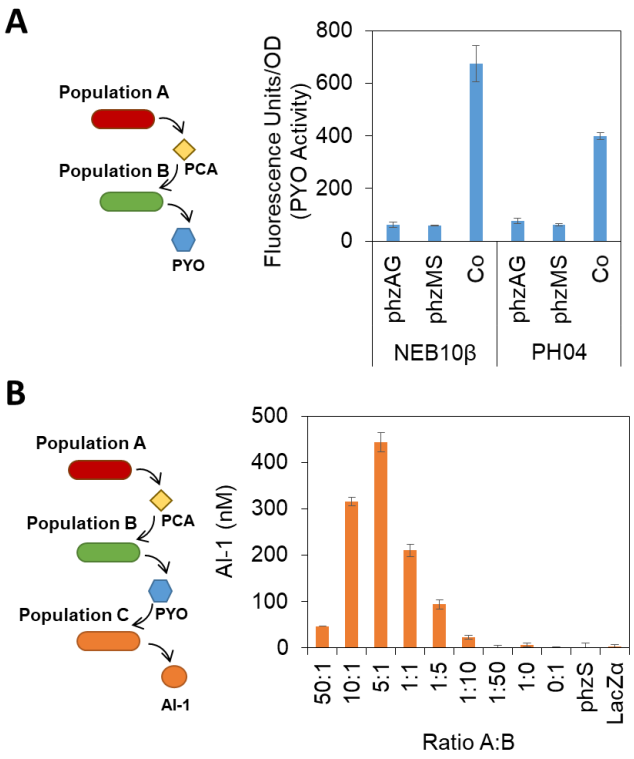

Figure 8.3 Population A and B co-cultures produce PYO.

a) NEB10β pZE-phzAG and NEB10β pZE-phzMS were cultured alone or together. Similarly, PH04 pZE-phzAG and PH04 pZE-phzMS were cultured alone or together. After overnight growth in M9 media, CM media was collected. PYO activity was assessed using the fluorescent reporter assay. **b**) NEB10β pZE-phzAG (Population A) and NEB10β pZE-phzMS (Population B) were co-cultured in LB media. After 5 hours of co-culture, PH04 pSox-LasI (Population C) was added to the co-cultures. After 1 additional hour of culture, CM samples were taken. An AI-1 reporter assay was used to measure the extracellular AI-1 levels in the culture. The controls "phzS" and "LacZα" indicate growth of monocultures NEB10β pZE-phzS or NEB10β pZE-lacZα, respectively, prior to addition of Population C.

8.2.3 Growth control module for user-modulated growth rate in Populations A and B

Having demonstrated that *E. coli* co-cultures expressing *phzA-G* and *phzMS* produce PYO, and that the culture composition likely affects the rate of PYO synthesis, we next sought to add our previously developed growth control module to either Population A or B in order to allow for user-modulated cell growth rate of either subpopulation. The growth controller module contains *ptsH* under the *lasI* promoter and *lasR* under a constitutive T5 promoter. AI-1 addition upregulates HPr (encoded by *ptsH*), which increases cell growth rate in a *ptsH* mutant host strain. Here, we added these components to the pZE-phzAG and pZE-phzMS plasmids to create plasmids pZE-phzAG-ptsH and pZE-phzMS-ptsH. We transformed these plasmids into the *ptsH* mutant strain PH04. We then grew PH04 pZE-phzAG-ptsH and PH04 pZE-phzMS-ptsH (separately) in M9 media with glucose, and tested whether AI-1 addition changed the culture growth rate (**Figure 8.4**). As expected, increasing AI-1 levels resulted in increasing cell growth rate. The expression of the *phz* operon genes did not interfere with the function of the growth control module.

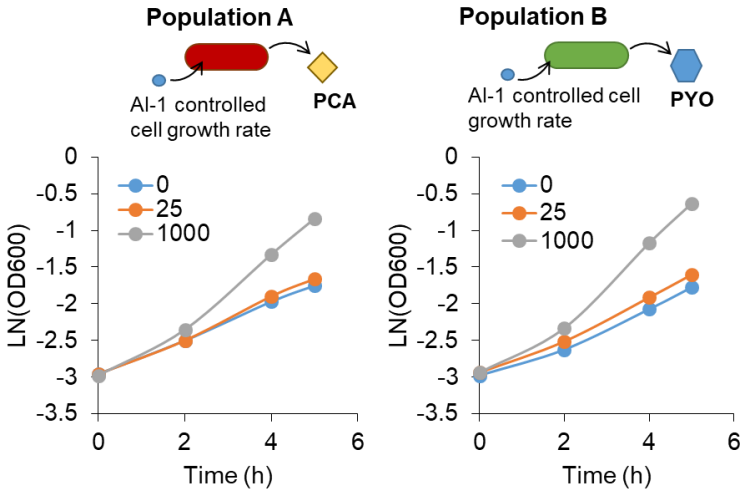

Figure 8.4 Growth control module enables regulation of cell growth rate in Populations A and B.

PH04 pZE-phzAG-ptsH (left panel) and PH04 pZE-phzMS-ptsH (right panel) were grown in M9 media with glucose. Either 0, 25, or 1000 nM AI-1 (as indicated) were added at t = 0. Cell density was recorded over time.

8.2.4 Co-culture PYO synthesis is modulated by tuning cell growth rate

We then tested co-cultures of Populations A and B, where Population A contained the growth control module. We grew Population A (PH04 pZE-phzAG-ptsH) and Population B (PH04 pZE-phzMS) in M9 media with glucose. The experiment was conducted with two different initial ratios of Populations A to B, 20 to 1 and 100 to 1. We added different concentrations of AI-1 one hour after inoculation. Then, after overnight growth, we collected conditioned media to test for extracellular pyocyanin using the fluorescent reporter assay. **Figure 8.5** shows fluorescence, indicative of PYO, in the reporter cells. Increasing AI-1 levels increased

the level of PYO produced in the overnight co-culture. The fold change in PYO produced is nearly 5 fold between the cultures without AI-1 and with 1 µM AI-1. This fold change holds true for the cultures that started with a 20:1 ratio and the cultures that started with a 100:1 ratio. This suggests that our ability to change the PYO synthesis of the co-culture by AI-1 addition (which modulates Population A growth rate) has a highly significant effect.

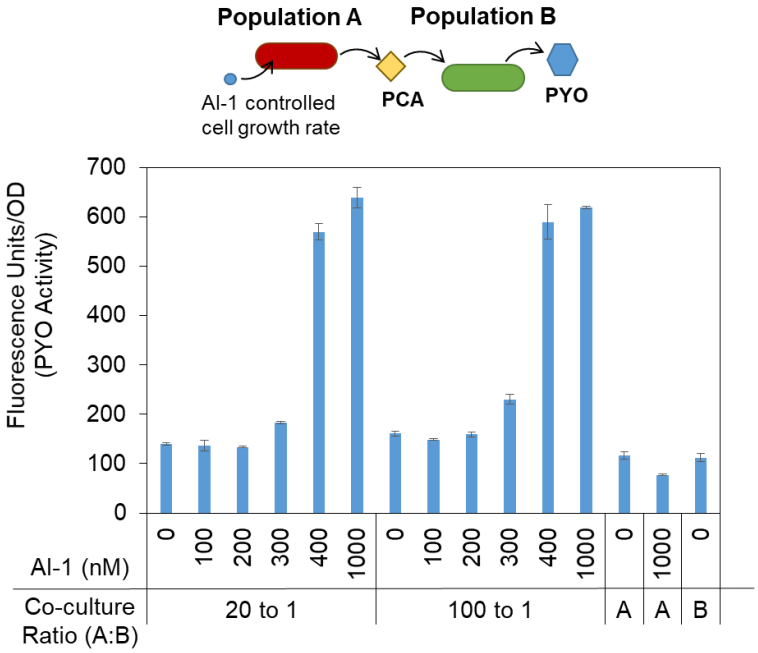

Figure 8.5. Regulating PYO synthesis in co-culture through modulation of Population A growth rate.

PH04 pZE-phzAG-ptsH and PH04 pZE-phzMS were co-cultured together with the initial inoculation ratios indicated. One hour after inoculation, the indicated concentration of AI-1 was added. After overnight growth, CM samples were collected and PYO activity was tested using the fluorescent reporter assay.

8.3 Discussion

In sum, we demonstrated the application of a method for user-controlled cell growth rate towards a co-culture that is cooperatively producing pyocyanin. We demonstrate modulation of pyocyanin synthesis by modulating growth rate of the PCA synthesizing strain, as opposed to directly regulating transcription in either strain. This strategy is likely to be broadly applicable as pyocyanin is derived from the shikimate pathway, a common starting point for many molecular products[198]. Strategies for modulating culture composition may further enable use of co-cultures by metabolic engineers and synthetic biologists. We also show that PYO can be used in *E. coli* as a molecule for cell-cell communication. By splitting the pathway for PYO synthesis between two populations, the behavior of the receiver or PYO modulating strain is dependent on the composition of the PYO producing strains. We believe the strategies developed here could be useful for many applications including for coordinating co-cultures that are synthesizing a product and for engineering cooperativity in synthetic biology systems.

8.4 Materials and Methods

Strains and Plasmids

The strains, plasmids, and primers used in this study are listed in Supplementary Tables 1 and 2. Plasmids pZE-phzAG, pZE-phzMS, and pZE-lacZα are derived from the commercial vector pZE12MCS (ExpresSys), a high copy colE1 origin plasmid. Each plasmid contains the genes of interest under the LlacO-1 promoter in the vector. The phzAG, phzM, and phzS genes were amplified from *P.*

aeuruginosa PA01 using primers KpnI-phzA1-FWD and HindIII-phzG1-RS, HindIII-phzM-FWD and HindIII-phzM-RVS, and KpnI-HindIII-RBS-phzS-FWD and BamHI-phzS-RVS, respectively. The *phzA1-G1* fragment and the pZE12MCS vector were digested with KpnI and HindIII, and ligated to form pZE-phzAG. Plasmid pZE-phzMS was cloned in a multi-step process. When amplifying *phzS* a ribosomal binding site was placed upstream of *phzS* along with KpnI and HindIII restriction digestion sites. A BamHI restriction digestion site was added downstream of *phzS*. This fragment and the pZE12MCS vector were digested with KpnI and BamHI restriction enzymes, and ligated to form pZE-phzS. Then, the *phzM* fragment and pZE-phzS were digested with the HindIII restriction enzyme, and ligated to form plasmid pZE-phzMS.

To construct plasmid pZE-lacZα, *lacZα* was amplified from a wild type *E. coli* strain (W3110 derivate), using primers KpnI-lacZalpha-FWD and BamHI-lacZalpha-RVS. The fragment and pZE12MCS vector were digested with KpnI and BamHI restriction enzymes, and ligated.

Plasmids pZE-phzAG-ptsH and pZE-phzMS-ptsH were generated by adding the growth control module to the pZE-phzAG and pZE-phzMS plasmids. The growth control module, consisting of *ptsH* under the *lasI* promoter and dsRedExpress2 and *lasR* under a constitutive T5 promoter, was amplified from pAHL-HPr. Primers PciI-t7-term-rvs and PciI-ptsH-rvs were used to amplify the control module and add a PciI restriction digestion site on either end of the fragment. Restriction digestion and ligation were used to insert the fragment into the pZE12MCS vector at the PciI restriction digestion site.

Cell culture conditions

LB media was used for cloning and overnight growth of cultures inoculated from glycerol stocks. M9 minimal media (1x M9 salts, 2mM $MgSO_4$, 0.1 mM $CaCl_2$, 0.2%, 0.4% glucose) or LB media was used for experiments as indicated in the figure captions. Cultures were grown at 37ºC with 250 rpm shaking. Ampicillin (50 µg/mL) and/or kanamycin (50 µg/mL) was used to maintain plasmids.

PYO fluorescent reporter assay

A fluorescent reporter assay was used to quantify PYO in experimental samples. CM samples were collected by filtration through a 0.2 µM filter and stored at -20ºC until analysis. The fluorescent reporter cells, SW101 pCT10 pET-dsRED, consist of a dual plasmid system (curtesy of Sally Wang). A single copy plasmid contains the pyocyanin sensitive *soxS* promoter. T7 polymerase is under the *soxS* promoter and activates dsRed on the high copy pET plasmid.

For the assay, reporter cells were reinoculated in LB media from overnight cultures and grown to approximately 0.2 OD. 180 µL of reporter cells and 20 µL of sample were added together in 96 well, black wall, clear bottom plates. Cultures were grown at 30ºC, 250 rpm shaking for approximately 4 hours. A SpectraMax M2e plate reader was used to read dsRed fluorescence and OD600. For fluorescence, the excitation wavelength was 550 nm, the emission wavelength was 579 nm, and a cutoff of 570 nm was used. The reported value was divided by the cell density (OD600).

AI-1 luminescent reporter assay

To measure extracellular AI-1, cell-free conditioned media samples were collected. *E. coli* AI-1 reporter cells with plasmid pAL105[141] were grown overnight in

LB media, and then diluted 2500 fold in fresh LB media. 10 µL of samples were added to 90 µL of reporter cells. If necessary, samples were diluted prior to the assay to be in the linear range of the assay. Samples making up a standard curve of known AI-1 concentrations 0, 12, 24, 36, 48, and 60 nM AI-1 were also added to the reporter cells. After three hours, luminescence was recorded. A linear fit was used to determine the standard curve, which was then used to calculate the AI-1 in the experimental samples. If the experimental samples were diluted prior to the assay, the results were multiplied by the dilution factor (usually 5 or 10) to back calculate to the AI-1 in the original sample.

Chapter 9: Summary and Future Directions

9.1 Conclusions

The dissertation research presented here describes investigations into the AI-2 QS process and explores methods for manipulating populations within microbial communities using cell-cell communication processes.

In Chapter 3, we discovered an interaction between the phospotransferase system (PTS) protein HPr and the AI-2 kinase, LsrK. This interaction is highly significant since HPr is involved in sugar uptake, including glucose, and is therefore part of a major metabolic process in the cell. We found that HPr inhibits LsrK activity, and that the phosphorylation state of HPr likely affects the extent of this inhibition. The data suggest bacteria have sophisticated methods to incorporate metabolic information into QS processes. This work was part of a collaboration with Dr. Kyoung-Seok Ryu and is published in *Science Advances*[33].

In Chapter 4, we manipulate cell response to AI-2 by both deleting genes that metabolize AI-2 (LsrFG) and overexpressing genes that increase AI-2 uptake (LsrK, LsrACDB). This led to a suite of reporter cells that have varied cell to response to AI-2. This suite of cells may be useful for interrogating AI-2 in native environments. This work led to a co-first author publication, with Amin Zargar, in *Biotechnology Progress*[170].

In Chapter 5, we then shifted focus to engineering control over bacterial co-cultures. Here, we designed a co-culture where one strain detects AI-2 and then secretes a signal in order to modify the growth rate of a second strain. The

composition of the co-culture follows a different trajectory based on the level of AI-2 initially in the environment. The demonstration of an engineered co-culture that responds to an important molecular cue by changing culture composition is a significant advancement to the synthetic biology field. This work led to a first author publication in *Nature Communications*[85].

In Chapter 6, we developed a programmable, dual-input AI-2 QS circuit. We used stronger, mutated versions of the *lsr* promoter in combination with controllable, induced expression of the repressor LsrR. We developed a model of the system that accounted for variations in promoter strength and took into account the inducible LsrR expression. We found that the model closely fit the experimental data over time for different *lsr* promoter activities. My main contribution to this work was conception and design of the mathematical model. This work is currently unpublished. I also contributed by assisting with characterization of the mutated *lsr* promoters, which were first described in an earlier manuscript published in *Nucleic Acids Research*[37]**.**

In Chapter 7, we built off the idea of QS signal controlled cell growth rate developed in Chapter 5, and we engineered electronic control of cell growth rate through generation of hydrogen peroxide at an electrode surface. We saw significant changes in cell growth. This suggests potential to remotely control cell-growth or culture composition in microbial communities via a wirelessly connected device. Further, we demonstrate control over a major cellular process using electronics. The work in this chapter was partially inspired by two other recently submitted

manuscripts that I contributed to, where target gene expression is controlled electrically and quorum sensing processes are used to enable cell-cell communication.

In Chapter 8, we demonstrate the application of the growth control module towards a co-culture that is cooperatively producing the redox molecule pyocyanin. We show that the growth control module can be used to adjust the growth rate of one of the strains, and subsequently alter the rate of synthesis of pyocyanin by the co-culture. This is significant, because although the importance of culture composition in co-cultures that are cooperatively producing a product is understood, few tools exist to dynamically change the culture composition. We further show that the pyocyanin produced can signal to a third strain, altering the behavior of the third strain based on the composition of the first two strains.

9.2 Future Directions

There are many exciting future avenues that could be pursed based on or inspired by this dissertation research. In regards to the AI-2 QS system, the mathematical model of the QS process developed here could easily be adjusted to explore *in silico* different genetic circuit designs in order to engineer varied cell responses to AI-2. Further, the AI-2 sensitive strains developed throughout this work could be used to interrogate or manipulate AI-2 in natural environments such as the GI tract. The discovery that *ptsH* knockout strains are able to uptake AI-2, even in the presence of glucose, may provide useful or interesting avenues to manipulate AI-2 QS processes in different environments which may have glucose. This ability to

uptake AI-2 in the presence of glucose could be turned on or off, expanding the programmability of synthetic biology systems using AI-2.

Chapters 5,7, and 8 demonstrated the utility of using signal modulated transcriptional regulation of *ptsH* to control cell growth rate, and also demonstrate the robustness of this strategy. This strategy could be applied by metabolic engineers to a co-culture system that is synthesizing a product where problems may arise due to differences in growth rate between the strains or an inability to control the composition of the co-culture. It would be interesting to investigate whether the control module would still work in different environments such as the GI tract (or model GI tract) or a continuous culture.

Finally, the development of the *E. coli* PCA and PYO producing strains in Chapter 8 are likely to inspire new strategies for connecting biology with electronics. Since both of these molecules are redox active, they have the potential to be measured electrochemically. Further, the promoter controlling the transcription of the genes required for PCA or PYO synthesis could likely be switched for a variety of promoters that are activated by molecules of interest. This would essentially allow electrochemical detection of the presence specific molecules. A similar idea has been explored, where the synthesis of LacZ can be detected electrochemically[199, 200]. Production of PCA or PYO may allow electrochemical monitoring of the activity of more than one promoter if used alongside LacZ production.

Appendices

Appendix A: Supplementary Information for Chapter 3

Chapter 3 Supplementary Tables

Supplementary Table 1: Strains and plasmids used in Chapter 3.

Strains	Genotype	Source
E. coli		
DH5α	Cloning strain	New England Biolabs
ZK126	W3110 Δ*lacU169 tna-2*	[201]
LW7	W3110 Δ*lacU169 tna-2* Δ*luxS*::Kan	[32]
PH01	W3110 Δ*lacU169 tna-2* Δ*ptsH*::Cm	[33]
PH02	W3110 Δ*lacU169 tna-2* Δ*luxS*::Kan Δ*ptsH*::Cm	[33]
V. harveyi		
BB170	BB120 luxN::Tn5 (sensor 1^- ,sensor 2^+), Km^r	[115]
Plasmids	**Relevant Property**	**Source**
pSkunk	p15a origin, f1 origin, AadA streptomycin/spectomycin resistance, and tac promoter	[113]
pLW11	pFZY1 derivative, containing *lsrACDBFG* promoter region	[33]

Appendix B: Supplementary Information for Chapter 4

Chapter 4 Supplementary Figures

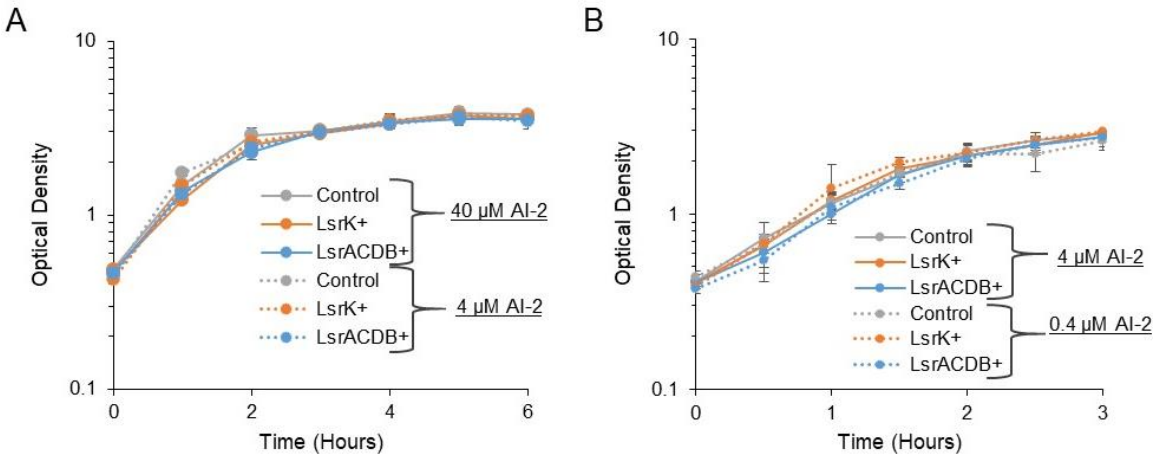

Supplementary Figure 1. Growth Curves

Growth curves of MDAI2 (**A**) and CT104 (**B**) with plasmids pCT6 and either pET (Control), pET-LsrK (LsrK+), or pET-LsrACDB (LsrACDB+). Each culture was grown to approximately OD_{600} 0.4 at which time cultures were supplemented with indicated AI-2 concentrations (t = 0 hr). Optical density was recorded over time. Error bars represent standard deviation of biological triplicates.

Chapter 4 Supplementary Tables

Supplementary Table 1: Strains and plasmids used in Chapter 4.

Strains	Genotype	Source
E. coli		
MDAI2	W3110 luxS::Tcr, W3110-derived luxS mutant strain	[202]
CT104	W3110 luxS::Tcr, lsrFG-, W3110-derived luxS, lsrFG mutant strain	[95]
V. harveyi		
BB170	BB120 luxN::Tn5 (sensor 1^- ,sensor 2^+), Km^r	[115]
Plasmids	**Relevant Property**	**Source**
pCT6	pFZY1 derivative, containing lsrR and lsrR promoter region fused with T7RPol, Ap^r	[36]
pET200/D-TOPO	Cloning vector, containing T7 promoter, Km^r	Invitrogen
pET-LsrK	pET200 derivative containing LsrK, Km^r	[28]
pET-LsrACDB	pET200 derivative containing LsrACDB, Km^r	[28]
pET-sfGFP	pET200 derivative, containing sfGFP, Km^r	[28]
pET-sfGFP-LsrK	pET-LsrK derivative, containing sfGFP upstream of LsrK sequence, Km^r	[28]
pET-sfGFP-LsrACDB	pET-LsrACDB derivative, containing sfGFP upstream of LsrACDB sequence, Km^r	[28]

Appendix C: Supplementary Information for Chapter 5

Chapter 5 Supplementary Figures

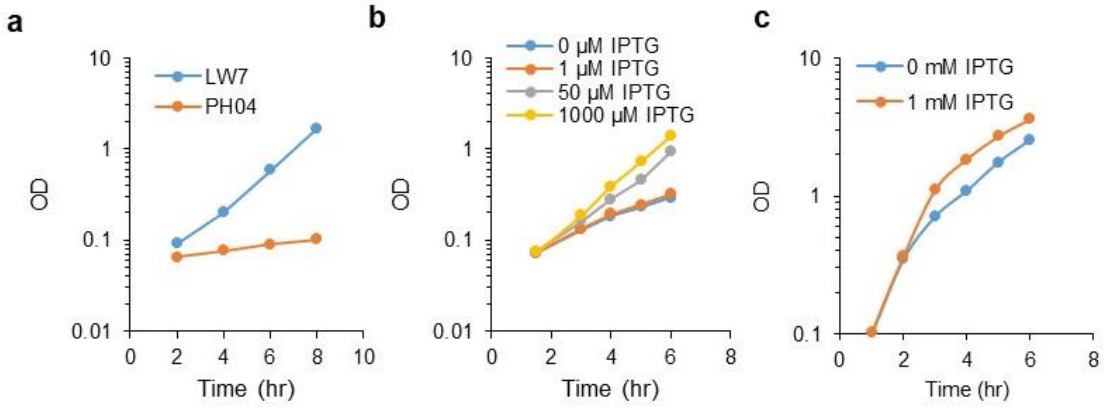

Supplementary Figure 1. Regulating cell growth rate through HPr.

(**a**) Growth curves of LW7 (W3110 Δ*luxS* Δ*lacZ*) and PH04 (W3110 Δ*luxS* Δ*lacZ* Δ*ptsH*) in M9 media (0.8% glucose). (**b**) Growth curves of PH03 (W3110 Δ*lacZ* Δ*ptsH*) pTac-HPr (containing *ptsH* under *tac* inducible promoter) induced with varying levels of IPTG supplemented at $t = 0$. Cultures grown in M9 media (0.8% glucose, 0.2% casamino acids). (**c**) Growth curves of PH03 pTac-HPr in LB media with and without IPTG (induced at $t = 0$). One biological replicate is shown in each panel.

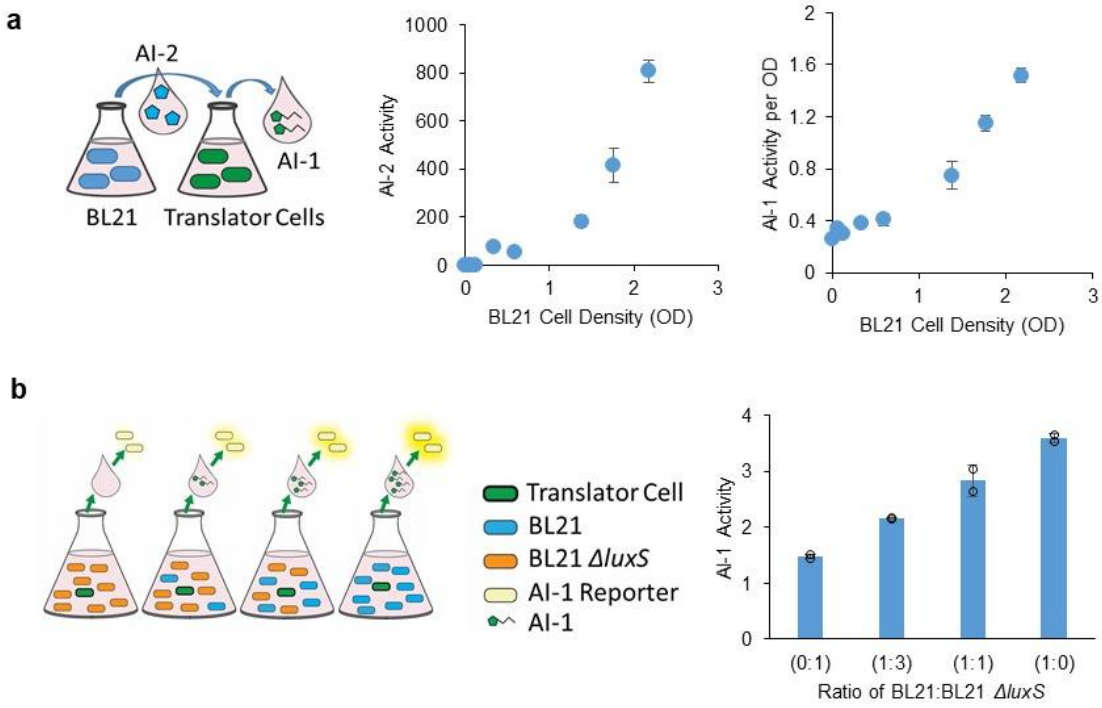

Supplementary Figure 2. AI-2 producing cells activate AI-1 synthesis in translator cells.

(a) BL21 cells were grown in LB media. At various cell densities, CM samples were collected to measure AI-2 activity (left panel). CT104 pCT6 pLasI translator cultures were grown to OD 0.1, resuspended in CM from the BL21 cultures and AI-1 activity per translator cell OD was measured after five hours (right panel). Error bars represent s.d. of technical duplicates. **(b)** CT104 pCT6 pLasI translator cells were added to consortia composed of varying ratios of BL21 (produces AI-2) to BL21 *ΔluxS* (does not produce AI-2) in LB media. Combined BL21 and BL21 *ΔluxS* initial OD was approximately 0.25 and initial translator OD was 0.02. After 5 hours CM samples were taken to measure AI-1 activity. Error bars represent s.d. of technical duplicates.

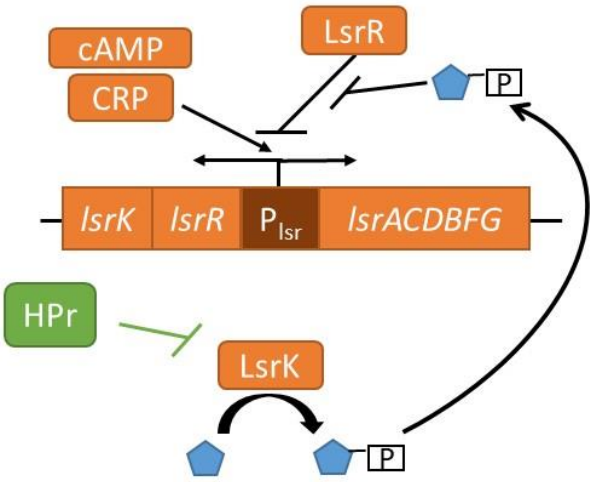

Supplementary Figure 3. Scheme of AI-2 pathway.

In the native AI-2 quorum sensing system, LsrACDB transports AI-2 into the cell. LsrK phosphorylates AI-2, which subsequently causes derepression of the *lsr* promoter by LsrR and transcription of the *lsr* operon. This creates a positive feedback loop and additional uptake of AI-2. LsrFG degrade the phosphorylated AI-2 signal. The *lsr* promoter is also partially regulated by global regulators cAMP/CRP that are affected by the availability of glucose. In addition, the PTS protein HPr (involved in sugar transport into the cell) has been shown to interact with LsrK and inhibit LsrK activity[33].

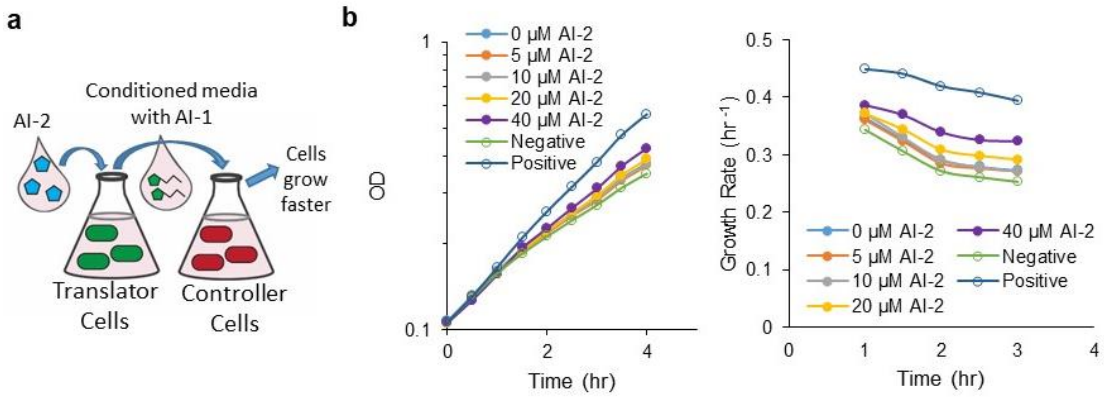

Supplementary Figure 4. Translator cells regulate controller cells based on initial AI-2 level.

(**a**) Schematic of process for conditioned media experiments. Translator cells (PH04 pCT6 pLasI) are grown with varying levels of AI-2. Conditioned media from translator cells is added to controller cells (PH03 pAHL-HPr). (**b**) Growth curves and growth rates of controller cultures grown in M9 media supplemented with conditioned media from translator cells. Translator cells were grown for 3 hours with varying levels of AI-2 as indicated. Conditioned media samples from translator cultures were added to controller cultures at a 5% final volume at t = 0. The negative and positive controls used conditioned media from cells not capable of producing AI-1. For the positive control, 2 µM AI-1 was added at t = 0. One biological replicate is shown.

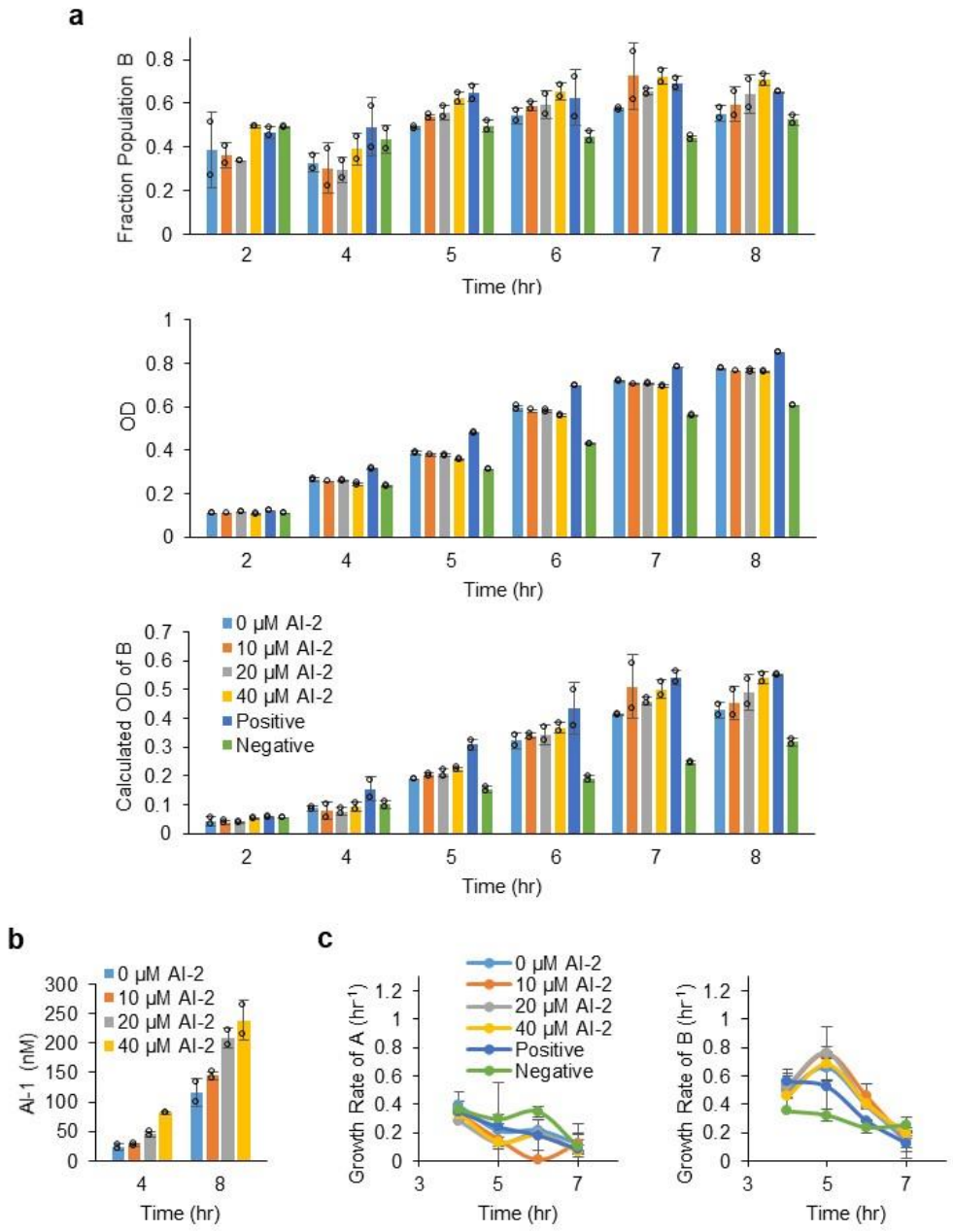

Supplementary Figure 5. Translator cells alter co-culture composition based on AI-2 level.

(**a**) Translator cells (Population A, PH04 pCT6 pLasI) and controller cells (Population B, PH04 pAHL-HPr) were co-cultured in M9 media with varying levels of AI-2. Population B fraction, total culture density, and calculated OD of Population B over

time are shown. Controller cells and translator cells were each inoculated 0.5% from overnight cultures and in media with AI-2 at $t = 0$. For the positive control 1 µM AI-1 was added at the start of the culture. The negative control used PH04 pAHL-sfGFP in place of controller cells. (**b**) Extracellular AI-1 level of co-culture. (**c**) Translator cell and controller cell growth rate in the co-culture. To determine the translator cell density in order to calculate growth rate, the red cell OD was subtracted from the total OD. Error bars represent s.d. between biological duplicates.

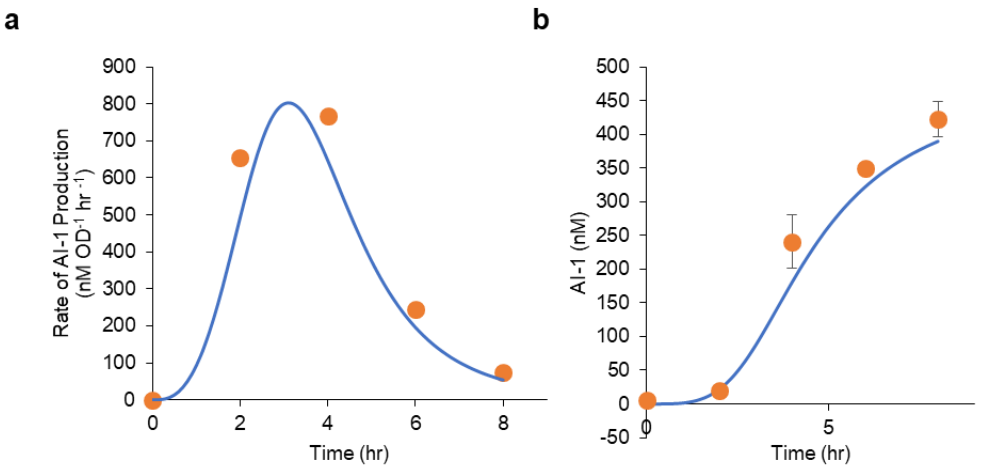

Supplementary Figure 6. Predicting translator cell behavior from co-culture data.

The rate of AI-1 production by the translator cells for an 80 µM AI-2 addition was predicted using co-culture data from Figure 6. To confirm the prediction, translator cells were inoculated to approximately OD 0.05 from overnight cultures in M9 media with 80 µM AI-2 at t = 0. **(a)** The blue line shows the predicted *fAI1* function. The predicted function has the form shown for the *fAI1* functions in Supplementary Table S2, where A = 0, B = 4, C = 3.6, D = 570, and E = 0.5. The dots show the rate of AI-1 production during the translator monoculture experiment. (**b**) The orange dots show the AI-1 level in the translator monoculture with 80 µM AI-2 over time. The blue line shows the simulation results for a translator cell culture using the predicted *fAI1* function. Error bars represent s.d. of technical duplicates.

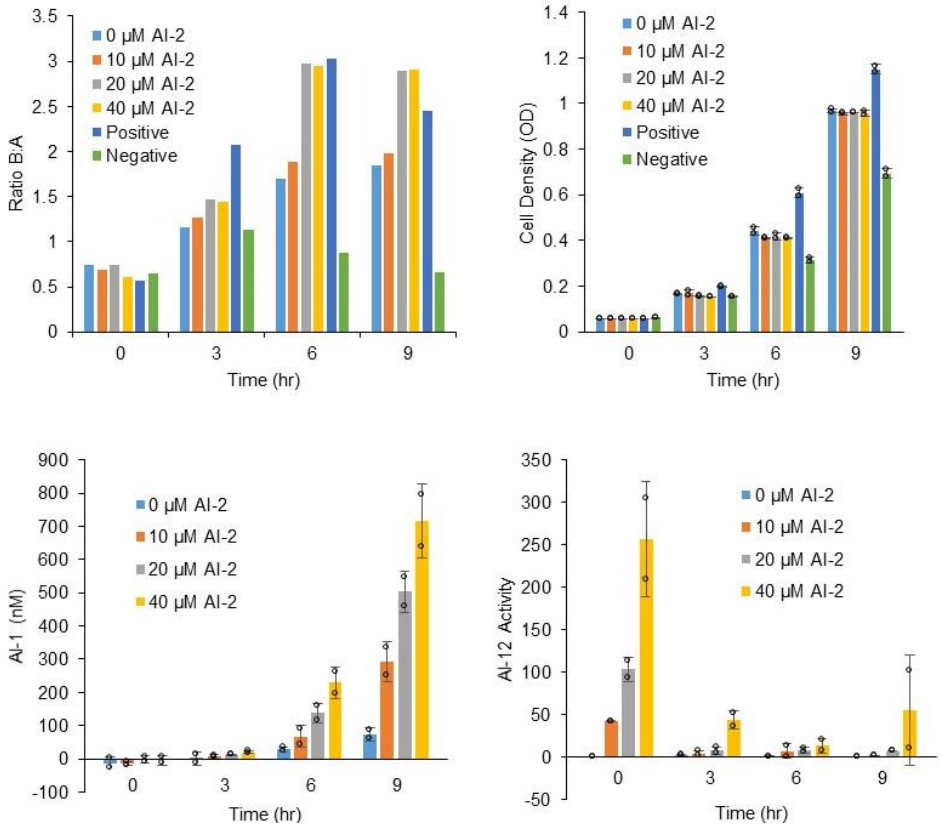

Supplementary Figure 7. Extended co-cultures of translator and controller cells. Populations A and B were each inoculated 0.5% with varying concentrations of AI-2 as indicated. For the positive control, 200 nM AI-1 was added in place AI-2. For the negative control, the AI-1 responsive cells were replaced with a cell line containing sfGFP in place of *ptsH* (PH04 pAHL-sfGFP). Every three hours cultures were spun down and resuspended in fresh media with either AI-2 or AI-1. Samples were collected at $t = 0$ and immediately prior to each resuspension for measurement of fraction Population B and cell density. Ratio of B:A was calculated using the average fraction Population B measurement. CM from experimental cultures were also collected for AI-1 and AI-2 activity measurements. Error bars represent s.d. of biological duplicates.

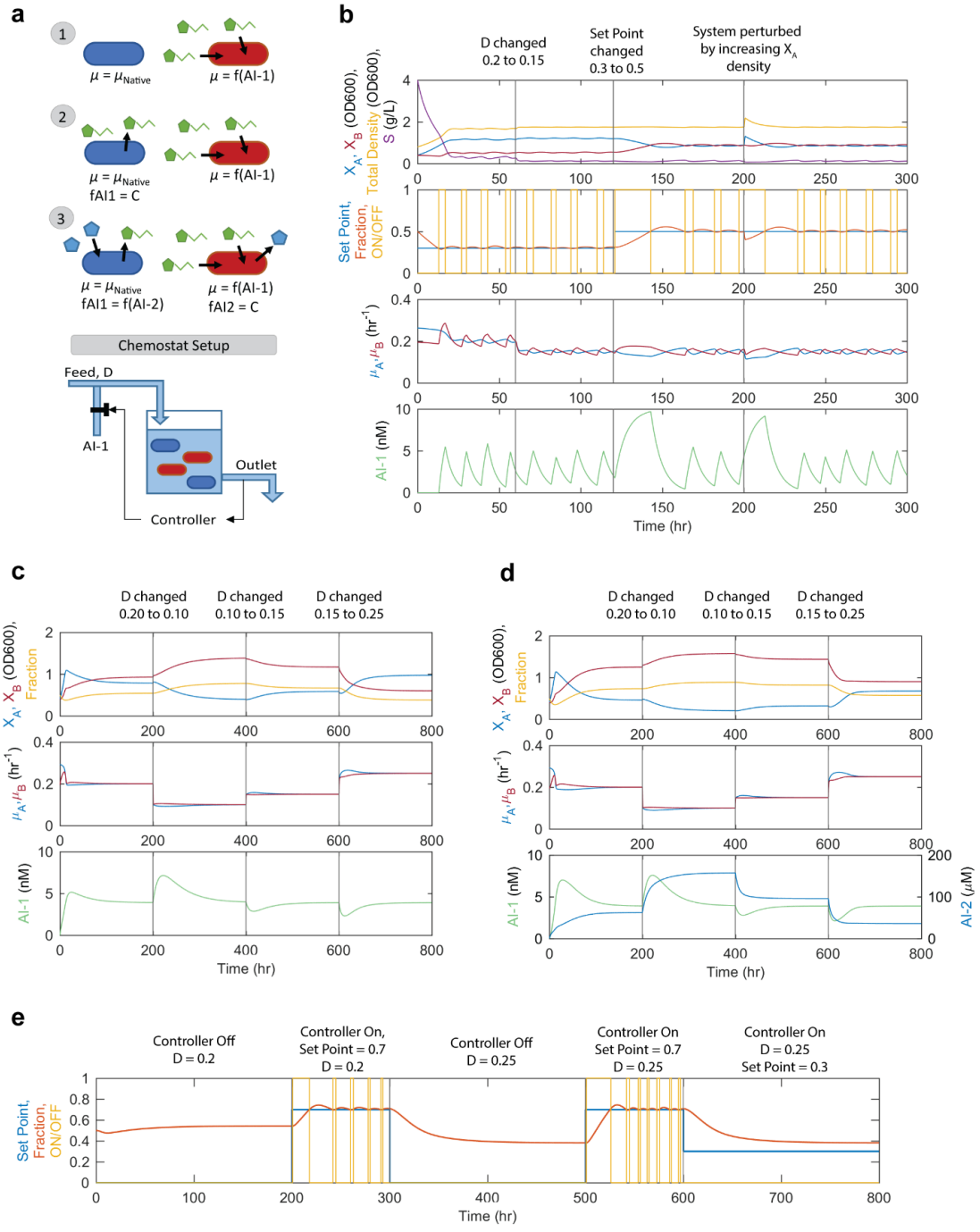
a
1
μ = μNative
μ = f(AI-1)
2
μ = μNative
fAI1 = C
μ = f(AI-1)
3
μ = μNative
fAI1 = f(AI-2)
μ = f(AI-1)
fAI2 = C
Chemostat Setup
Feed, D
AI-1
Outlet
Controller
b
D changed 0.2 to 0.15
Set Point changed 0.3 to 0.5
System perturbed by increasing XA density
XA, XB (OD600), Total Density S (g/L)
Set Point, Fraction, ON/OFF
μA, μB (hr-1)
AI-1 (nM)
Time (hr)
c
D changed 0.20 to 0.10
D changed 0.10 to 0.15
D changed 0.15 to 0.25
XA, XB (OD600), Fraction
μA, μB (hr-1)
AI-1 (nM)
Time (hr)
d
D changed 0.20 to 0.10
D changed 0.10 to 0.15
D changed 0.15 to 0.25
XA, XB (OD600), Fraction
μA, μB (hr-1)
AI-1 (nM)
AI-2 (μM)
Time (hr)
e
Controller Off D = 0.2
Controller On, Set Point = 0.7 D = 0.2
Controller Off D = 0.25
Controller On Set Point = 0.7 D = 0.25
Controller On D = 0.25 Set Point = 0.3
Set Point, Fraction, ON/OFF
Time (hr)

Supplementary Figure 8. Chemostat simulations using various populations and control schemes.

a) Scheme depicting various co-culture designs consisting of Populations A (blue) and B (red). Each population produces QS signals as indicated. The growth rate of Population A is not controlled, but the growth rate of Population B is modulated by AI-1. The co-culture behavior is modeled in a chemostat with a continuous feed into and removal of culture from the reactor set by the dilution rate, D. Each co-culture set can be simulated with a control scheme where the culture composition is sampled hourly, compared to a set point, and a fixed concentration of AI-1 is either added or not to the feed. **b)** Model simulation of co-culture set 1 in a chemostat with the controller. An initial Set Point of 0.7 (fraction of Population B) is simulated. The controller adds or stops adding AI-1 to the feed (ON/OFF, where ON = 1 and OFF = 0) to maintain the desired set point. At the times indicated, the dilution rate is changed, the set point is changed, or the system is perturbed by simulating a sudden increase in Population A density. **c)** Simulation of co-culture set 2 in a chemostat without the "controller." Over time the system reaches steady state and a specific culture composition. Changing the dilution rate changes the steady state culture composition. **d**) Simulation of co-culture set 3 in a chemostat without the controller. **e)** Simulation of co-culture set 2 with the controller. As in (**c**), a steady state culture composition is reached based on the dilution rate. Then, a set point can be programmed to control the composition at a higher (but not a lower) level than the system would naturally achieve. See Supplementary Note 3 for further details on the model.

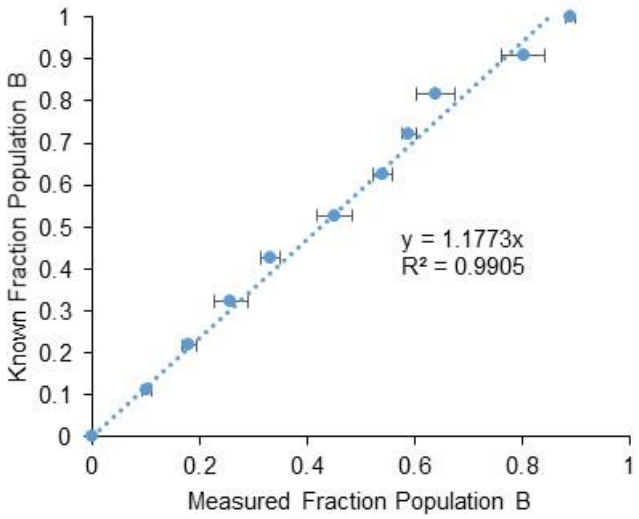

Supplementary Figure 9. Standard curve for measurement of fraction Population B.

Translator cells and controller cells (expressing constitutive dsRedExpress2) were each inoculated 1% from overnight cultures and grown as monocultures in M9 media for five hours. After five hours, OD was recorded, and used to create co-cultures of known compositions. Microscopy and ImageJ were used to determine measured compositions. Error bars show s.d. between technical quadruplicates.

Chapter 5 Supplementary Tables

Supplementary Table 1: Function for AI-1 production in translator cells.

Equation	Description
$Extracellular\ AI1 = D + \frac{A - D}{\left(1 + \left(\frac{t}{C}\right)^{B}\right)^{E}}$	Fits experimental results (Figure 5a) for translator culture extracellular AI-1 levels over time for different initial AI-2 concentrations.
$Cell\ Density = EXP(0.28t - 2.89)$	Fits experimental results (Figure 5c) for translator culture cell density over time.
$fAI1(t, AI2) = \frac{\frac{d}{dt}(Extracellular\ AI1(t))}{EXP(0.28t - 2.89)}$	AI-1 produced by translator cells over time in response to initial AI-2 level.

Where

fAI1	Rate of AI-1 produced (nM AI-1/(hr × OD))
t	Time (hr)
A, B, C, D, E	Constants dependent on initial AI-2 concentration (see below)

	0 µM	**10 µM**	**20 µM**	**40 µM**
A	0	0	0	0
B	4.4	3.5	3.5	3.8
C	6.4	9	6.48	4.40
D	295	300	350	505
E	0.83	2.75	1.19	0.49

Supplementary Table 2: System of ordinary differential equations used to model co-culture system.

Reaction	Differential Equation
Strain A Density	$\frac{dX_A}{dt} = \frac{\mu_{b\_A} \times S}{K_A + S} \times X_A$
Strain B Density	$\frac{dX_B}{dt} = \frac{S}{K_B + S} \times \mu_{b\_B} \times fHPr(AI1) \times X_B$
Substrate Concentration	$\frac{dS}{dt} = -\frac{1}{Y_A}\frac{\mu_{b_A} \times S}{K_A + S} \times X_A - \frac{1}{Y_B}\frac{S}{K_B + S} \times \mu_{b\_B} \times fHPr(AI1) \times X_B$
AI-1 Concentration	$\frac{dAI1}{dt} = fAI1(AI2) \times X_A$
Where	
Function for increased growth rate (caused by HPr) in Population B	$fHPr(AI1) = D + \frac{A - D}{\left(1 + \left(\frac{AI1}{C}\right)^B\right)^E}$ Where A = 1, B = 1, C = 29, D = 2.1, E = 0.48
Function for production of AI-1 in Population A as a function of AI-2 and time from AI-2 addition	$fAI1(t, AI2)$ Varies depending on initial AI-2 concentration. See Table S1 and Figure 2d.

Supplementary Table 3: Initial conditions and constants used in model.

Species	**Description**
X_A	Population A concentration (OD600)
X_B	Population B concentration (OD600)
S	Substrate Concentration (g/L)
$AI1$	AI-1 Concentration (nM)
$AI2$	Supplemented AI-2 Concentration (μM)
S_0	Initial substrate conc. (8 g/L for media used)
t	Time (hr)

Parameter	**Description**	**Value**
μ_{b_A}	Basal specific growth rate of Population A (hr^{-1})	0.28
μ_{b_B}	Basal specific growth rate of Population B (hr^{-1})	0.32
K_A & K_B	Substrate concentration for half max growth (g/L)	0.1
Y_A & Y_B	Yield (OD600 cells)/(g/L substrate)	0.45

Supplementary Table 4: System of ordinary differential equations used in chemostat simulations.

Reaction	Differential Equation	
Strain A Density	$\frac{dX_A}{dt} = -D \times X_A + \frac{\mu_{b\_A} \times S}{K_A + S} \times X_A$	(1)
Strain B Density	$\frac{dX_B}{dt} = -D \times X_B + \frac{S}{K_B + S} \times \mu_{b\_B} \times fHPr(AI1) \times X_B$	(2)
Substrate Concentration	$\frac{dS}{dt} = D \times (S_0 - S) - \frac{1}{Y_A}\frac{\mu_{b\_A} \times S}{K_A + S} \times X_A - \frac{1}{Y_B}\frac{\mu_{b\_B} \times S}{K_B + S} \times fHPr(AI1) \times X_B$	(3)
AI-1 Concentration	$\frac{dAI1}{dt} = D \times (AI1_{feed} - AI1)$	(4)
	$\frac{dAI1}{dt} = D \times (AI1_{feed} - AI1) + AI1_{rate} \times X_A$	(5)
	$\frac{dAI1}{dt} = -D \times AI1 + fAI1(AI2) \times X_A$	(6)
AI-2 Concentration	$\frac{dAI2}{dt} = -D \times AI2 + AI2_{rate} \times X_B$	(7)
Where		
Function for increased growth rate (caused by HPr) in Population B	$fHPr(AI1) = D + \frac{A - D}{\left(1 + \left(\frac{AI1}{C}\right)^B\right)^E}$ Where A = 1, B = 1, C = 29, D = 2.1, E = 0.48	
Function for rate of AI-1 production in Population A as a function of AI-2	$fAI1(AI2) = D + \frac{A - D}{\left(1 + \left(\frac{AI2}{C}\right)^B\right)^E}$ Where A = 0, B = 1, C = 40, D = 2, E =2	

Simulation	Differential Equations
Co-culture Set 1 (Supplementary Figure 9b)	Equations (1), (2), (3), (4)
Co-culture Set 2 (Supplementary Figures 9c and 9e)	Equations (1), (2), (3), (5)
Co-culture Set 3 (Supplementary Figure 9d)	Equations (1), (2), (3), (6), (7)

Supplementary Table 5: Initial conditions and constants used in chemostat simulations.

Species	**Description**	**Initial Condition**
X_A	Population A concentration (OD600)	0.4
X_B	Population B concentration (OD600)	0.4
S	Substrate Concentration ($g \times L^{-1}$)	4
AI1	AI-1 Concentration (nM)	0
AI2	Supplemented AI-2 Concentration (μM)	0
t	Time (hr)	0
Parameter	**Description**	**Value**
D	Dilution rate (hr^{-1})	varied
S_0	Feed substrate concentration ($g \times L^{-1}$)	4
μ_{b_A}	Basal specific growth rate of Population A (hr^{-1}) (Used for simulation in Supplementary Figure 9b)	0.3
μ_{b_A}	Basal specific growth rate of Population A (hr^{-1}) (Used for simulations in Supplementary Figures 9c-9e)	0.27
μ_{b_B}	Basal specific growth rate of Population B (hr^{-1})	0.2
K_A & K_B	Substrate concentration for half max growth (g/L)	0.1
Y_A & Y_B	Yield (OD600 cells)/(g/L substrate)	0.45
$AI1_{rate}$	Rate of AI-1 production by Population A ($nM \times OD600^{-1} \times hr^{-1}$)	1
$AI2_{rate}$	Rate of AI-2 production by Population B ($\mu M \times OD600^{-1} \times hr^{-1}$)	10
$AI1_{feed}$	AI-1 in feed when controller is ON (nM)	10

Supplementary Table 6: Strains and Plasmids used in Chapter 5

Strains	Relevant Genotype	Source
E. coli		
W3110	K12 strain, wild type, λ-, F-, IN(*rrnD-rrnE*)1, *rph-1s*	Genetic Stock Center Yale University, New Haven, CT
TOP10	F- *mcrA* Δ(*mrr-hsd*RMS-*mcr*BC) Φ80*lac*ZΔM15 Δ*lac*X74 *rec*A1 *ara*D139 Δ(*araleu*)7697 *gal*U *gal*K *rps*L (StrR) *end*A1 *nup*G	Invitrogen
BL21	B strain, F-*ompT* [*dcm*][*lon*]*hsdS*(r_B-M_B-)*gal*	Novagen
BL21 luxS$^-$	BL21 Δ*luxS*:: Kan	[203]
ZK126	W3110 Δ*lacU169 tna-2*	[201]
LW7	W3110 Δ*lacU169 tna-2* Δ*luxS*::Kan	[32]
PH01	W3110 Δ*lacU169 tna-2* Δ*ptsH*::Cm	[33]
PH02	W3110 Δ*lacU169 tna-2* Δ*luxS*::Kan Δ*ptsH*::Cm	[33]
PH03	W3110 Δ*lacU169 tna-2* Δ*ptsH*	This study
PH04	W3110 Δ*lacU169 tna-2* Δ*luxS* Δ*ptsH*	This study
CT104	W3110 *luxS*::Tcr, lsrFG-, W3110-derived *luxS, lsrFG* mutant strain	[27]
V. harveyi		
BB170	BB120 *luxN*::Tn5 (sensor 1- ,sensor 2+), Km^r	[115]

Plasmids	Description	Source
pET200	Cloning vector, containing *T7* promoter, Km^r	Invitrogen
pFZY1	*galK'-lacZYA* transcriptional fusion vector, Ap^r	[204]
pCT6	pFZY1 derivative, containing *lsrR* and *lsrR* promoter region fused with T7RPol, Ap^r	[36]
pSkunk-HPr	containing *ptsH* under tac promoter, streptomycin/spectomycin resistance	[33]
pLSR	pTS40 derivative, containing SpeI and PvuI restriction digestion sites, Cm^r	[37]
pT5G	eGFP under constitutive T5 promoter, Km^r	[125]
pTT01	pBR322, *soxR* gene and the overlapping divergent *soxR* and *soxS* promoters, phiLOV downstream of *soxS* promoter, Ap^r	[125]
pSox-LasI	pTT01 derivate, containing *lasI* under *soxS* promoter, Ap^r	This study

pAHL-Reporter_Red-Green (pAHL-sfGFP)	pET21a derivative, containing *sfGFP* under *lasI* promoter and *lasR* and *dsRedExpress2* under constitutive promoter, Ap^r	[139]
pLasI	pET200 derivate, containing *lasI* under *T7* promoter, Km^r	This study
pTac-HPr	pLSR derivate, containing *ptsH* under *tac* promoter, Cm^r	This study
pAHL-HPr	pAHL-Reporter_Red-Green derivative, containing *ptsH* under *lasI* promoter, Ap^r	This study
pAL105	$lasR^+$ *lasI::luxCDABE*; Tet^r p15A origin	[141]

Supplementary Table 7: Primers used in Chapter 5

Primer	Sequence
LasI-F	CACCATGATCGTACAAATTGGTCGGCGC
LasI-R	TCATGAAACCGCCAGTCGCTG
TacProm-PvuI-F	TGCATCGATCGTACGACTCACTATAGGGCGAATTCTG
Sox-R-GB	AATATCGATGATAAGCTGTCAAACATG
Sox-F-GB	AAGCTTAAATCTGCCTCTTTTCAG
pSoxLasI-F-GB	ACTGAAAAGAGGCAGATTTAAGCTTATGATCGTACAAATTGGTC
pSoxLasI-R-GB	CATGTTTGACAGCTTATCATCGATATTATGAAACCGCCAGT
HPr-SpeI-R	AGTCTAGACTAGTTTACTCGAGTTCCGCCATCAGTTTAACCAG
HPr-SpeI-F	TGCATACTAGTATGTTCCAGCAAGAAGTTACCG
HPr-SacI-R	TTCTTAGAGCTCTTACTCGAGTTCCGCCATC

Chapter 5 Supplementary Notes

Supplementary Note 1

We estimated the growth rate of Population B and the AI-1 levels during the extended co-culture experiment (data points in **Figure 5.7d**) using a combination of the experimental data and the model. To estimate the growth of Population B, we first estimated the cell density of Population A over time. Assuming a constant specific growth rate for Population A (μ_{b_A}) and an initial inoculation density of X_{A_i}, we calculated the Population A density at 0, 3, 6 and 9 hours. X_{A_i} was determined using the average of the initial total OD (0.053) and the average of the initial "Fraction Population B" experimental data. We then calculated the Population B density at 0, 3, 6 and 9 hours using the calculated Population A density and the experimental "Fraction Population B" data. We plotted the natural log of the Population B density over time and fitted a 2nd order polynomial trend line through the data for each AI-2 concentration. We used the slope of the trend lines to estimate the growth rate of Population B over 9 hours in increments of 0.1 hours for each AI-2 concentration. For each three hour time segment (0-3 hr, 3-6 hr, and 6-9 hr), we calculated the average growth rate by averaging the values of each 0.1 hour increment. We normalized these values to μ_{b_B} in order to obtain relative growth rate. We used the model to determine corresponding average AI-1 levels. To do this, we modeled Population A using the adjusted model (see **Supplementary Note 2**) to determine the AI-1 level at 0.1 hour increments over the 9 hour experiment. We determined average AI-1 for each three

hour segment and each AI-2 concentration. The average relative growth rate vs average AI-1 levels are plotted as data points in **Figure 5.7d**.

Supplementary Note 2

To model the extended co-culture experiments, including resuspension of the cells in fresh media containing AI-2, we used an adjusted model where additional assumptions were incorporated based on the experimental results. The experiment consisted of an initial co-culture inoculated into media with AI-2. At 3 and 6 hours, the culture was resuspended in fresh media. We note that to simulate each resuspension, the cell densities at the end of each three hour simulation were input back into the model along with the parameters for the fresh media (8 g/L glucose, supplemented AI-2 level, and 0 nM AI-1) and the simulation was restarted. For all simulations of the extended co-culture experiments, the total initial OD used at $t = 0$ was 0.053.

The first assumption used in the adjusted model was to account for the increased level of AI-1 produced by Population A with each resuspension. This increase likely occurred because the AI-1 synthase, LasI, did not immediately degrade each time the cells were resuspended. In the adjusted model, the rate of AI-1 produced (*fAI1*) was assumed to be the value of the *fAI1* function at the end of the prior three hours plus the value of the *fAI1* function calculated from the time and initial AI-2 level during the current simulation. The second change in the model was an adjustment to the AI-1 regulated growth rate (*fHPr*) in Population B. The *fHPr* logistic function had the form $f(x) = D + (A-D)/(1+(x/C)^B)^E$ as in the original model. In the adjusted model the

constants used were A = 1, B = 1, C =3, and E = 0.48. We assumed the value of D to be a function of time. In the adjusted model $D(t) = -0.27t + 3$ where t ranges from 0 to 9 hours. This results in reduced AI-1 mediated increase in growth rate and decreased growth rate at later time periods. We also assumed that the value of the *fHPr* function did not immediately revert back to basal level when resuspended in media without AI-1 (presumably the protein HPr would still be present). To do this, the function *fHPr* for relative growth rate, used the AI-1 level from the end of the prior three hours ($AI1_{prior}$) until the current AI-1 level surpassed $AI1_{prior}$ at which point the current AI-1 level was used in the *fHPr* function.

Supplementary Note 3

The mathematical model can be used to investigate *in silico* how the strategies developed in this manuscript could be used to design co-culture systems with varied or controlled behaviors in continuous cultures. For instance, we designed three theoretical co-cultures of increasing complexity and simulated their behaviors in chemostats with or without a controller (**Supplementary Figure 8a**). In the first case (**Supplementary Figure 8b**), the co-culture (set 1) consists of one population that is not directly controlled (Population A) and one population where growth rate is a function of the AI-1 signal (Population B). An on-off (bang-bang) control scheme is used to control the culture composition at a programmed set point. The controller samples the culture composition hourly and compares the measured fraction of Population B to the set point. If the fraction of Population B is lower than the set point, an AI-1 feed pump is actuated, enabling a fixed concentration of AI-1 in the

feed. The AI-1 increases the growth rate of Population B, driving the fraction of Population B up (closer to the set point). The AI-1 remains in the feed for the next 60 minutes (the sample frequency selected for these simulations), after which the controller samples the culture composition again. If the fraction is higher than the set point, AI-1 is no longer added to the feed. If it is still lower, AI-1 continues to be added in the feed. In the simulations depicted, eventually, the correct composition is reached and AI-1 is removed from the feed. At this point, AI-1 that has accumulated in the chemostat causes some overshoot of the set point while the dilution rate and removal of AI-1 (in the outlet) results in eventual decrease in Population B growth rate and return to the set point. This cycle continues and allows the culture composition to target the set point. Importantly, the minimum (without AI-1) and maximum (with AI-1) specific growth rates of Population B must span the specific growth rate of Population A for the system to work. In this way, the Population B growth rate can be increased or decreased as necessary so that neither population outgrows the other over time. We note that changing the dilution rate (depicted in **Supplementary Figure 8b**) results in a change in growth rates of both populations (as is typical of a chemostat) but the controller maintains the system at the set point. Also in this figure, we show that the controller allows for the set point to be changed or for the system to recover from perturbations.

We simulated a second case (co-culture set 2) without the controller. In this case (**Supplementary Figure 8c**), Population A produces AI-1 at a constant rate (per cell) and Population B growth rate is a function of AI-1. There is no AI-1 in the feed. Interestingly, a change in dilution rate causes an initial increase or decrease in AI-1

levels (due to increased or decreased removal of AI-1 in the feed) resulting in a change in Population B growth rate and a gradual change in culture composition. As the AI-1 producing population (Population A) decreases or increases, the AI-1 level approaches the steady state level, which is the same regardless of dilution rate. This steady state AI-1 level is the concentration of AI-1 at which the growth rates of both populations are identical. Thus, setting the dilution rate sets the culture composition and there is no set point for the fraction of Population B. The case in **Supplementary Figure 8d** shows similar behavior (co-culture set 3). Set 3 populations are the same as set 2, except that Population B produces AI-2 at a constant rate and Population A produces AI-1 at a rate that is a function of AI-2 level. Changing the dilution rate in this case also changes the steady state culture composition. This case results in higher levels of Population B for a set dilution rate than the case shown in **Supplementary Figure 8c** using co-culture set 2. In both of these examples, the culture composition is regulated autonomously by the cells and can only be changed by changing the dilution rate. In a sense, this condition is hands off and could be anticipated or otherwise designed in advance using the model. A user specified fraction is not achieved via this simple control process.

By extensions, in **Supplementary Figure 8e**, co-culture set 2 is now simulated in a chemostat with the on-off controller, adding an additional layer of control. Here, when the controller is off, the system reaches a specific composition at steady state (based on the dilution rate). Turning the controller on allows the system to target a higher set point, independent of the dilution rate. We note, however, a lower set point than what would naturally be achieved by the co-culture cannot be targeted since

Population A is producing a background level of AI-1. That is, the system is designed to operate within certain bounds and can only be fine-tuned within those bounds.

Several assumptions are made in these analyses that simplify the actual system. First, there are no delays in responses to signals. Removal of a signal results in an immediate decrease in the cell response to that signal (e.g. growth rate immediately decreases upon removal of AI-1). This type of response is a consequence of the simple Monod growth kinetics. Experimentally, incorporation of degradation tags on expressed proteins could result in quicker responses to changes in signal levels. Moreover, cell growth dynamics could be introduced as process lags. We have also assumed that the populations produce QS signals at constant rates independent of cell growth rate. However, the rate of AI-2 production in a chemostat actually changes as a function of the dilution rate[202]. Nevertheless, we suggest that the model offers insight into how co-cultures could be designed to operate in a continuous mode and how changes to the design may affect the outcome.

In sum, these scenarios provide a basis for how a cell-based autonomous controller system could be integrated into a reactor scheme that is operated based on user input. In all cases, one needs to provide a dilution rate. In some scenarios, this will define the composition irrespective of the genetic regulatory structure developed in this manuscript. In other words, although the genetic regulatory structure allows both populations to be maintained in continuous culture (something that would not normally happen), the engineered co-culture does not target a user-defined composition. In other scenarios, our autonomous controller system can be integrated with chemostats that do enable a user defined set point, including when simple on-off

controllers provide an additional external input (e.g., AI-1) feed. We note, however, that it is unlikely that a composition sampling system and autoinducer feed would ever be implemented in a continuous system owing to the associated cost. That said, the cascaded control scheme in **Supplementary Figure 8e** suggests that the cell-based autonomous controller can be designed to operate within certain parameters and then adjusted within those parameters by addition of exogenous signals or inducers.

Simulink Version 8.7 (R2016a) was used for the chemostat simulations. The systems of ordinary differential equations (**Supplementary Tables 4 and 5**) were solved using the ode45 solver. To model the controller in Simulink, a chart block was used. The chart block was designed to take an input (the culture composition from the model) and report a "0" if the input was greater than the set point and a "1" if the input was less than the set point. A "1" value directed the model to add AI-1 to the chemostat feed. A "0" value directed the model to stop adding AI-1 to the feed. The sample time for the block was set to 1 hour so that the controller would only perform this check every 60 minutes.

Appendix D: Supplementary Information for Chapter 6

Chapter 6 Supplementary Figures

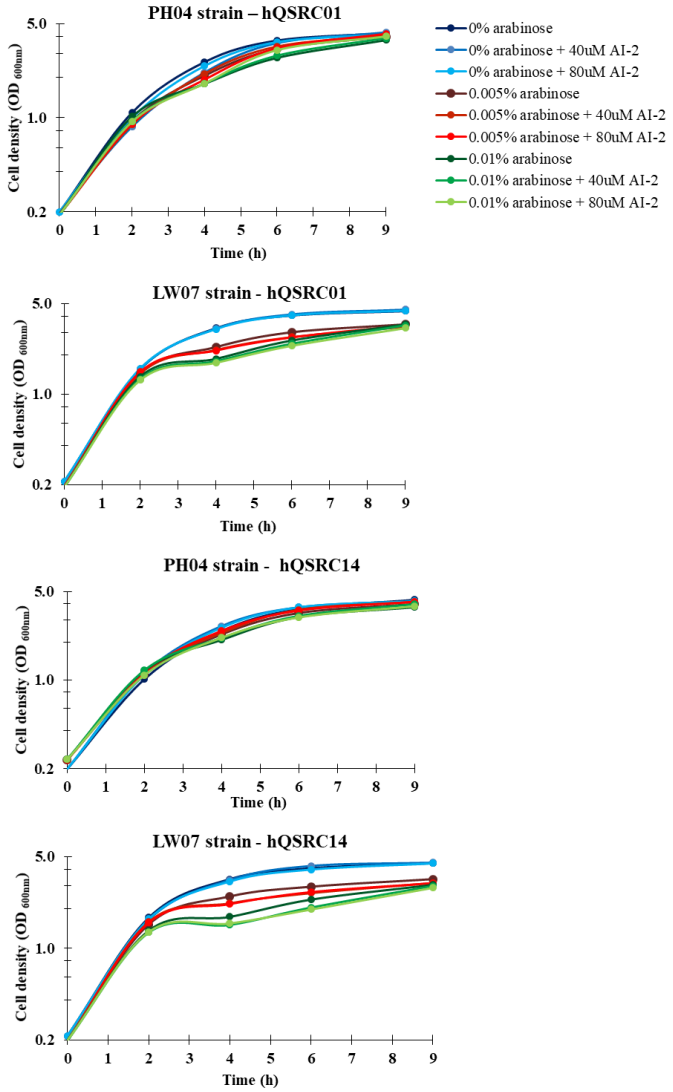

Supplementary Figure 1. Growth of the PH04 (Δ*lux*S Δ*pts*H) and LW7 (Δ*lux*S) strain.

Overnight cultures of E. coli PH04 and LW7 strain were diluted in LB or LB plus arabinose (0, 0.005% and 0.01%) and/or AI-2 (40 and 80 µM) to an OD_{600nm} of about 0.02. At different time points during cell growth, aliquots were collected for measurement of the OD_{600nm}.

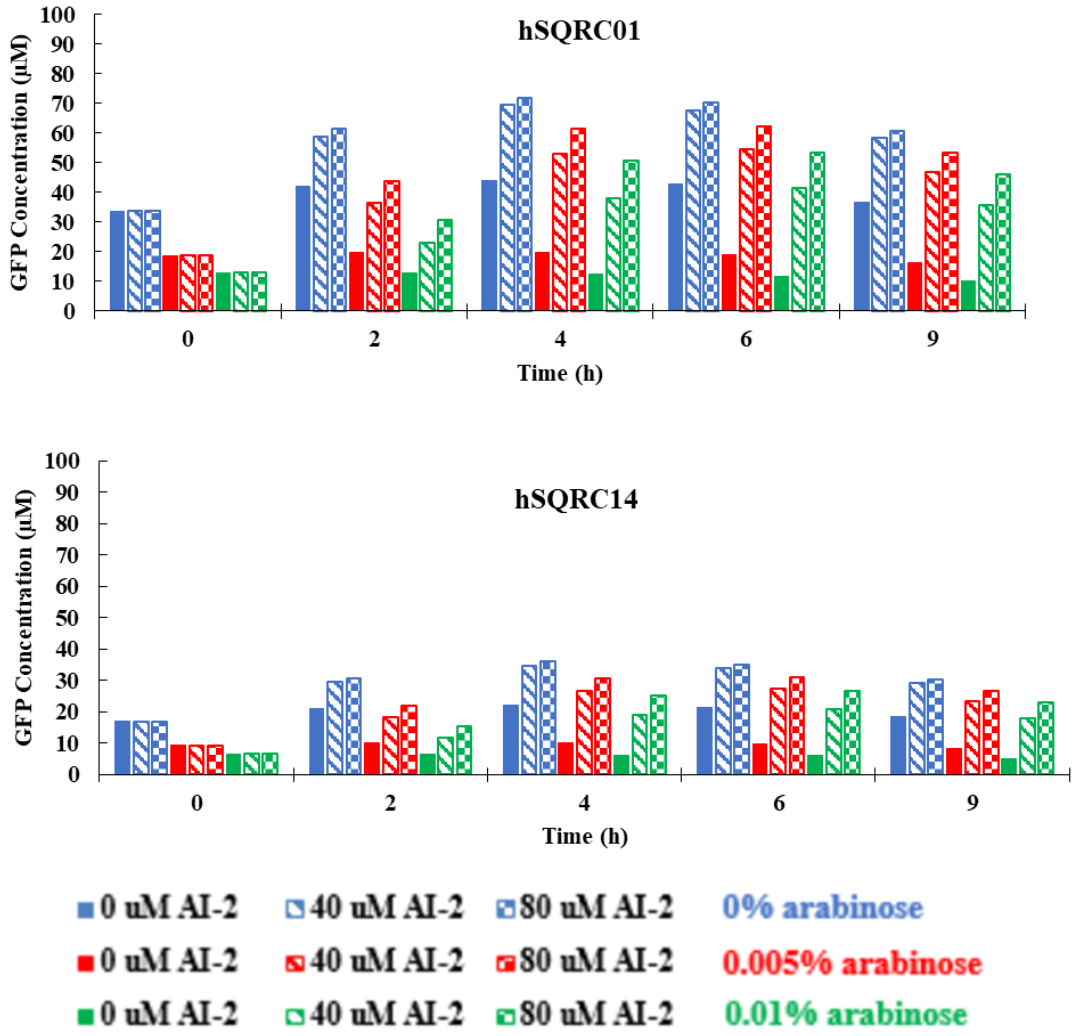

Supplementary Figure 2. Model simulation of GFP expression in hQSRC01 and hQSRC14.

Simulation assumed arabinose addition at OD 0.05, and AI-2 addition at OD 0.2. Time indicates time from AI-2 addition. Level of arabinose or AI-2 additions are indicated. Experimental setup and conditions in the simulations were designed to match the experimental setup and conditions in **Figure 6.3**.

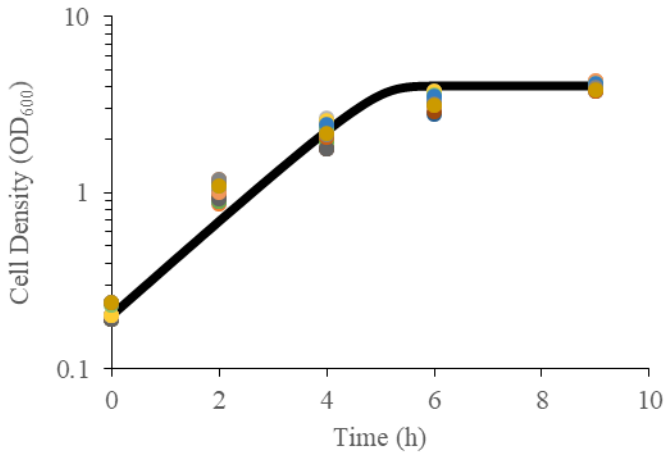

Supplementary Figure 3. Model simulated growth curve.

The growth curve generated by the mathmatical model is shown in black. Dots represent experimental PH04 hQSRC01 and hQSRC14 cultures grown with or without arabinose and AI-2.

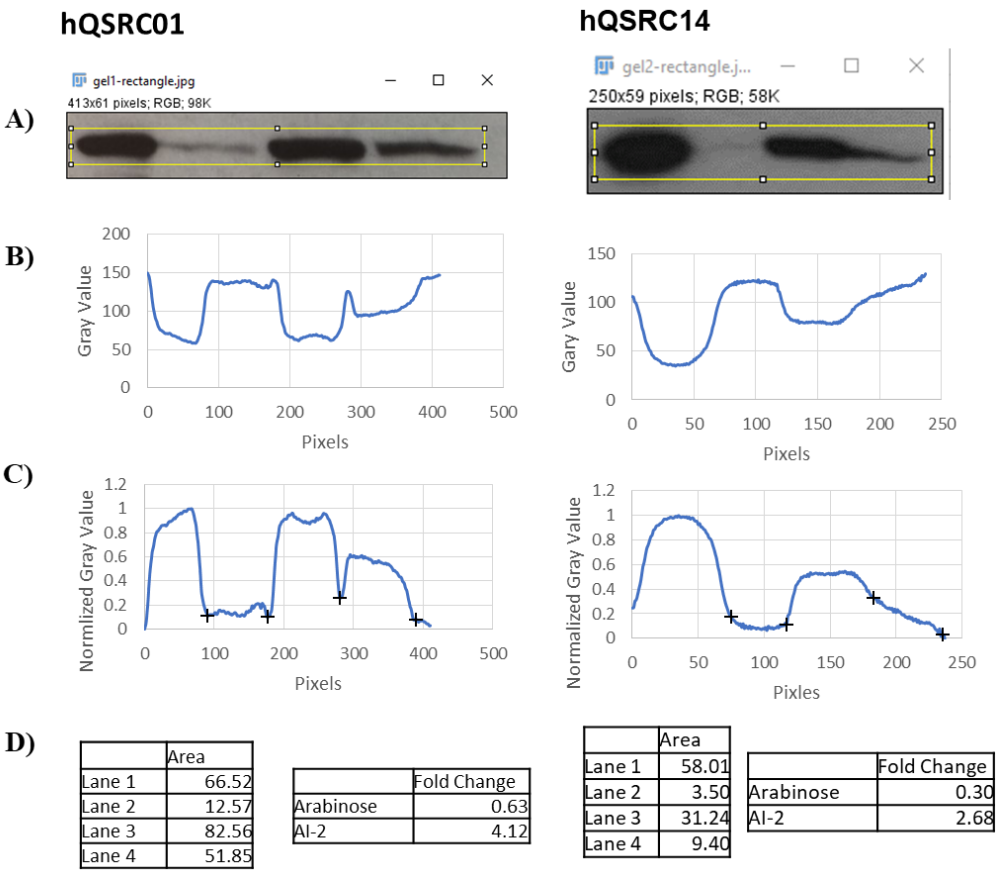

	Area
Lane 1	66.52
Lane 2	12.57
Lane 3	82.56
Lane 4	51.85

	Fold Change
Arabinose	0.63
AI-2	4.12

	Area
Lane 1	58.01
Lane 2	3.50
Lane 3	31.24
Lane 4	9.40

	Fold Change
Arabinose	0.30
AI-2	2.68

Supplementary Figure 4. Description of rh-GM-CSF chimera gel image quantification. To quantify gel images, images were opened in ImageJ (A). A narrow box (seen in yellow) was drawn around the bands. The "plot profile" feature under "analyze" was used to plot the gray value across the image (B). This gray value was then normalized so that the maximum gray value became zero and the minimum gray value became 1 for each image (C). The crosses indicate the pixel where each lane ended and the next lane started. The area under the curve for each lane was then determined (D). Lane 1 = Positive Control, Lane 2 = 0.01% arabinose, Lane 3 = 0% arabinose + 40 μM AI-2, Lane 4 = 0.01% arabinose + 40 μM AI-2. The AI-2 (Lane 4 divided by Lane 2) and arabinose (Lane 4 divided by Lane 3) mediated fold changes were then calculated.

Chapter 6 Supplementary Tables

Supplementary Table 1: Strains and plasmids used in Chapter 6

***E. coli* strains**	**Relevant genotype and property**	**Reference or source**
DH5α	Used for cloning	New England labs
LW7	W3110 Δ*lacU169 tna-2* Δ*lux*S::Kan	Wang *et al*., 2005
LW6 pLSR14	W3110 Δ*lacU169 tna-2* Δ*lsr*R::Kan harboring pLSR14	Hauk et al., 2016
Nissle1917 (EcN)	Probiotic *E. coli* strain	Mutaflor®
PH04	LW7 Δ*pts*H	This study
PH08	EcN Δ*lux*S Δ*pts*H	This study
Plasmids		
pBAD HisA	pBR322, ampicillin resistance and pBAD promoter	Invitrogen
pBAD-*lsrR*	Template used to amplify *araC*-pBAD-*lsrR* sequence	This study
pLSR	pTS40 plasmid backbone, containing *lsr*ACDBFG promoter region, Cm^r	Hauk *et al*., 2016
pLSR01	pLSR derivative, containing EP01rec promoter, Cm^r	Hauk *et al*., 2016
pLSR14	pLSR derivative, containing EP14rec promoter, Cm^r	Hauk *et al*., 2016
pPHT	pLSR derivative, containing LsrR expression under pBAD promoter, Cm^r	This study
pPHT01	pLSR01 derivative, containing LsrR expression under pBAD promoter, Cm^r	This study
pPHT14	pLSR14 derivative, containing LsrR expression under pBAD promoter, Cm^r	This study
pAES40	ColE1 origin, YebF export vector, Ap^r	AthenaES
pGM29OmpA	Template sequence used to amplify hGM-CSF	Sletta *et al*., 2007
pAES40-GM-CSF	Template sequence used to amplify yebF-hGM-CSF sequence	This study
pPHT01-*yebF*-hGM-CSF-Histag	YebF-hGM-CSF-Histag expression under EP01 promoter	This study
pPHT14-*yebF*-hGM-CSF-Histag	YebF-hGM-CSF-Histag expression under EP14 promoter	This study
pSkunk	p15a origin, f1 origin, AadA streptomycin/spectomycin resistance and *tac* promoter	Wright *et al*., 2014
pSkunk-*lsrK*	LsrK expression under *tac* promoter	This study

Supplementary Table 3: Mathematical model

Equation	No.
$\frac{dAI2_{in}}{dt} = k_{in} \times LsrACDB \times AI2_{out} - k_{out} \times AI2_{in} - k_p \times LsrK \times AI2_{in} - k_{d1} \times AI2_{in}$	(1)
$\frac{dAI2_{out}}{dt} = -k_{in} \times LsrACDB \times AI2_{out} \times OD + k_{out} \times AI2_{in} \times OD$	(2)
$\frac{dAI2_P}{dt} = k_p \times LsrK \times AI2_{in} - k_{FG} \times AI2_P \times LsrFG - k_{on} \times LsrR \times AI2_P + k_{off} \times LsrR{:}AI2_P - k_{d1} \times AI2_P$	(3)
$\frac{dLsrACDB}{dt} = \frac{k_a \times \beta_{LsrACDB}}{1 + K_{LsrR} \times LsrR} - (k_{d1} + k_{d2}) \times LsrACDB$	(4)
$\frac{dLsrK}{dt} = \frac{k_a \times \beta_{LsrK}}{1 + K_{LsrR} \times LsrR} + k_2 - (k_{d1} + k_{d2}) \times LsrK$	(5)
$\frac{dLsrFG}{dt} = \frac{k_a \times \beta_{LsrFG}}{1 + K_{LsrR} \times LsrR} - (k_{d1} + k_{d2}) \times LsrFG$	(6)
$\frac{dLsrR}{dt} = \frac{k_a \times \beta_{LsrR}}{1 + K_{LsrR} \times LsrR} + k_1 \times Ara - k_{on} \times AI2_P \times LsrR + k_{off} \times LsrR{:}AI2_P - (k_{d1} + k_{d2}) \times LsrR$	(7)
$\frac{dLsrR{:}AI2_P}{dt} = k_{on} \times AI2_P \times LsrR - k_{off} \times LsrR{:}AI2_P - k_{d1} \times LsrR{:}AI2_P$	(8)
$\frac{dGFP}{dt} = \frac{k_a \times \beta_{GFP}}{1 + K_{LsrR} \times LsrR} - (k_{d1} + k_{d2}) \times GFP$	(9)
$\frac{dOD}{dt} = \frac{\mu \times OD \times S}{K_\mu + S}$	(10)
$\frac{dS}{dt} = -\frac{\mu \times OD \times S}{Y \times (K_\mu + S)}$	(11)

Where k_a and k_{d1} are functions of growth rate:

$k_a = \frac{S}{K_\mu + S}$
$k_{d1} = \frac{\mu \times S}{K_\mu + S}$

Supplementary Table 4: Description of variables and constants in model

Variable	Definition	Initial Condition or Value
$AI2_{in}$	Intracellular AI-2 concentration (μM)	0
$AI2_{out}$	Extracellular AI-2 concentration (μM) added at OD 0.2	0, 40, or 80
$AI2_P$	Phosphorylated AI-2 concentration (μM)	0
$LsrACDB$	LsrACDB concentration (μM)	0.0045
$LsrK$	LsrK concentration (μM)	0.0055
$LsrR$	LsrR concentration (μM)	0.01
$LsrFG$	LsrFG concentration (μM)	0.0045
$LsrR{:}AI2_P$	Concentration of bound LsrR and phosphorylated AI-2 complexes (μM)	0
GFP	GFP concentration (μM)	0
OD	Cell density (OD600)	0.05
S	Substrate concentration (g/L)	4
k_{in}	Rate constant describing transport of AI-2 into the cell by LsrACDB ($\mu M^{-1} \times hr^{-1}$)	60
k_{out}	Rate constant describing transport of AI-2 out of the cell (hr^{-1})	1
k_P	Rate constant describing phosphorylation of intracellular AI-2 by LsrK ($\mu M^{-1} \times hr^{-1}$)	15
k_{FG}	Rate constant describing degradation of phosphorylated AI-2 by LsrFG ($\mu M^{-1} \times hr^{-1}$)	50
k_{on}	Rate constant describing binding of free LsrR and AI-2P ($\mu M^{-1} \times hr^{-1}$)	30
k_{off}	Rate constant describing dissociation of LsrR:AI-2P complex (hr^{-1})	4
$\beta_{LsrACDB}$	Describes rate of transcription/translation of LsrACDB from *lsr* promoter in genome ($\mu M \times hr^{-1}$)	.012

β_{LsrK}	Describes rate of transcription/translation of LsrK from *lsr* promoter in genome (μM × hr^{-1})	.012
β_{LsrR}	Describes rate of transcription/translation of LsrR from *lsr* promoter in genome (μM × hr^{-1})	.01
β_{GFP}	Describes rate of transcription/translation of GFP from *lsr* promoter on plasmid (μM × hr^{-1})	30 (hQSRC14) 60 (hQSRC01)
K_{LsrR}	Describes repression of *lsr* promoter by LsrR (μM^{-1})	100
k_1	Describes rate of transcription/translation of LsrR from arabinose promoter (μM × hr^{-1})	0.04
Ara	Presence of arabinose (unitless)	0.5 (0.005% arabinose) 1 (0.01% arabinose) 0 (no arabinose)
k_2	Elevated levels of LsrK (0, if LsrK plasmid is not used) (μM × hr^{-1})	0.005
μ	Maximum specific growth rate (hr^{-1})	0.7
K_μ	Substrate concentration that yield ½ maximum specific growth rate (g/L)	0.5
Y	Yield (OD cells)/(g/L substrate)	1
k_{d1}	Dilution of intracellular proteins/complexes/AI-2 due to growth rate.	$k_{d1} = \frac{\mu \times S}{K_\mu + S}$
k_{d2}	Degradation of intracellular proteins (hr^{-1})	0.05
k_a	Dependence of transcription/translation on growth rate (at decreased growth rates, the rate of protein expression decreases)	$k_a = \frac{S}{K_\mu + S}$

Chapter 6 Supplementary Notes

Supplementary Note 1

The mathematical model is comprised of 11 ordinary differential equations. The equations describe the AI-2 uptake proteins (LsrABCD, Equation 4), the AI-2 kinase (LsrK, Equation 5), the repressor (LsrR, Equation 7), and proteins that metabolize AI-2 (LsrFG, Equation 6). An equation describing the LsrR/phosphorylated-AI-2 complex (Equation 8) is incorporated as well. The concentration of AI-2 both extracellularly and intracellularly (Equations 1 and 2), as well as the concentration of phosphorylated AI-2 (Equation 3) is described. Equations 10 and 11 describe cell density and substrate concentration. Finally, Equation 9 describes target protein expression. The equations themselves are based on knowledge of the AI-2 quorum sensing process and on the hQSRC design.

To set initial values for parameters, we started with the equations for cell density and substrate concentration. We assumed the LB media started with 4 g/L substrate (S_i), and then we chose values for K_μ, μ, and Y so that the growth curves generated by the model approximate the experimental growth curves. We then assumed an initial value for extracellular AI-2 of 40 μM, and set parameters (assuming no arabinose induced LsrR) so that the simulated culture took up AI-2 and that AI-2 resulted in an increase in *lsr* operon proteins, as expected. Then we adjusted parameters to fit the experimental data in Figure 3. At this point, we also added a parameter (k_a) that describes a decrease in transcription and translation at low growth rates (due to depleted media).

The mathematical model was solved in MATLAB Version R2016a using the ODE45 solver. To obtain the results in Fig. S3, the model was simulated with a starting cell density of 0.05 OD, with an initial addition of arabinose and without any initial AI-2 addition. In the simulation, the cells were grown for 2.24 hours until cell density was 0.2 OD. The system of equations was then solved again, assuming AI-2 addition and inputting in initial conditions from the end of the previous simulation. This matches the experimental set-up, where cultures were grown from OD 0.05 to OD 0.2, with arabinose added at OD 0.05 and AI-2 added at OD 0.2. In all figures and charts, $t = 0$ indicates time of AI-2 addition.

Appendix E: Supplementary Information for Chapter 7

Chapter 7 Supplementary Tables

Supplementary Table 1: Strains and plasmids used in Chapter 7

Strains	Genotype	Source
E. coli		
NEB10β	Δ*(ara-leu) 7697 araD139 fhuA* Δ*lacX74 galK16 galE15e14- ϕ80*d*lacZ*Δ*M15 recA1 relA1 endA1 nupG rpsL* (Str^R) *rph spoT1* Δ*(mrr-hsdRMS-mcrBC)*	New England Biolabs
PH04	W3110 Δ*lacU169 tna-2* Δ*luxS* Δ*ptsH*	[85]
V. harveyi		
BB170	BB120 luxN::Tn5 (sensor 1^- ,sensor 2^+), Km^r	[115]
Plasmids	**Relevant Property**	**Source**
pAHL-HPr	pET21a derivative, containing *ptsH* under the *lasI* promoter and dsRedExpress2 and *lasR* under constitutive T5 promoter, Ap^r	[85]
pOxyRS-LasI	pBR322 origin, containing *lasI* under *oxyS* promoter, Ap^r	This study
pOxyRS-LasI-ssrA	pBR322 origin, containing *lasI-ssrA* under *oxyS* promoter, Ap^r	This study

Supplementary Table 2: Primers used in Chapter 7

Primer	Sequence
OxySv2Assem-R	GGTACCTTTCTCCTCTTTAATGAATTCGTGTGAG
OxySAssem-F	TAATGCGGTAGTTTATCACAGTTAAATTGCTAACG CAG
OxySv2-LasI-F	GAGGAGAAAGGTACCATGATCGTACAAATTGGTCG GCGC
LasI-oxyS-R	GATAAACTACCGCATTATGAAACCGCCAGTCGCTG
ssrA-F	GCAGCGAACGACGAAAATTACGC
LasI-ssrA-R	TTCGTCGTTCGCTGCTGAAACCGCCAGTCGCTG

Appendix F: Supplementary Information for Chapter 8

Chapter 8 Supplementary Tables

Supplementary Table 1: Strains and plasmids used in Chapter 8

Strains	Genotype	Source
E. coli		
NEB10β	Δ*(ara-leu) 7697 araD139 fhuA* Δ*lacX74 galK16 galE15e14- ϕ80*d*lacZ*Δ*M15 recA1 relA1 endA1 nupG rpsL* (Str^R) *rph spoT1* Δ*(mrr-hsdRMS-mcrBC)*	New England Biolabs
PH04	W3110 Δ*lacU169 tna-2* Δ*luxS* Δ*ptsH*	[85]
LW7	W3110 Δ*lacU169 tna-2* Δ*luxS*::Kan	[32]

Plasmids	Relevant Property	Source
pZE12MCS	colEI origin, LlacO-1 promoter followed by multi-cloning site, Ap^r	ExpresSys
pZE-phzAG	pZE12MCS derivate, containing *phzA1-G1* under LlacO-1 promoter, Ap^r	This study
pZE-phzMS	pZE12MCS derivate, containing *phzMS* under LlacO-1 promoter, Ap^r	This study
pZE-LacZα	pZE12MCS derivate, containing *lacZα* under LlacO-1 promoter, Ap^r	This study
pZE-phzAG-ptsH	pZE-phzAG derivated, containing growth control module	This study
pZE-phzMS-ptsH	pZE-phzAG derivated, containing growth control module	This study
pTT01	pBR322, *soxR* gene and the overlapping divergent *soxR* and *soxS* promoters, phiLOV downstream of *soxS* promoter, Ap^r	[125]
pSox-LasI	pTT01 derivate, containing *lasI* under *soxS* promoter, Ap^r	[85]

Supplementary Table 2: Primers used in Chapter 8

Primer	Sequence
PciI-t7-term-RVS	TCGTACATGTCAAAAAACCCCTCAAGACCCGT
PciI-ptsH-RVS	ATCTACATGTTACTCGAGTTCCGCCATCAG
HindIII-phzM-RVS	CCTAGTAAGCTTTCATCAGGCCCTGGCA

HindIII-phzM-FWD	CACTGAAGCTTATGAATAATTCGAATCTTGCTGCTGC
KpnI-phzA-FWD	TGCATGGTACCATGAACGGTCAGCGGTAC
HindIII-phzG1-RVS	CATACAAGCTTCACGGTTGCAGGTAGC
KpnI-HindIII-RBS-phzS-FWD	TACGTGGTACCAAGCTTAAAGAGGAGAAAGCACCCATGAGCGAA
BamHI-phzS-RVS	AAGTAGGATCCTAGCGTGGCCGTTC

References

1. Wong, C.K., Tan, M.H., Rasouliha, B.H., Hwang, I.Y., Ling, H. et al. Therapeutic microbes for infectious disease. *Methods Mol Biol* **1151**, 117-133 (2014).
2. Keasling, J.D. Manufacturing Molecules Through Metabolic Engineering. *Science* **330**, 1355-1358 (2010).
3. Jawed, K., Yazdani, S.S. & Koffas, M.A. Advances in the development and application of microbial consortia for metabolic engineering. *Metab Eng Commun* **9**, e00095 (2019).
4. Miller, M.B. & Bassler, B.L. Quorum sensing in bacteria. *Annu Rev Microbiol* **55**, 165-199 (2001).
5. Mukherjee, S. & Bassler, B.L. Bacterial quorum sensing in complex and dynamically changing environments. *Nat Rev Microbiol* **17**, 371-382 (2019).
6. Whiteley, M., Diggle, S.P. & Greenberg, E.P. Progress in and promise of bacterial quorum sensing research. *Nature* **551**, 313-320 (2017).
7. Cameron, D.E., Bashor, C.J. & Collins, J.J. A brief history of synthetic biology. *Nat Rev Microbiol* **12**, 381-390 (2014).
8. You, L., Cox, R.S., 3rd, Weiss, R. & Arnold, F.H. Programmed population control by cell-cell communication and regulated killing. *Nature* **428**, 868-871 (2004).
9. Basu, S., Gerchman, Y., Collins, C.H., Arnold, F.H. & Weiss, R. A synthetic multicellular system for programmed pattern formation. *Nature* **434**, 1130-1134 (2005).

10. Nealson, K.H. & Hastings, J.W. Bacterial bioluminescence: its control and ecological significance. *Microbiol Rev* **43**, 496-518 (1979).

11. Papenfort, K. & Bassler, B.L. Quorum sensing signal-response systems in Gram-negative bacteria. *Nat Rev Microbiol* **14**, 576-588 (2016).

12. Wang, B., Barahona, M. & Buck, M. Amplification of small molecule-inducible gene expression via tuning of intracellular receptor densities. *Nucleic Acids Res* **43**, 1955-1964 (2015).

13. Shong, J. & Collins, C.H. Engineering the esaR promoter for tunable quorum sensing- dependent gene expression. *ACS Synth Biol* **2**, 568-575 (2013).

14. Collins, C.H., Arnold, F.H. & Leadbetter, J.R. Directed evolution of Vibrio fischeri LuxR for increased sensitivity to a broad spectrum of acyl-homoserine lactones. *Mol Microbiol* **55**, 712-723 (2005).

15. Zeng, W., Du, P., Lou, Q., Wu, L., Zhang, H.M. et al. Rational Design of an Ultrasensitive Quorum-Sensing Switch. *ACS Synth Biol* **6**, 1445-1452 (2017).

16. Liu, C., Fu, X., Liu, L., Ren, X., Chau, C.K. et al. Sequential establishment of stripe patterns in an expanding cell population. *Science* **334**, 238-241 (2011).

17. Swofford, C.A., Van Dessel, N. & Forbes, N.S. Quorum-sensing Salmonella selectively trigger protein expression within tumors. *Proc Natl Acad Sci U S A* **112**, 3457-3462 (2015).

18. Doong, S.J., Gupta, A. & Prather, K.L.J. Layered dynamic regulation for improving metabolic pathway productivity in Escherichia coli. *Proc Natl Acad Sci U S A* **115**, 2964-2969 (2018).

19. Gupta, A., Reizman, I.M., Reisch, C.R. & Prather, K.L. Dynamic regulation of metabolic flux in engineered bacteria using a pathway-independent quorum-sensing circuit. *Nat Biotechnol* **35**, 273-279 (2017).

20. Basu, S., Mehreja, R., Thiberge, S., Chen, M.T. & Weiss, R. Spatiotemporal control of gene expression with pulse-generating networks. *Proc Natl Acad Sci U S A* **101**, 6355-6360 (2004).

21. Shong, J. & Collins, C.H. Quorum sensing-modulated AND-gate promoters control gene expression in response to a combination of endogenous and exogenous signals. *ACS Synth Biol* **3**, 238-246 (2014).

22. Tamsir, A., Tabor, J.J. & Voigt, C.A. Robust multicellular computing using genetically encoded NOR gates and chemical 'wires'. *Nature* **469**, 212-215 (2011).

23. Danino, T., Mondragon-Palomino, O., Tsimring, L. & Hasty, J. A synchronized quorum of genetic clocks. *Nature* **463**, 326-330 (2010).

24. Andrews, L.B., Nielsen, A.A.K. & Voigt, C.A. Cellular checkpoint control using programmable sequential logic. *Science* **361** (2018).

25. Pereira, C.S., Thompson, J.A. & Xavier, K.B. AI-2-mediated signalling in bacteria. *FEMS Microbiol Rev* **37**, 156-181 (2013).

26. Kamaraju, K., Smith, J., Wang, J., Roy, V., Sintim, H.O. et al. Effects on membrane lateral pressure suggest permeation mechanisms for bacterial quorum signaling molecules. *Biochemistry* **50**, 6983-6993 (2011).

27. Servinsky, M.D., Terrell, J.L., Tsao, C.Y., Wu, H.C., Quan, D.N. et al. Directed assembly of a bacterial quorum. *ISME J* **10**, 158-169 (2016).

28. Zargar, A., Quan, D.N. & Bentley, W.E. Enhancing Intercellular Coordination: Rewiring Quorum Sensing Networks for Increased Protein Expression through Autonomous Induction. *ACS Synth Biol* **5**, 923-928 (2016).

29. Stephens, K., Zargar, A., Emamian, M., Abutaleb, N., Choi, E. et al. Engineering Escherichia coli for enhanced sensitivity to the autoinducer-2 quorum sensing signal. *Biotechnol Prog*, e2881 (2019).

30. Torcato, I.M., Kasal, M.R., Brito, P.H., Miller, S.T. & Xavier, K.B. Identification of novel autoinducer-2 receptors in Clostridia reveals plasticity in the binding site of the LsrB receptor family. *J Biol Chem* **294**, 4450-4463 (2019).

31. Quan, D.N. & Bentley, W.E. Gene network homology in prokaryotes using a similarity search approach: queries of quorum sensing signal transduction. *PLoS Comput Biol* **8**, e1002637 (2012).

32. Wang, L., Hashimoto, Y., Tsao, C.Y., Valdes, J.J. & Bentley, W.E. Cyclic AMP (cAMP) and cAMP receptor protein influence both synthesis and uptake of extracellular autoinducer 2 in Escherichia coli. *J Bacteriol* **187**, 2066-2076 (2005).

33. Ha, J.H., Hauk, P., Cho, K., Eo, Y., Ma, X. et al. Evidence of link between quorum sensing and sugar metabolism in Escherichia coli revealed via cocrystal structures of LsrK and HPr. *Sci Adv* **4**, eaar7063 (2018).

34. Pereira, C.S., Santos, A.J., Bejerano-Sagie, M., Correia, P.B., Marques, J.C. et al. Phosphoenolpyruvate phosphotransferase system regulates detection and

processing of the quorum sensing signal autoinducer-2. *Mol Microbiol* **84**, 93-104 (2012).

35. Zargar, A., Quan, D.N., Abutaleb, N., Choi, E., Terrell, J.L. et al. Constructing "quantized quorums" to guide emergent phenotypes through quorum quenching capsules. *Biotechnol Bioeng* **114**, 407-415 (2017).

36. Tsao, C.Y., Hooshangi, S., Wu, H.C., Valdes, J.J. & Bentley, W.E. Autonomous induction of recombinant proteins by minimally rewiring native quorum sensing regulon of *E. coli*. *Metab Eng* **12**, 291-297 (2010).

37. Hauk, P., Stephens, K., McKay, R., Virgile, C.R., Ueda, H. et al. Insightful directed evolution of Escherichia coli quorum sensing promoter region of the lsrACDBFG operon: a tool for synthetic biology systems and protein expression. *Nucleic Acids Res* **44**, 10515-10525 (2016).

38. Ueda, H., Stephens, K., Trivisa, K. & Bentley, W.E. Bacteria Floc, but Do They Flock? Insights from Population Interaction Models of Quorum Sensing. *MBio* **10** (2019).

39. Zargar, A., Quan, D.N., Emamian, M., Tsao, C.Y., Wu, H.C. et al. Rational design of 'controller cells' to manipulate protein and phenotype expression. *Metab Eng* **30**, 61-68 (2015).

40. Quan, D.N., Tsao, C.Y., Wu, H.C. & Bentley, W.E. Quorum Sensing Desynchronization Leads to Bimodality and Patterned Behaviors. *PLoS Comput Biol* **12**, e1004781 (2016).

41. Hooshangi, S. & Bentley, W.E. LsrR quorum sensing "switch" is revealed by a bottom-up approach. *PLoS Comput Biol* **7**, e1002172 (2011).

42. Oliphant, K. & Allen-Vercoe, E. Macronutrient metabolism by the human gut microbiome: major fermentation by-products and their impact on host health. *Microbiome* **7**, 91 (2019).

43. Lam, K.N., Alexander, M. & Turnbaugh, P.J. Precision Medicine Goes Microscopic: Engineering the Microbiome to Improve Drug Outcomes. *Cell Host Microbe* **26**, 22-34 (2019).

44. Fung, T.C., Olson, C.A. & Hsiao, E.Y. Interactions between the microbiota, immune and nervous systems in health and disease. *Nat Neurosci* **20**, 145-155 (2017).

45. Thompson, J.A., Oliveira, R.A., Djukovic, A., Ubeda, C. & Xavier, K.B. Manipulation of the quorum sensing signal AI-2 affects the antibiotic-treated gut microbiota. *Cell Rep* **10**, 1861-1871 (2015).

46. Piewngam, P., Zheng, Y., Nguyen, T.H., Dickey, S.W., Joo, H.S. et al. Pathogen elimination by probiotic Bacillus via signalling interference. *Nature* **562**, 532-537 (2018).

47. Bridges, A.A. & Bassler, B.L. The intragenus and interspecies quorum-sensing autoinducers exert distinct control over Vibrio cholerae biofilm formation and dispersal. *PLoS Biol* **17**, e3000429 (2019).

48. Zhu, J., Miller, M.B., Vance, R.E., Dziejman, M., Bassler, B.L. et al. Quorum-sensing regulators control virulence gene expression in Vibrio cholerae. *Proc Natl Acad Sci U S A* **99**, 3129-3134 (2002).

49. Duan, F. & March, J.C. Engineered bacterial communication prevents Vibrio cholerae virulence in an infant mouse model. *Proc Natl Acad Sci U S A* **107**, 11260-11264 (2010).

50. Mao, N., Cubillos-Ruiz, A., Cameron, D.E. & Collins, J.J. Probiotic strains detect and suppress cholera in mice. *Sci Transl Med* **10** (2018).

51. Hwang, I.Y., Koh, E., Wong, A., March, J.C., Bentley, W.E. et al. Engineered probiotic Escherichia coli can eliminate and prevent Pseudomonas aeruginosa gut infection in animal models. *Nat Commun* **8**, 15028 (2017).

52. Jayaraman, P., Holowko, M.B., Yeoh, J.W., Lim, S. & Poh, C.L. Repurposing a Two-Component System-Based Biosensor for the Killing of Vibrio cholerae. *ACS Synth Biol* **6**, 1403-1415 (2017).

53. Gupta, S., Bram, E.E. & Weiss, R. Genetically programmable pathogen sense and destroy. *ACS Synth Biol* **2**, 715-723 (2013).

54. Silpe, J.E. & Bassler, B.L. A Host-Produced Quorum-Sensing Autoinducer Controls a Phage Lysis-Lysogeny Decision. *Cell* **176**, 268-280 e213 (2019).

55. Kim, S., Kerns, S.J., Ziesack, M., Bry, L., Gerber, G.K. et al. Quorum Sensing Can Be Repurposed To Promote Information Transfer between Bacteria in the Mammalian Gut. *ACS Synth Biol* **7**, 2270-2281 (2018).

56. Sedlmayer, F., Jaeger, T., Jenal, U. & Fussenegger, M. Quorum-Quenching Human Designer Cells for Closed-Loop Control of Pseudomonas aeruginosa Biofilms. *Nano Lett* **17**, 5043-5050 (2017).

57. Sedlmayer, F., Hell, D., Muller, M., Auslander, D. & Fussenegger, M. Designer cells programming quorum-sensing interference with microbes. *Nat Commun* **9**, 1822 (2018).

58. Szafranski, S.P., Deng, Z.L., Tomasch, J., Jarek, M., Bhuju, S. et al. Quorum sensing of Streptococcus mutans is activated by Aggregatibacter actinomycetemcomitans and by the periodontal microbiome. *BMC Genomics* **18**, 238 (2017).

59. Muras, A., Mayer, C., Otero-Casal, P., Exterkate, R.A.M., Brandt, B.W. et al. Short chain N-acylhomoserine lactone quorum sensing molecules promote periodontal pathogens in in vitro oral biofilms. *Appl Environ Microbiol* (2019).

60. Chng, K.R., Tay, A.S., Li, C., Ng, A.H., Wang, J. et al. Whole metagenome profiling reveals skin microbiome-dependent susceptibility to atopic dermatitis flare. *Nat Microbiol* **1**, 16106 (2016).

61. Grice, E.A., Kong, H.H., Conlan, S., Deming, C.B., Davis, J. et al. Topographical and temporal diversity of the human skin microbiome. *Science* **324**, 1190-1192 (2009).

62. Williams, M.R., Costa, S.K., Zaramela, L.S., Khalil, S., Todd, D.A. et al. Quorum sensing between bacterial species on the skin protects against epidermal injury in atopic dermatitis. *Sci Transl Med* **11** (2019).

63. Turner, T.R., James, E.K. & Poole, P.S. The plant microbiome. *Genome Biol* **14**, 209 (2013).

64. Busby, P.E., Soman, C., Wagner, M.R., Friesen, M.L., Kremer, J. et al. Research priorities for harnessing plant microbiomes in sustainable agriculture. *PLoS Biol* **15**, e2001793 (2017).

65. Compant, S., Samad, A., Faist, H. & Sessitsch, A. A review on the plant microbiome: Ecology, functions, and emerging trends in microbial application. *J Adv Res* **19**, 29-37 (2019).

66. Garge, S.S. & Nerurkar, A.S. Attenuation of Quorum Sensing Regulated Virulence of Pectobacterium carotovorum subsp. carotovorum through an AHL Lactonase Produced by Lysinibacillus sp. Gs50. *PLoS One* **11**, e0167344 (2016).

67. Valente, R.S., Nadal-Jimenez, P., Carvalho, A.F.P., Vieira, F.J.D. & Xavier, K.B. Signal Integration in Quorum Sensing Enables Cross-Species Induction of Virulence in Pectobacterium wasabiae. *MBio* **8** (2017).

68. Zuniga, A., Fuente, F., Federici, F., Lionne, C., Bonnet, J. et al. An Engineered Device for Indoleacetic Acid Production under Quorum Sensing Signals Enables Cupriavidus pinatubonensis JMP134 To Stimulate Plant Growth. *ACS Synth Biol* **7**, 1519-1527 (2018).

69. Meyer, J.L., Gunasekera, S.P., Scott, R.M., Paul, V.J. & Teplitski, M. Microbiome shifts and the inhibition of quorum sensing by Black Band Disease cyanobacteria. *ISME J* **10**, 1204-1216 (2016).

70. Terrell, J.L., Wu, H.C., Tsao, C.Y., Barber, N.B., Servinsky, M.D. et al. Nano-guided cell networks as conveyors of molecular communication. *Nat Commun* **6**, 8500 (2015).

71. Roy, V., Smith, J.A., Wang, J., Stewart, J.E., Bentley, W.E. et al. Synthetic analogs tailor native AI-2 signaling across bacterial species. *J Am Chem Soc* **132**, 11141-11150 (2010).

72. Shong, J., Jimenez Diaz, M.R. & Collins, C.H. Towards synthetic microbial consortia for bioprocessing. *Curr Opin Biotechnol* **23**, 798-802 (2012).

73. Zhou, K., Qiao, K., Edgar, S. & Stephanopoulos, G. Distributing a metabolic pathway among a microbial consortium enhances production of natural products. *Nat Biotech* **33**, 377-383 (2015).

74. Dinh, C.V., Chen, X. & Prather, K.L.J. Development of a Quorum-Sensing Based Circuit for Control of Coculture Population Composition in a Naringenin Production System. *ACS Synth Biol* (2020).

75. Chen, Y., Kim, J.K., Hirning, A.J., Josic, K. & Bennett, M.R. Emergent genetic oscillations in a synthetic microbial consortium. *Science* **349**, 986-989 (2015).

76. Brenner, K., Karig, D.K., Weiss, R. & Arnold, F.H. Engineered bidirectional communication mediates a consensus in a microbial biofilm consortium. *Proc Natl Acad Sci U S A* **104**, 17300-17304 (2007).

77. Lentini, R., Martin, N.Y., Forlin, M., Belmonte, L., Fontana, J. et al. Two-Way Chemical Communication between Artificial and Natural Cells. *ACS Cent Sci* **3**, 117-123 (2017).

78. Rampioni, G., D'Angelo, F., Messina, M., Zennaro, A., Kuruma, Y. et al. Synthetic cells produce a quorum sensing chemical signal perceived by Pseudomonas aeruginosa. *Chem Commun (Camb)* **54**, 2090-2093 (2018).

79. Lentini, R., Santero, S.P., Chizzolini, F., Cecchi, D., Fontana, J. et al. Integrating artificial with natural cells to translate chemical messages that direct E. coli behaviour. *Nat Commun* **5**, 4012 (2014).

80. Marchand, N. & Collins, C.H. Peptide-based communication system enables Escherichia coli to Bacillus megaterium interspecies signaling. *Biotechnol Bioeng* **110**, 3003-3012 (2013).

81. Scott, S.R. & Hasty, J. Quorum Sensing Communication Modules for Microbial Consortia. *ACS Synth Biol* **5**, 969-977 (2016).

82. Kylilis, N., Tuza, Z.A., Stan, G.B. & Polizzi, K.M. Tools for engineering coordinated system behaviour in synthetic microbial consortia. *Nat Commun* **9**, 2677 (2018).

83. Grant, P.K., Dalchau, N., Brown, J.R., Federici, F., Rudge, T.J. et al. Orthogonal intercellular signaling for programmed spatial behavior. *Mol Syst Biol* **12**, 849 (2016).

84. Wellington, S. & Greenberg, E.P. Quorum Sensing Signal Selectivity and the Potential for Interspecies Cross Talk. *MBio* **10** (2019).

85. Stephens, K., Pozo, M., Tsao, C.Y., Hauk, P. & Bentley, W.E. Bacterial co-culture with cell signaling translator and growth controller modules for autonomously regulated culture composition. *Nat Commun* **10**, 4129 (2019).

86. Scott, S.R., Din, M.O., Bittihn, P., Xiong, L., Tsimring, L.S. et al. A stabilized microbial ecosystem of self-limiting bacteria using synthetic quorum-regulated lysis. *Nat Microbiol* **2**, 17083 (2017).

87. Din, M.O., Danino, T., Prindle, A., Skalak, M., Selimkhanov, J. et al. Synchronized cycles of bacterial lysis for in vivo delivery. *Nature* **536**, 81-85 (2016).

88. Balagadde, F.K., Song, H., Ozaki, J., Collins, C.H., Barnet, M. et al. A synthetic Escherichia coli predator-prey ecosystem. *Mol Syst Biol* **4**, 187 (2008).

89. Kong, W., Meldgin, D.R., Collins, J.J. & Lu, T. Designing microbial consortia with defined social interactions. *Nat Chem Biol* **14**, 821-829 (2018).

90. Wu, F., Lopatkin, A.J., Needs, D.A., Lee, C.T., Mukherjee, S. et al. A unifying framework for interpreting and predicting mutualistic systems. *Nat Commun* **10**, 242 (2019).

91. Abisado, R.G., Benomar, S., Klaus, J.R., Dandekar, A.A. & Chandler, J.R. Bacterial Quorum Sensing and Microbial Community Interactions. *MBio* **9** (2018).

92. Ozkaya, O., Balbontin, R., Gordo, I. & Xavier, K.B. Cheating on Cheaters Stabilizes Cooperation in Pseudomonas aeruginosa. *Curr Biol* **28**, 2070-2080 e2076 (2018).

93. Honjo, H., Iwasaki, K., Soma, Y., Tsuruno, K., Hamada, H. et al. Synthetic microbial consortium with specific roles designated by genetic circuits for cooperative chemical production. *Metab Eng* **55**, 268-275 (2019).

94. Luo, X., Tsao, C.Y., Wu, H.C., Quan, D.N., Payne, G.F. et al. Distal modulation of bacterial cell-cell signalling in a synthetic ecosystem using partitioned microfluidics. *Lab Chip* **15**, 1842-1851 (2015).

95. Wu, H.C., Tsao, C.Y., Quan, D.N., Cheng, Y., Servinsky, M.D. et al. Autonomous bacterial localization and gene expression based on nearby cell receptor density. *Mol Syst Biol* **9**, 636 (2013).

96. Wood, T.L., Guha, R., Tang, L., Geitner, M., Kumar, M. et al. Living biofouling-resistant membranes as a model for the beneficial use of engineered biofilms. *Proc Natl Acad Sci U S A* **113**, E2802-2811 (2016).

97. Hong, S.H., Hegde, M., Kim, J., Wang, X., Jayaraman, A. et al. Synthetic quorum-sensing circuit to control consortial biofilm formation and dispersal in a microfluidic device. *Nat Commun* **3**, 613 (2012).

98. Teschler, J.K., Zamorano-Sanchez, D., Utada, A.S., Warner, C.J., Wong, G.C. et al. Living in the matrix: assembly and control of Vibrio cholerae biofilms. *Nat Rev Microbiol* **13**, 255-268 (2015).

99. Harms, A., Maisonneuve, E. & Gerdes, K. Mechanisms of bacterial persistence during stress and antibiotic exposure. *Science* **354** (2016).

100. Vendeville, A., Winzer, K., Heurlier, K., Tang, C.M. & Hardie, K.R. Making 'sense' of metabolism: autoinducer-2, LuxS and pathogenic bacteria. *Nat Rev Microbiol* **3**, 383-396 (2005).

101. Khalil, A.S. & Collins, J.J. Synthetic biology: applications come of age. *Nat Rev Genet* **11**, 367-379 (2010).

102. Ford, T.J. & Silver, P.A. Synthetic biology expands chemical control of microorganisms. *Curr Opin Chem Biol* **28**, 20-28 (2015).

103. Saeidi, N., Wong, C.K., Lo, T.M., Nguyen, H.X., Ling, H. et al. Engineering microbes to sense and eradicate Pseudomonas aeruginosa, a human pathogen. *Mol Syst Biol* **7**, 521 (2011).

104. Xavier, K.B., Miller, S.T., Lu, W., Kim, J.H., Rabinowitz, J. et al. Phosphorylation and processing of the quorum-sensing molecule autoinducer-2 in enteric bacteria. *ACS Chem Biol* **2**, 128-136 (2007).

105. Xue, T., Zhao, L., Sun, H., Zhou, X. & Sun, B. LsrR-binding site recognition and regulatory characteristics in Escherichia coli AI-2 quorum sensing. *Cell Res* **19**, 1258-1268 (2009).

106. Xavier, K.B. & Bassler, B.L. Regulation of uptake and processing of the quorum-sensing autoinducer AI-2 in Escherichia coli. *J Bacteriol* **187**, 238-248 (2005).

107. Byrd, C.M. (University of Maryland at College Park, 2011).

108. Graff, S.M. & Bentley, W.E. Mathematical model of LsrR-binding and derepression in Escherichia coli K12. *J Bioinform Comput Biol* **15**, 1650039 (2017).

109. Deutscher, J., Francke, C. & Postma, P.W. How phosphotransferase system-related protein phosphorylation regulates carbohydrate metabolism in bacteria. *Microbiol Mol Biol Rev* **70**, 939-1031 (2006).

110. Deutscher, J., Ake, F.M., Derkaoui, M., Zebre, A.C., Cao, T.N. et al. The bacterial phosphoenolpyruvate:carbohydrate phosphotransferase system: regulation by protein phosphorylation and phosphorylation-dependent protein-protein interactions. *Microbiol Mol Biol Rev* **78**, 231-256 (2014).

111. Isaza, M.P., Duncan, M.S., Kaplan, J.B. & Kachlany, S.C. Screen for leukotoxin mutants in Aggregatibacter actinomycetemcomitans: genes of the phosphotransferase system are required for leukotoxin biosynthesis. *Infect Immun* **76**, 3561-3568 (2008).

112. Datsenko, K.A. & Wanner, B.L. One-step inactivation of chromosomal genes in Escherichia coli K-12 using PCR products. *Proc Natl Acad Sci U S A* **97**, 6640-6645 (2000).

113. Wright, R.C., Khakhar, A., Eshleman, J.R. & Ostermeier, M. Advancements in the development of HIF-1alpha-activated protein switches for use in enzyme prodrug therapy. *PLoS One* **9**, e114032 (2014).

114. Miller, J.H. Experiments in molecular genetics. (Cold Spring Harbor Laboratory Press, Cold Spring Harbor, N.Y. ; 1972).

115. Bassler, B.L., Greenberg, E.P. & Stevens, A.M. Cross-species induction of luminescence in the quorum-sensing bacterium Vibrio harveyi. *J Bacteriol* **179**, 4043-4045 (1997).

116. Waters, C.M. & Bassler, B.L. Quorum sensing: cell-to-cell communication in bacteria. *Annu Rev Cell Dev Biol* **21**, 319-346 (2005).

117. Rutherford, S.T. & Bassler, B.L. Bacterial quorum sensing: its role in virulence and possibilities for its control. *Cold Spring Harb Perspect Med* **2** (2012).

118. Zargar, A., Quan, D.N., Carter, K.K., Guo, M., Sintim, H.O. et al. Bacterial secretions of nonpathogenic Escherichia coli elicit inflammatory pathways: a closer investigation of interkingdom signaling. *MBio* **6**, e00025 (2015).

119. Brenner, K., You, L. & Arnold, F.H. Engineering microbial consortia: a new frontier in synthetic biology. *Trends in Biotechnology* **26**, 483-489 (2008).

120. Siegele, D.A. & Hu, J.C. Gene expression from plasmids containing the araBAD promoter at subsaturating inducer concentrations represents mixed populations. *Proc Natl Acad Sci U S A* **94**, 8168-8172 (1997).

121. McKay, R., Hauk, P., Quan, D. & Bentley, W.E. Development of Cell-Based Sentinels for Nitric Oxide: Ensuring Marker Expression and Unimodality. *ACS Synth Biol* **7**, 1694-1701 (2018).

122. Smith, J.A., Wang, J., Nguyen-Mau, S.M., Lee, V. & Sintim, H.O. Biological screening of a diverse set of AI-2 analogues in Vibrio harveyi suggests that receptors which are involved in synergistic agonism of AI-2 and analogues are promiscuous. *Chem Commun*, 7033-7035 (2009).

123. Woolston, B.M., Edgar, S. & Stephanopoulos, G. Metabolic engineering: past and future. *Annu Rev Chem Biomol Eng* **4**, 259-288 (2013).

124. McKay, R., Ghodasra, M., Schardt, J., Quan, D., Pottash, A.E. et al. A platform of genetically engineered bacteria as vehicles for localized delivery of therapeutics: Toward applications for Crohn's disease. *Bioeng Transl Med* **3**, 209-221 (2018).

125. Tschirhart, T., Kim, E., McKay, R., Ueda, H., Wu, H.C. et al. Electronic control of gene expression and cell behaviour in Escherichia coli through redox signalling. *Nat Commun* **8**, 14030 (2017).

126. Bittihn, P., Din, M.O., Tsimring, L.S. & Hasty, J. Rational engineering of synthetic microbial systems: from single cells to consortia. *Curr Opin Microbiol* **45**, 92-99 (2018).

127. Hays, S.G., Patrick, W.G., Ziesack, M., Oxman, N. & Silver, P.A. Better together: engineering and application of microbial symbioses. *Curr Opin Biotechnol* **36**, 40-49 (2015).

128. Lindemann, S.R., Bernstein, H.C., Song, H.S., Fredrickson, J.K., Fields, M.W. et al. Engineering microbial consortia for controllable outputs. *ISME J* **10**, 2077-2084 (2016).

129. Jones, J.A., Vernacchio, V.R., Sinkoe, A.L., Collins, S.M., Ibrahim, M.H.A. et al. Experimental and computational optimization of an Escherichia coli co-culture for the efficient production of flavonoids. *Metab Eng* **35**, 55-63 (2016).

130. Zhang, H. & Stephanopoulos, G. Co-culture engineering for microbial biosynthesis of 3-amino-benzoic acid in Escherichia coli. *Biotechnol J* **11**, 981-987 (2016).

131. Shin, H.D., McClendon, S., Vo, T. & Chen, R.R. Escherichia coli binary culture engineered for direct fermentation of hemicellulose to a biofuel. *Appl Environ Microbiol* **76**, 8150-8159 (2010).

132. Tsai, S.L., Goyal, G. & Chen, W. Surface display of a functional minicellulosome by intracellular complementation using a synthetic yeast consortium and its application to cellulose hydrolysis and ethanol production. *Appl Environ Microbiol* **76**, 7514-7520 (2010).

133. Gamby, S., Roy, V., Guo, M., Smith, J.A., Wang, J. et al. Altering the communication networks of multispecies microbial systems using a diverse toolbox of AI-2 analogues. *ACS Chem Biol* **7**, 1023-1030 (2012).

134. Marchand, N. & Collins, C.H. Synthetic Quorum Sensing and Cell-Cell Communication in Gram-Positive Bacillus megaterium. *ACS Synth Biol* **5**, 597-606 (2016).

135. Pereira, C.S., de Regt, A.K., Brito, P.H., Miller, S.T. & Xavier, K.B. Identification of functional LsrB-like autoinducer-2 receptors. *J Bacteriol* **191**, 6975-6987 (2009).

136. Milias-Argeitis, A., Rullan, M., Aoki, S.K., Buchmann, P. & Khammash, M. Automated optogenetic feedback control for precise and robust regulation of gene expression and cell growth. *Nat Commun* **7**, 12546 (2016).

137. Postma, P.W., Lengeler, J.W. & Jacobson, G.R. Phosphoenolpyruvate:carbohydrate phosphotransferase systems of bacteria. *Microbiol Rev* **57**, 543-594 (1993).

138. DeLisa, M.P., Valdes, J.J. & Bentley, W.E. Quorum signaling via AI-2 communicates the "Metabolic Burden" associated with heterologous protein production in Escherichia coli. *Biotechnol Bioeng* **75**, 439-450 (2001).

139. Rhoads, M.K., Hauk, P., Gupta, V., Bookstaver, M.L., Stephens, K. et al. Modification and Assembly of a Versatile Lactonase for Bacterial Quorum Quenching. *Molecules* **23**, 341 (2018).

140. Cherepanov, P.P. & Wackernagel, W. Gene disruption in Escherichia coli: TcR and KmR cassettes with the option of Flp-catalyzed excision of the antibiotic-resistance determinant. *Gene* **158**, 9-14 (1995).

141. Lindsay, A. & Ahmer, B.M. Effect of sdiA on biosensors of N-acylhomoserine lactones. *J Bacteriol* **187**, 5054-5058 (2005).

142. Kang, M., Lu, Y., Chen, S. & Tian, F. Harnessing the power of an expanded genetic code toward next-generation biopharmaceuticals. *Curr Opin Chem Biol* **46**, 123-129 (2018).

143. Forbes, N.S. Engineering the perfect (bacterial) cancer therapy. *Nat Rev Cancer* **10**, 785-794 (2010).

144. Panteli, J.T., Van Dessel, N. & Forbes, N.S. Detection of tumors with fluoromarker-releasing bacteria. *Int J Cancer* **146**, 137-149 (2020).

145. Hwang, I.Y. & Chang, M.W. Engineering commensal bacteria to rewire host-microbiome interactions. *Curr Opin Biotechnol* **62**, 116-122 (2019).

146. Hwang, I.Y., Tan, M.H., Koh, E., Ho, C.L., Poh, C.L. et al. Reprogramming microbes to be pathogen-seeking killers. *ACS Synth Biol* **3**, 228-237 (2014).

147. Geldart, K.G., Kommineni, S., Forbes, M., Hayward, M., Dunny, G.M. et al. Engineered E. coli Nissle 1917 for the reduction of vancomycin-resistant Enterococcus in the intestinal tract. *Bioeng Transl Med* **3**, 197-208 (2018).

148. Geldart, K., Forkus, B., McChesney, E., McCue, M. & Kaznessis, Y.N. pMPES: A Modular Peptide Expression System for the Delivery of Antimicrobial Peptides to the Site of Gastrointestinal Infections Using Probiotics. *Pharmaceuticals (Basel)* **9** (2016).

149. Van Dessel, N., Swofford, C.A. & Forbes, N.S. Potent and tumor specific: arming bacteria with therapeutic proteins. *Ther Deliv* **6**, 385-399 (2015).

150. Duan, F.F., Liu, J.H. & March, J.C. Engineered commensal bacteria reprogram intestinal cells into glucose-responsive insulin-secreting cells for the treatment of diabetes. *Diabetes* **64**, 1794-1803 (2015).

151. Hwang, I.Y., Lee, H.L., Huang, J.G., Lim, Y.Y., Yew, W.S. et al. Engineering microbes for targeted strikes against human pathogens. *Cell Mol Life Sci* **75**, 2719-2733 (2018).

152. Ou, B., Jiang, B., Jin, D., Yang, Y., Zhang, M. et al. Engineered Recombinant Escherichia coli Probiotic Strains Integrated with F4 and F18 Fimbriae Cluster Genes in the Chromosome and Their Assessment of Immunogenic Efficacy in Vivo. *ACS Synth Biol* **9**, 412-426 (2020).

153. Rottinghaus, A.G., Amrofell, M.B. & Moon, T.S. Biosensing in Smart Engineered Probiotics. *Biotechnol J*, e1900319 (2019).

154. El Hage, R., Hernandez-Sanabria, E. & Van de Wiele, T. Emerging Trends in "Smart Probiotics": Functional Consideration for the Development of Novel Health and Industrial Applications. *Front Microbiol* **8**, 1889 (2017).

155. Landry, B.P. & Tabor, J.J. Engineering Diagnostic and Therapeutic Gut Bacteria. *Microbiol Spectr* **5** (2017).

156. Mimee, M., Tucker, A.C., Voigt, C.A. & Lu, T.K. Programming a Human Commensal Bacterium, Bacteroides thetaiotaomicron, to Sense and Respond to Stimuli in the Murine Gut Microbiota. *Cell Syst* **2**, 214 (2016).

157. Virgile, C., Hauk, P., Wu, H.C., Shang, W., Tsao, C.Y. et al. Engineering bacterial motility towards hydrogen-peroxide. *PLoS One* **13**, e0196999 (2018).

158. Shang, W., Tsao, C.Y., Luo, X., Teodoro, M., McKay, R. et al. A simple and reusable bilayer membrane-based microfluidic device for the study of gradient-mediated bacterial behaviors. *Biomicrofluidics* **11**, 044114 (2017).

159. Panteli, J.T. & Forbes, N.S. Engineered bacteria detect spatial profiles in glucose concentration within solid tumor cell masses. *Biotechnol Bioeng* **113**, 2474-2484 (2016).

160. Forbes, N.S., Coffin, R.S., Deng, L., Evgin, L., Fiering, S. et al. White paper on microbial anti-cancer therapy and prevention. *J Immunother Cancer* **6**, 78 (2018).

161. Duan, F. & March, J.C. Interrupting Vibrio cholerae infection of human epithelial cells with engineered commensal bacterial signaling. *Biotechnol Bioeng* **101**, 128-134 (2008).

162. Wang, L., Li, J., March, J.C., Valdes, J.J. & Bentley, W.E. luxS-dependent gene regulation in Escherichia coli K-12 revealed by genomic expression profiling. *J Bacteriol* **187**, 8350-8360 (2005).

163. Tsao, C.Y., Wang, L., Hashimoto, Y., Yi, H., March, J.C. et al. LuxS coexpression enhances yields of recombinant proteins in Escherichia coli in part through posttranscriptional control of GroEL. *Appl Environ Microbiol* **77**, 2141-2152 (2011).

164. Adams, B.L., Carter, K.K., Guo, M., Wu, H.C., Tsao, C.Y. et al. Evolved Quorum sensing regulator, LsrR, for altered switching functions. *ACS Synth Biol* **3**, 210-219 (2014).

165. Zhou, K., Qiao, K., Edgar, S. & Stephanopoulos, G. Distributing a metabolic pathway among a microbial consortium enhances production of natural products. *Nat Biotechnol* **33**, 377-383 (2015).

166. Dinh, C.V., Chen, X. & Prather, K.L.J. Development of a quorum-sensing based circuit for control of co-culture population composition in a naringenin production system. *ACS Synth Biol* (2020).

167. Swift, C.L., Brown, J.L., Seppala, S. & O'Malley, M.A. Co-cultivation of the anaerobic fungus Anaeromyces robustus with Methanobacterium bryantii enhances transcription of carbohydrate active enzymes. *J Ind Microbiol Biotechnol* **46**, 1427-1433 (2019).

168. Bhagwat, A., Collins, C.H. & Dordick, J.S. Selective antimicrobial activity of cell lytic enzymes in a bacterial consortium. *Appl Microbiol Biotechnol* **103**, 7041-7054 (2019).

169. Gilmore, S.P., Lankiewicz, T.S., Wilken, S.E., Brown, J.L., Sexton, J.A. et al. Top-Down Enrichment Guides in Formation of Synthetic Microbial Consortia for Biomass Degradation. *ACS Synth Biol* **8**, 2174-2185 (2019).

170. Stephens, K., Zargar, A., Emamian, M., Abutaleb, N., Choi, E. et al. Engineering Escherichia coli for enhanced sensitivity to the autoinducer-2 quorum sensing signal. *Biotechnol Prog* **35**, e2881 (2019).

171. Guzman, L.M., Belin, D., Carson, M.J. & Beckwith, J. Tight regulation, modulation, and high-level expression by vectors containing the arabinose PBAD promoter. *J Bacteriol* **177**, 4121-4130 (1995).

172. He, L., Yang, H., Tang, J., Liu, Z., Chen, Y. et al. Intestinal probiotics E. coli Nissle 1917 as a targeted vehicle for delivery of p53 and Tum-5 to solid tumors for cancer therapy. *J Biol Eng* **13**, 58 (2019).

173. He, L., Yang, H., Liu, F., Chen, Y., Tang, S. et al. Escherichia coli Nissle 1917 engineered to express Tum-5 can restrain murine melanoma growth. *Oncotarget* **8**, 85772-85782 (2017).

174. Isabella, V.M., Ha, B.N., Castillo, M.J., Lubkowicz, D.J., Rowe, S.E. et al. Development of a synthetic live bacterial therapeutic for the human metabolic disease phenylketonuria. *Nat Biotechnol* **36**, 857-864 (2018).

175. Duan, F., Curtis, K.L. & March, J.C. Secretion of insulinotropic proteins by commensal bacteria: rewiring the gut to treat diabetes. *Appl Environ Microbiol* **74**, 7437-7438 (2008).

176. Klampfer, L., Zhang, J. & Nimer, S.D. GM-CSF rescues TF-1 cells from growth factor withdrawal-induced, but not differentiation-induced apoptosis: the role of BCL-2 and MCL-1. *Cytokine* **11**, 849-855 (1999).

177. Nagai, Y., Garrett, K.P., Ohta, S., Bahrun, U., Kouro, T. et al. Toll-like receptors on hematopoietic progenitor cells stimulate innate immune system replenishment. *Immunity* **24**, 801-812 (2006).

178. Sletta, H., Tondervik, A., Hakvag, S., Aune, T.E., Nedal, A. et al. The presence of N-terminal secretion signal sequences leads to strong stimulation

of the total expression levels of three tested medically important proteins during high-cell-density cultivations of Escherichia coli. *Appl Environ Microbiol* **73**, 906-912 (2007).

179. Roggo, C. & van der Meer, J.R. Miniaturized and integrated whole cell living bacterial sensors in field applicable autonomous devices. *Curr Opin Biotechnol* **45**, 24-33 (2017).

180. Cai, S., Shen, Y., Zou, Y., Sun, P., Wei, W. et al. Engineering highly sensitive whole-cell mercury biosensors based on positive feedback loops from quorum-sensing systems. *Analyst* **143**, 630-634 (2018).

181. Kang, Y., Lee, W., Kim, S., Jang, G., Kim, B.G. et al. Enhancing the copper-sensing capability of Escherichia coli-based whole-cell bioreporters by genetic engineering. *Appl Microbiol Biotechnol* **102**, 1513-1521 (2018).

182. McKay, R., Hauk, P., Wu, H.C., Pottash, A.E., Shang, W. et al. Controlling localization of Escherichia coli populations using a two-part synthetic motility circuit: An accelerator and brake. *Biotechnol Bioeng* **114**, 2883-2895 (2017).

183. Weber, W., Luzi, S., Karlsson, M., Sanchez-Bustamante, C.D., Frey, U. et al. A synthetic mammalian electro-genetic transcription circuit. *Nucleic Acids Res* **37**, e33 (2009).

184. Tsaneva, I.R. & Weiss, B. soxR, a locus governing a superoxide response regulon in Escherichia coli K-12. *J Bacteriol* **172**, 4197-4205 (1990).

185. Dietrich, L.E., Teal, T.K., Price-Whelan, A. & Newman, D.K. Redox-active antibiotics control gene expression and community behavior in divergent bacteria. *Science* **321**, 1203-1206 (2008).

186. Rubens, J.R., Selvaggio, G. & Lu, T.K. Synthetic mixed-signal computation in living cells. *Nat Commun* **7**, 11658 (2016).

187. Qiang, Z., Chang, J.H. & Huang, C.P. Electrochemical generation of hydrogen peroxide from dissolved oxygen in acidic solutions. *Water Res* **36**, 85-94 (2002).

188. Sanchez-Sanchez, C.M. & Bard, A.J. Hydrogen peroxide production in the oxygen reduction reaction at different electrocatalysts as quantified by scanning electrochemical microscopy. *Anal Chem* **81**, 8094-8100 (2009).

189. Deutscher, J. The mechanisms of carbon catabolite repression in bacteria. *Curr Opin Microbiol* **11**, 87-93 (2008).

190. Andersen, J.B., Sternberg, C., Poulsen, L.K., Bjorn, S.P., Givskov, M. et al. New unstable variants of green fluorescent protein for studies of transient gene expression in bacteria. *Appl Environ Microbiol* **64**, 2240-2246 (1998).

191. Mimee, M., Nadeau, P., Hayward, A., Carim, S., Flanagan, S. et al. An ingestible bacterial-electronic system to monitor gastrointestinal health. *Science* **360**, 915-918 (2018).

192. Choi, K.R., Jang, W.D., Yang, D., Cho, J.S., Park, D. et al. Systems Metabolic Engineering Strategies: Integrating Systems and Synthetic Biology with Metabolic Engineering. *Trends in Biotechnology* **37**, 817-837 (2019).

193. Roell, G.W., Zha, J., Carr, R.R., Koffas, M.A., Fong, S.S. et al. Engineering microbial consortia by division of labor. *Microb Cell Fact* **18**, 35 (2019).

194. Zhang, H., Pereira, B., Li, Z. & Stephanopoulos, G. Engineering Escherichia coli coculture systems for the production of biochemical products. *Proc Natl Acad Sci U S A* **112**, 8266-8271 (2015).

195. Li, Z., Wang, X. & Zhang, H. Balancing the non-linear rosmarinic acid biosynthetic pathway by modular co-culture engineering. *Metab Eng* **54**, 1-11 (2019).

196. Mavrodi, D.V., Bonsall, R.F., Delaney, S.M., Soule, M.J., Phillips, G. et al. Functional analysis of genes for biosynthesis of pyocyanin and phenazine-1-carboxamide from Pseudomonas aeruginosa PAO1. *J Bacteriol* **183**, 6454-6465 (2001).

197. Jimenez, P.N., Koch, G., Thompson, J.A., Xavier, K.B., Cool, R.H. et al. The multiple signaling systems regulating virulence in Pseudomonas aeruginosa. *Microbiol Mol Biol Rev* **76**, 46-65 (2012).

198. Cao, M., Gao, M., Suastegui, M., Mei, Y. & Shao, Z. Building microbial factories for the production of aromatic amino acid pathway derivatives: From commodity chemicals to plant-sourced natural products. *Metab Eng* (2019).

199. Tschirhart, T., Zhou, X.Y., Ueda, H., Tsao, C.Y., Kim, E. et al. Electrochemical Measurement of the beta-Galactosidase Reporter from Live Cells: A Comparison to the Miller Assay. *ACS Synth Biol* **5**, 28-35 (2016).

200. VanArsdale, E., Tsao, C.Y., Liu, Y., Chen, C.Y., Payne, G.F. et al. Redox-Based Synthetic Biology Enables Electrochemical Detection of the Herbicides Dicamba and Roundup via Rewired Escherichia coli. *ACS Sens* **4**, 1180-1184 (2019).

201. Connell, N., Han, Z., Moreno, F. & Kolter, R. An E. coli promoter induced by the cessation of growth. *Mol Microbiol* **1**, 195-201 (1987).

202. DeLisa, M.P., Valdes, J.J. & Bentley, W.E. Mapping stress-induced changes in autoinducer AI-2 production in chemostat-cultivated Escherichia coli K-12. *J Bacteriol* **183**, 2918-2928 (2001).

203. Fernandes, R. & Bentley, W.E. AI-2 biosynthesis module in a magnetic nanofactory alters bacterial response via localized synthesis and delivery. *Biotechnol Bioeng* **102**, 390-399 (2009).

204. Koop, A.H., Hartley, M.E. & Bourgeois, S. A low-copy-number vector utilizing beta-galactosidase for the analysis of gene control elements. *Gene* **52**, 245-256 (1987).